(1)

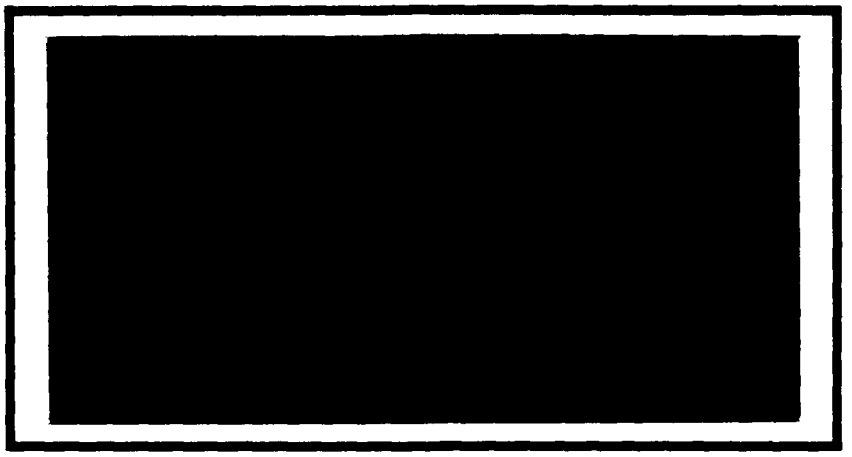

DEPARTMENT OF THE AIR FORCE

AIR UNIVERSITY

AIR FORCE INSTITUTE OF TECHNOLOGY

Wright-Patterson Air Force Base, Ohio

AFIT/GAE/ENY/89D-34

(1)

IMPACT DAMAGE TOLERANCE OF COMPOSITE CYLINDRICAL PANELS

THESIS

Eugene A. Senn
Captain, USAF

AFIT/GAE/ENY/89D-34

REPORT DOCUMENTATION PAGE

Form Approved
OMB No. 0704-0188

1a. REPORT SECURITY CLASSIFICATION UNCLASSIFIED	1b. RESTRICTIVE MARKINGS
2a. SECURITY CLASSIFICATION AUTHORITY	3. DISTRIBUTION/AVAILABILITY OF REPORT Approved for public release; distribution unlimited
2b. DECLASSIFICATION/DOWNGRADING SCHEDULE	
4. PERFORMING ORGANIZATION REPORT NUMBER(S) AFIT/GAE/ENY/89D-34	5. MONITORING ORGANIZATION REPORT NUMBER(S)
6a. NAME OF PERFORMING ORGANIZATION School of Engineering 6b. OFFICE SYMBOL (If applicable) AFIT/ENY	7a. NAME OF MONITORING ORGANIZATION
6c. ADDRESS (City, State, and ZIP Code) Air Force Institute of Technology (AU) Wright-Patterson AFB, OH 45433-6583	7b. ADDRESS (City, State, and ZIP Code)
8a. NAME OF FUNDING/SPONSORING ORGANIZATION AF Flight Dynamics Laboratory 8b. OFFICE SYMBOL (If applicable) WRDC/FI	9. PROCUREMENT INSTRUMENT IDENTIFICATION NUMBER
8c. ADDRESS (City, State, and ZIP Code) Wright-Patterson AFB, OH 45433	10. SOURCE OF FUNDING NUMBERS PROGRAM ELEMENT NO. / PROJECT NO. / TASK NO / WORK UNIT ACCESSION NO.

11. TITLE (Include Security Classification)
IMPACT DAMAGE TOLERANCE OF COMPOSITE CYLINDRICAL PANELS (UNCLASSIFIED)

12. PERSONAL AUTHOR(S)
Eugene A. Senn, Capt, USAF

13a. TYPE OF REPORT	13b. TIME COVERED	14. DATE OF REPORT (Year, Month, Day)	15. PAGE COUNT
MS Thesis	FROM _____ TO _____	1989 December	132

16. SUPPLEMENTARY NOTATION

17. COSATI CODES			18. SUBJECT TERMS (Continue on reverse if necessary and identify by block number)
FIELD	GROUP	SUB-GROUP	Composite cylindrical panels, Graphite/Epoxy, Kevlar/ Polyester, low velocity impact, damage, compression, imperfections
11	04		
20	11		

19. ABSTRACT (Continue on reverse if necessary and identify by block number)

See reverse side for abstract.

Thesis Advisor: Dr. Anthony Palazotto
Professor of Aerospace Engineering
Department of Aeronautical and Astronautical Engineering

20. DISTRIBUTION/AVAILABILITY OF ABSTRACT ☒ UNCLASSIFIED/UNLIMITED ☐ SAME AS RPT. ☐ DTIC USERS	21. ABSTRACT SECURITY CLASSIFICATION UNCLASSIFIED
22a. NAME OF RESPONSIBLE INDIVIDUAL Anthony Palazotto, Professor	22b. TELEPHONE (Include Area Code) (513) 255-2998 22c. OFFICE SYMBOL AFIT/ENY

BLOCK 19 (UNCLASSIFIED)

This thesis studied the impact damage tolerance of composite cylindrical panels subjected to low velocity impacts. Graphite/Epoxy and Kevlar/Polyester panels with ply lay-ups of [0/90]2s, [±45/90/0]s, and [0/90]3s were investigated.

STAGSC-1, the finite element program used to perform the analysis, can not analyze a laminated woven material such as Kevlar/Polyester, so a simple method was devised to model the material as an orthotropic laminate. The equivalent material properties agreed to within 5% of the experimental properties determined by standard material property tensile tests.

A nonlinear collapse analysis was performed to predict the strength of the undamaged panels. The experimental collapse loads differed by as much as 62% (lower) from the finite element predicted loads. The sensitivity of the composite panel to small imperfections accounts for the difference between analytical and experimental loads. Imposing a transverse sinusoidal imperfection with a maximum amplitude equal to the thickness of one ply resulted in analytical loads that agreed with experimental loads to within 16% at worst.

Graphite/Epoxy and Kevlar/Polyester curved panels were impacted with energies of 1-3 ft-lbs (velocities of 3.40-5.36 ft/sec). No damage occurred for energies below 1-3 ft-lbs, depending on the ply lay-up. The residual strength of the damaged panel was only 2-6% lower than the strength of the undamaged panels.

Ultrasonic C-scan and microphotographs were taken of panels impacted with energies between 8-17 ft-lbs (velocities of 9.62-13.89 ft/sec) to investigate and characterize impact damage from the material response point of view. Even at low impact energies, C-scans and stereo X-rays show that internal damage occurs even though no exterior signs of damage are visible. The damage can be characterized by matrix cracking, delamination, and fiber breakage.

AFIT/GAE/ENY/89D-34

IMPACT DAMAGE TOLERANCE OF COMPOSITE CYLINDRICAL PANELS

THESIS

Presented to the Faculty of the School of Engineering
of the Air Force Institute of Technology
Air University
in Partial Fulfillment of the
Requirements for the Degree of
Master of Science in Aeronautical Engineering

Eugene A. Senn
Captain, USAF

December 1989

Approved for public release; distribution unlimited

ACKNOWLEDGEMENTS

This thesis would not have been possible without the help of a great many people. First I'd like to thank my advisor, Dr. Anthony Palazotto, for his help and guidance. I also thank him for his encouragement to continue my education beyond a Master's degree.

I would like Dr. R. S. Sandhu and Kevin Spitzer of the Flight Dynamic Laboratory (WRDC/FI) for all their help with the impact experimentation. A special thanks goes to Jack Smith for his patience, understanding, and encouragement. It was also a real pleasure to work with Larry Bates, Don Cook, and Harold Stalnaker on the compression work.

The Materials Laboratory (WRDC/ML) was of great help in performing the C-scan, stereo X-ray, and microphotography on the panels.

Lastly and most importantly, I thank my wife Susan for putting up with me during this ordeal. She rarely understood anything I was doing but, whether she realizes it or not, she helped just by being there.

TABLE OF CONTENTS

LIST OF FIGURES

LIST OF TABLES

LIST OF SYMBOLS

$( )_{,x}$	Partial derivative with respect to x
$( )_{,y}$	Partial derivative with respect to y
g	Acceleration of Gravity (32.174 ft/sec^2)
h	Drop Height
m	Mass of Impactor
t	Mid-Side Node Displacements for QUAF 411 Element
u,v,w	Displacements in the x,y,z directions, respectively
x,y,z	Structural Axes
E	Energy
F	Force
V	Impact Velocity
W	Weight of Impactor
WAMP	Amplitude of Imperfection
XL, YL	Half-Wavelength of Imperfection in x and y directions, respectively
X1, Y1	Location of Center of Imperfection
A_{ij}	Extensional Stiffness Matrix
B_{ij}	Extensional-Bending Coupling Stiffness Matrix
D_{ij}	Bending Stiffness Matrix
E_I	Impact Energy
E_x, E_y	Effective Engineering Young's Modulus
G_{xy}	Effective Engineering Shear Modulus
M_x, M_y, M_{xy}	Moments Acting on a Plate

N_x, N_y, N_{xy}	In-plane Forces on a Plate
E_1, E_2	Material Longitudinal and Transverse Young's Modulus
G_{12}	Material Shear Modulus
W_o	Imperfection Function
1,2,3	Fiber Axis Directions
θ	Fiber Orientation Angle
β_x, β_y	Rotations in Cylindrical Coordinates
ε_x^o, ε_y^o	Normal Mid-Surface Strains
ε_x, ε_y	Normal Strains
γ_{xy}^o	Shear Strain at Mid-Surface
γ_{xy}, γ_{xz}, γ_{yz}	Shear Strains
K_x, K_y, K_{xy}	Curvatures
θ_x, θ_y, θ_z	Rotations in a Flat Plate
ν_{xy}	Effective Engineering Poisson's Ratio
ν_{12}	Material Poisson's Ratio
$\{\varepsilon\}$	Strain Vector
$[Q]$	Reduced Stiffness Matrix
$[\bar{Q}]$	Transformed Reduced Stiffness Matrix
$\{\sigma\}$	Stress Vector

ABSTRACT

This thesis studied the impact damage tolerance of composite cylindrical panels subjected to low velocity impacts. Graphite/Epoxy and Kevlar/Polyester panels with ply lay-ups of $[0/90]_{2s}$, $[\pm 45/90/0]_{s}$, and $[0/90]_{3s}$ were investigated.

STAGSC-1, the finite element program used to perform the analysis, can not analyze a laminated woven material such as Kevlar/Polyester, so a simple method was devised to model the material as an orthotropic laminate. The equivalent material properties agreed to within 5% of the experimental properties determined by standard material property tensile tests.

A nonlinear collapse analysis was performed to predict the strength of the undamaged panels. The experimental collapse loads differed by as much as 62% (lower) from the finite element predicted loads. The sensitivity of the composite panel to small imperfections accounts for the difference between analytical and experimental loads. Imposing a transverse sinusoidal imperfection with a maximum amplitude equal to the thickness of one ply resulted in analytical loads that agreed with experimental loads to within 16% at worst.

Graphite/Epoxy and Kevlar/Polyester curved panels were impacted with energies of 1-3 ft-lbs (velocities of 3.40-5.36 ft/sec). No damage occurred for impact energies below 1-3 ft-lbs, depending on the ply lay-up. The residual strength of the damaged panel was only 2-6% lower than the strength of undamaged panels.

Ultrasonic C-Scan and microphotographs were taken of panels impacted with energies between 8-17 ft-lbs (velocities of 9.62-13.89 ft/sec) to investigate and characterize impact damage from the material response point of view. Even at low impact energies, C-scans and stereo X-rays show that internal damage occurs even though no exterior signs of damage are visible. The damage can be characterized by matrix cracking, delamination, and fiber breakage.

IMPACT DAMAGE TOLERANCE OF COMPOSITE CYLINDRICAL PANELS

1. INTRODUCTION

BACKGROUND

Compression of composite cylindrical panels has been studied at the Air Force Institute of Technology (AFIT) since the late 1970's. Wilder [1] presents a good background on the study of shell collapse. Becker [2] investigated the instability of composite cylindrical panels at AFIT in 1979. Janisse [3] studied the effects of surface imperfections and small cutouts in 1982.

Fiber breakage, matrix cracking, and/or delamination of composite materials may result from low energy impacts even though no damage can be seen on the surface. Little information is available on impact damage and impact damage tolerance of composite cylindrical panels. Much has been written about impact damage of flat plates and their compressive residual strength after impact [4-10]. In most cases, the impacted plates were cut into tensile or compression coupons with the majority of the damage contained in one coupon. This was done since compression fixtures for flat plates were not available. While testing this way gives some insight into how impact damage can weaken a structure, it confines all the damage to one

concentrated area. The true structural reaction to the damage is not shown.

Meyer [11] did investigate low energy impact of filament-wound Kevlar/Epoxy panels. He was able to characterize the damage by calculating the energy absorbed by the panel and by inspecting cross-sections of the damaged curved panels. Wilder [1] performed a study where impact damage to a cylindrical Graphite/Epoxy panel was simulated by implanting a teflon insert into the panel when it was manufactured. The insert left a completely debonded region between two plies similar to the delamination that occurs in flat plates.

PURPOSE

The purpose of this thesis was to study the damage tolerance of composite cylindrical panels subjected to a single low energy impact. Two materials and three ply orientations were studied. The compressive residual strength was obtained. Another purpose was to investigate and characterize impact damage of composite cylindrical panels. Ultrasonic C-scan, stereo X-ray, and microphotography were used to perform the investigation.

SCOPE

One set of panels tested in this thesis was made of AS4/3501-6 Graphite/Epoxy with ply orientations of $[0/90]_{2s}$,

$[\pm 45/90/0]_s$, and $[0/90]_{3s}$. Panels with the same ply orientations but made of Kevlar/Polyester, which is a weave material, were also tested. Panels from each group were tested in compression to establish the original strength of the panels. Similarly, panels from each group were subjected to low energy impacts of between 1-3 ft-lbs. C-scans and stereo X-rays were taken of these panels to determine damage size. They were then tested in compression to determine residual strength. Lastly, panels from each group were subjected to higher impact energies (8-17 ft-lbs). C-scans and microphotographs were taken of these panels in an effort to characterize the damage.

2. Experimentation

The main purpose of this thesis is to investigate how well composite cylindrical panels made of Graphite/Epoxy and Kevlar/Polyester resist low velocity impacts. Testing this resistance took the form of finding the residual strength of the panels after they have been impacted. With this in mind, panels of each material were subjected to low velocity impacts and tested in compression. In addition to residual strength testing, several techniques were used to capture and characterize the damage from a material point of view.

Impact of Composite Cylindrical Panels

A great deal of work has been done in the area of impact on composite flat plates [4-10]. However, the author could find very little published work regarding impact of composite cylindrical panels (or shells for that matter). While it is not the primary purpose of this thesis to study the dynamics of impact, a brief discussion on the phenomenon as it relates to the testing of the cylindrical panels is presented. The approach is from the impact testing point of view.

Impact tests were carried out on Graphite/Epoxy and Kevlar/Polyester panels with the geometry shown in Figure 2.1. Displacements in the x- and z-directions are measured

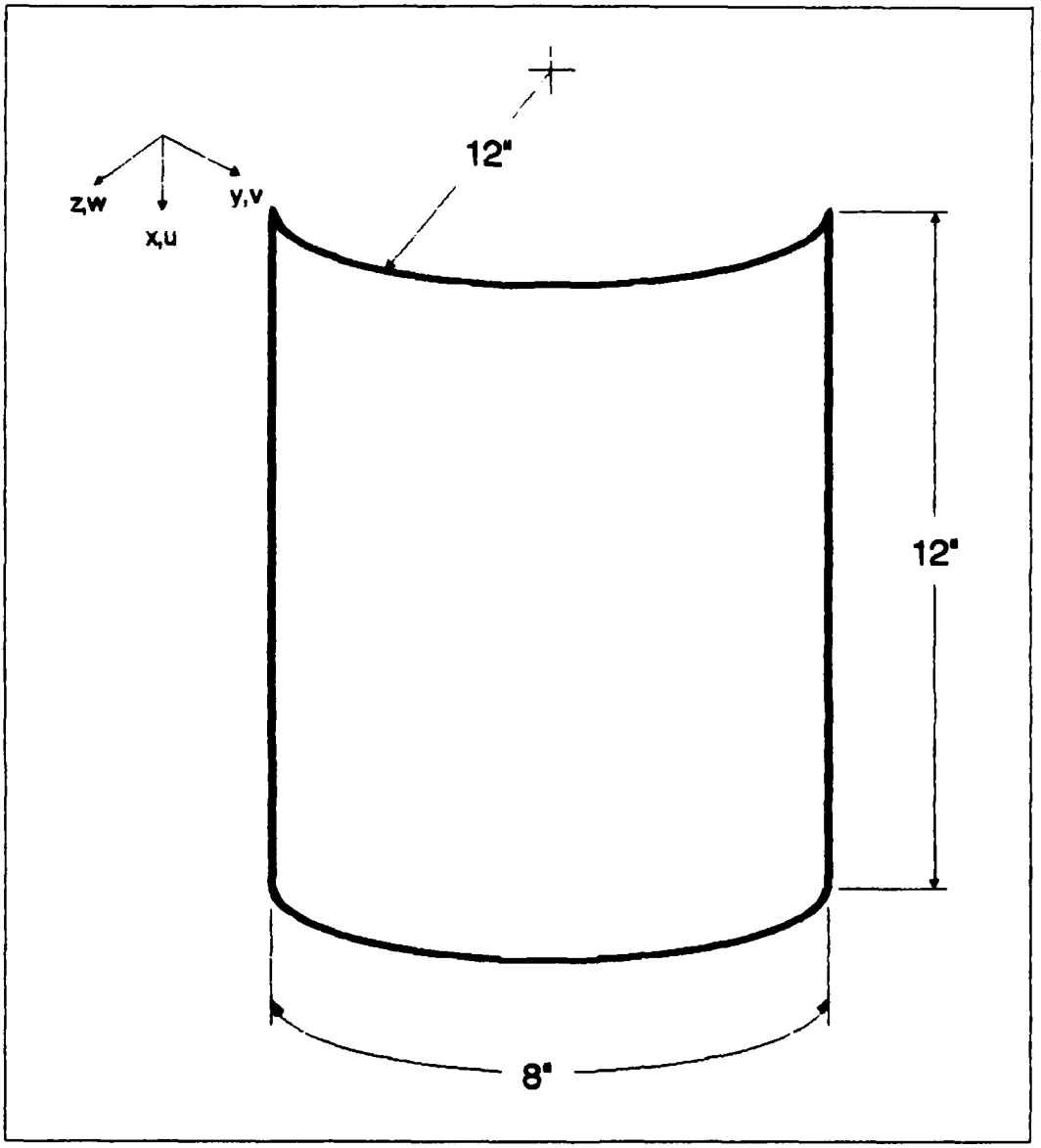

Figure 2.1 - Panel Geometry

in units of length while displacements in the y-direction are measured in radians.

The panels were subjected to a single, transverse (-z direction) impact normal to the surface of the panels. A GRC 8250 Dynatup Impact Test Machine (hereafter called Dynatup) made by General Research Corporation, was the test fixture used (see Figure 2.2) [12]. The impactor used was a 1/2" diameter tup weighing approximately 5.5 pounds and instrumented with an accelerometer to measure the contact force between the tup and the panel. The data obtained from the accelerometer is acquired and analyzed by a GRC 730-I Instrumented Impact Test Data System.

Two quantities important in discussing impact problems are the impact energy and the impact velocity. The Dynatup Test Data System calculates the impact energy from the simple relation

$$E_I = Wh \qquad (2.1)$$

where W is the weight of the impactor in pounds and h is the drop height in feet. The impact energy is also simply the kinetic energy of the impactor at the instant it contacts the panel.

$$E_I = 1/2(mV^2) \qquad (2.2)$$

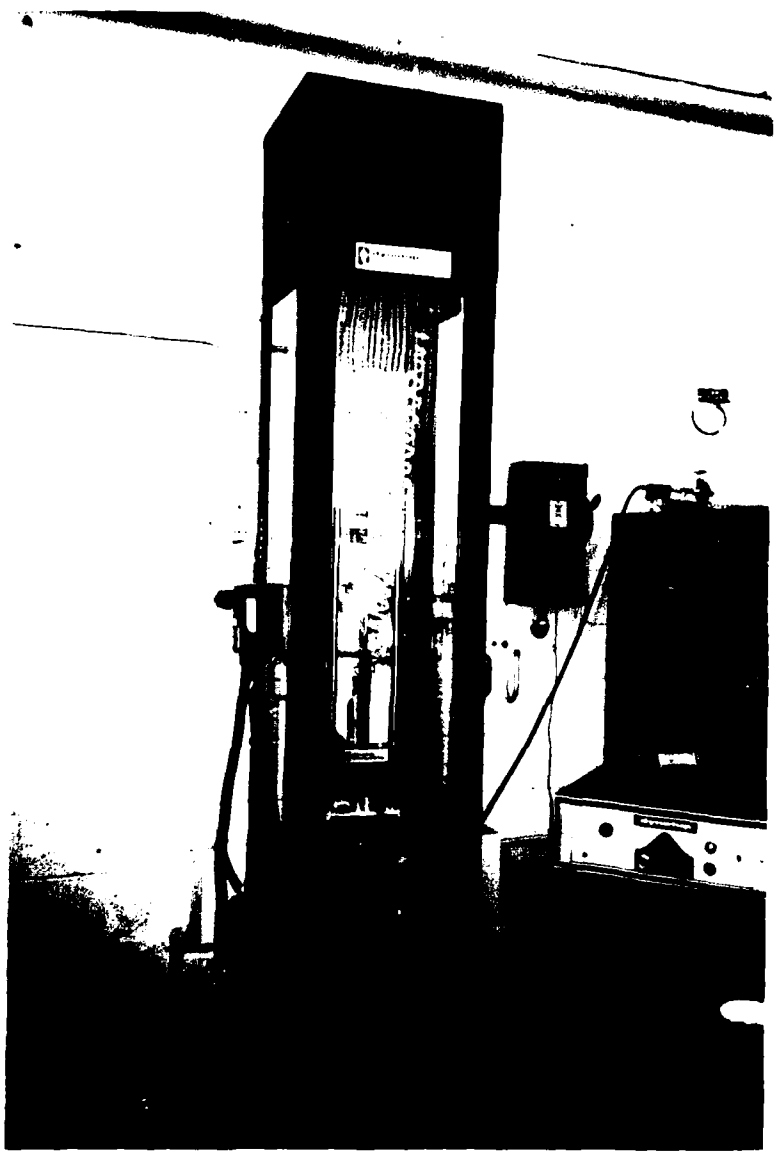

Figure 2.2 - Dynatup Impact Test Machine

Realizing that the impactor weight is just W=mg, we can substitute this into Equation (2.1), set Equations (2.1) and (2.2) equal to each other and solve for the impact velocity, V.

$$V = \sqrt{2gh} \qquad (2.3)$$

where g is the local acceleration of gravity (nominally 32.174 ft/sec^2).

The Dynatup actually calculates the impact velocity by use of a velocity flag. A metal "flag" similar to the one shown in Figure 2.3 is attached to the impactor. The flag is adjusted so that just prior to impact it trips a beam of light. The beam remains off as the first prong passes through the beam. After the first prong passes through the beam, the beam is then intact as the space between the prongs pass through. The second prong then breaks the beam again. The data acquisition system measures the amount of time that passes between the two breaks in the light beam. Knowing the distance between the edges of the two prongs, the system calculates the impact velocity by dividing this distance by the measured time.

Information available from the Dynatup on an impact test include Load vs. Time, Deflection vs. Time, Velocity vs. Time, Load vs. Deflection, Energy vs. Time, or any other combination of these parameters. An example of Load vs.

Time and Energy vs. Time is shown in Figure 2.4. The load is nothing more than the acceleration of the tup as obtained from the accelerometer, multiplied by the the mass of the impactor. The Deflection vs. Time curve shown in Figure 2.5 is obtained by integrating the acceleration vs. time curve twice with respect to time. (Recall from simple dynamics that the acceleration is the second derivative of displacement with respect to time). Knowing the load and deflection at every instant of time, a Load vs. Deflection curve, as shown in Figure 2.6, can be constructed. Lastly, the Energy vs. Time curve shown in Figure 2.4 is found by integrating the Load vs. Deflection curve [13] since

$$E = \int F \, dx \tag{2.4}$$

One last thing to discuss is the kinematic relations for a cylindrical panel and how they might affect impact test (and damage) results as compared to flat plates. Even though the structure under study here is a cylindrical panel, the kinematics are the same as for a complete cylindrical shell. Thus, the nonlinear strains and curvatures for a cylindrical shell as a function displacements can be written as [14]

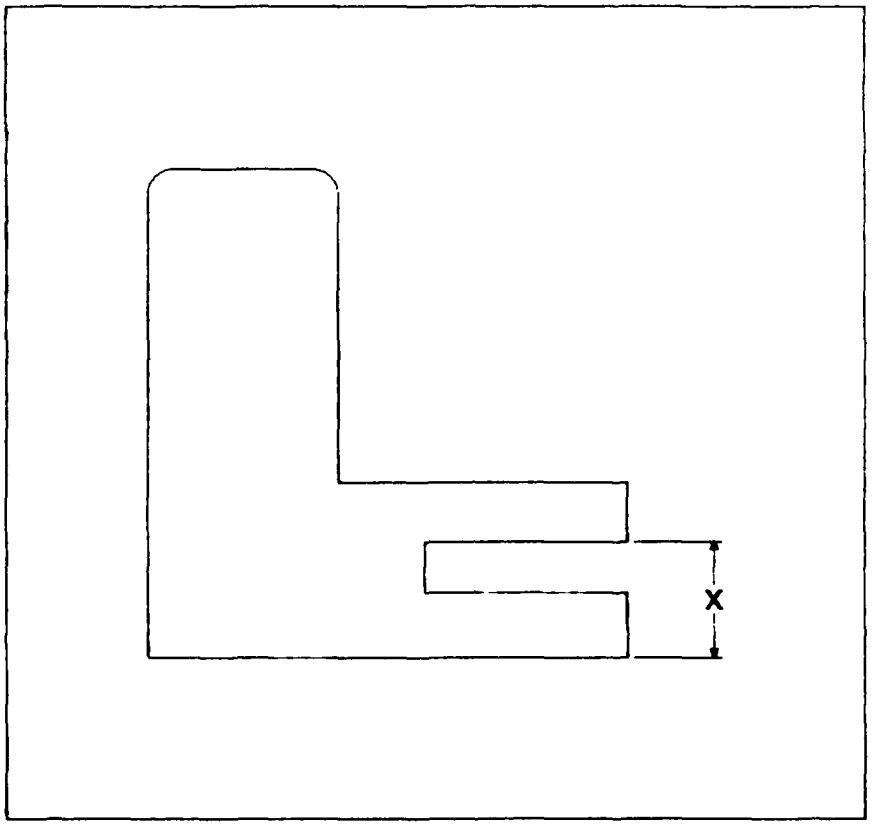

Figure 2.3 - Dynatup Velocity Flag

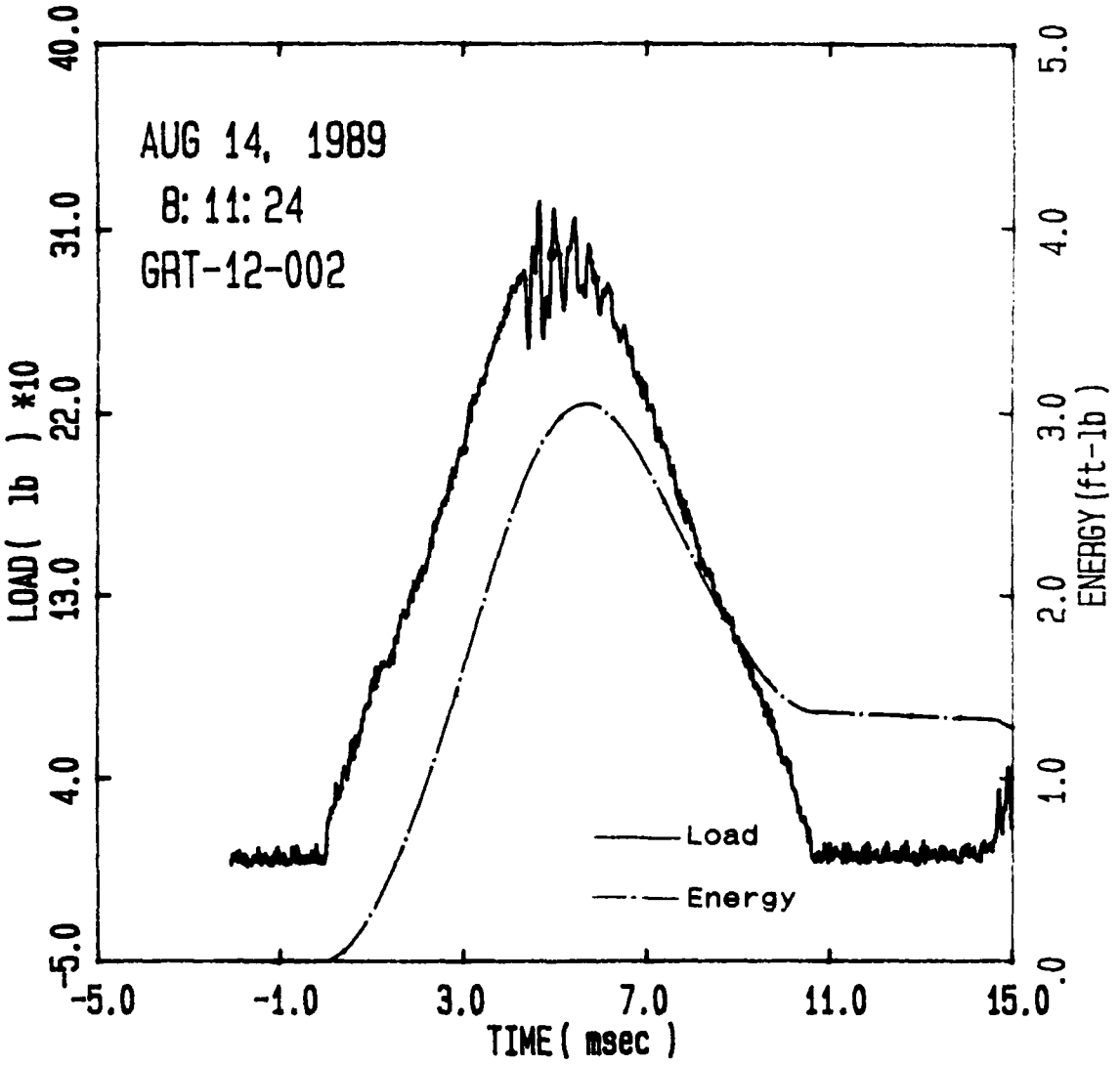

Specimen Id	Temp (f)	Impact Veloc. (ft/sec)	Impact Energy (ft-lb)	Time (msec) Max Ld	Time (msec) Total	Load (lb) Max	Energy (ft-lb) Max Ld	Energy (ft-lb) Total
GRT-12-002	72.	5.79	2.94	4.65	10.65	329.2	2.815	1.300

Figure 2.4
Example Plot of Load and Energy vs. Time for Impact Test

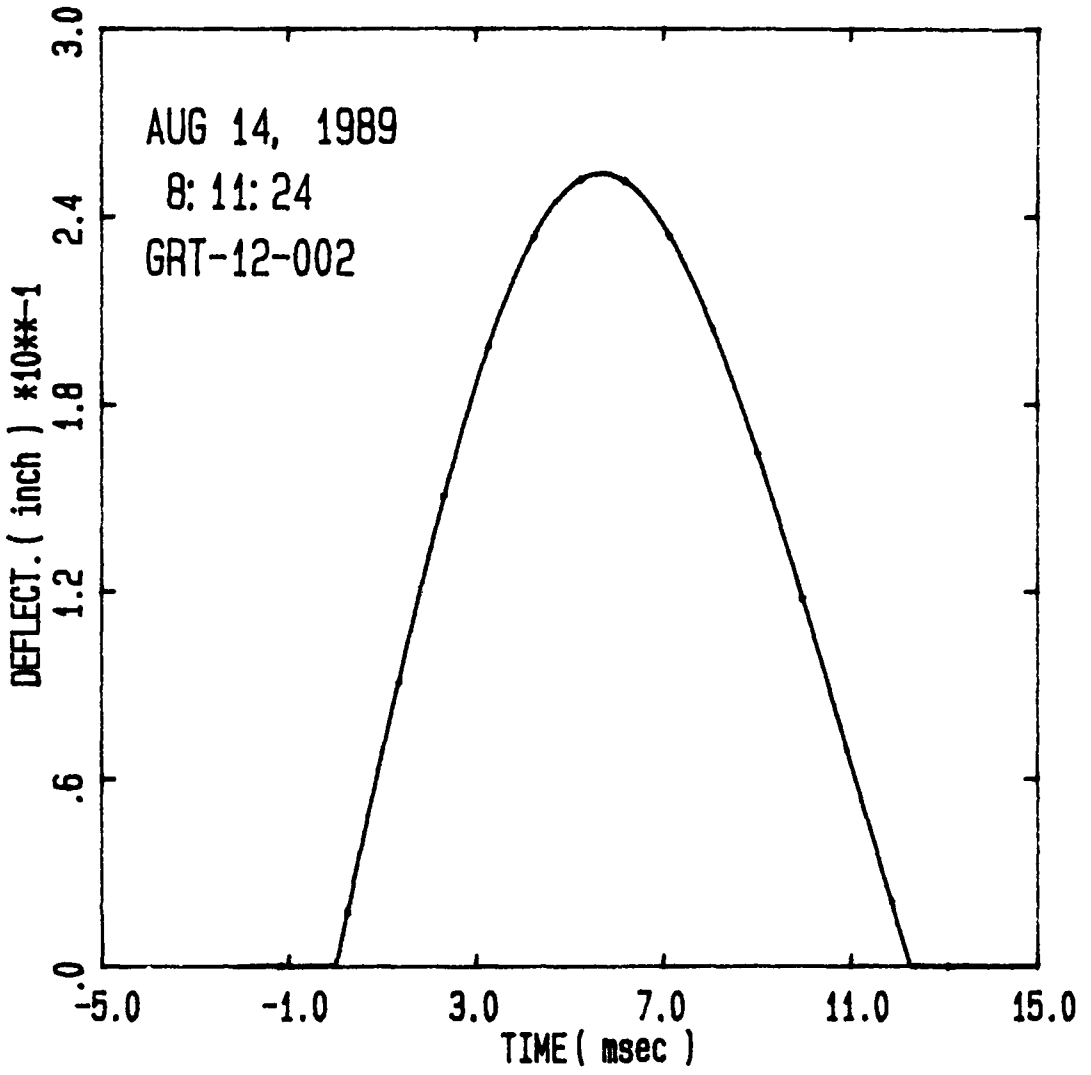

Specimen Id	Temp (f)	Impact Veloc. (ft/sec)	Energy (ft-lb)	Time (msec) Max Ld	Time (msec) Total	Load (lb) Max	Energy (ft-lb) Maxld	Energy (ft-lb) Total
GRT-12-002	72.	5.79	2.94	4.65	10.65	323.2	2.815	1.360

Figure 2.5
Example Plot of Deflection vs. Time for Impact Test

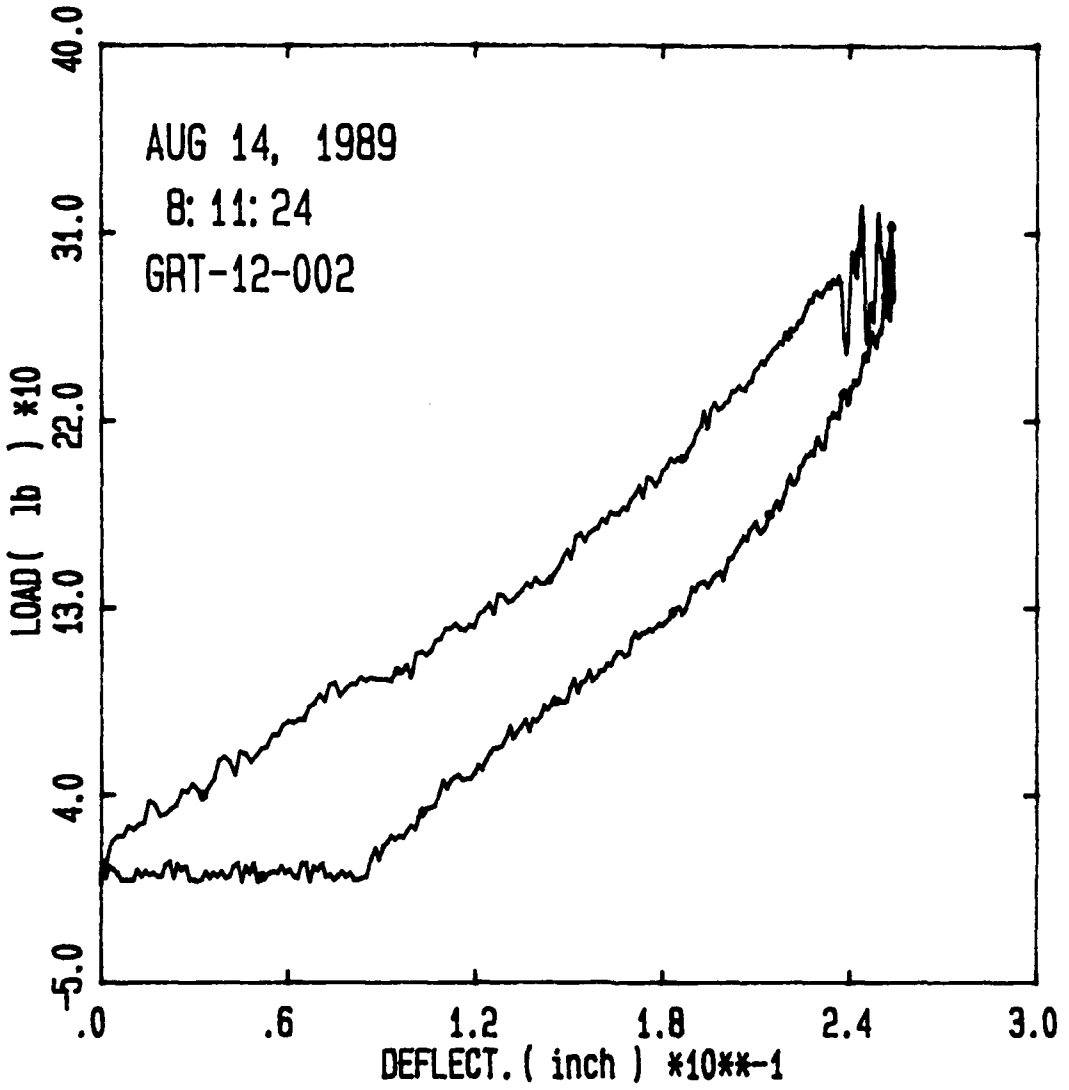

Specimen Id	Temp	Impact Veloc.	Impact Energy	Time		Load	Energy	
	(f)	(ft/sec)	(ft-lb)	(msec)		(lb)	(ft-lb)	
				Max Ld	Total	Max	Max Id	Total
GRT-12-002	72.	5.79	2.94	4.65	10.65	323.2	2.815	1.360

Figure 2.6
Example Plot of Load vs. Deflection for Impact Test

$$\varepsilon_x^\circ = u_{,x} + 1/2\ \beta_x^2$$

$$\varepsilon_y^\circ = \frac{v_{,y}}{R} + \frac{w}{R} + 1/2\ \beta_y^2$$

$$\gamma_{xy}^\circ = \frac{u_{,y}}{R} + v_{,x} + \beta_x\beta_y \qquad (2.5)$$

$$K_x = \beta_{x,x}$$

$$K_y = \beta_{y,y} / R$$

$$K_{xy} = 1/2 \left(\beta_{x,y} / R + \beta_{y,x} \right)$$

where

$$\beta_x = - w_{,x}$$

$$\beta_y = \frac{v}{R} - \frac{w_{,y}}{R} \qquad (2.6)$$

R is the radius of curvature of the cylindrical shell and u, v, and w are the middle surface displacements. Equations (2.5) and (2.6) represent the Sanders kinematic relations for shells specialized for cylindrical coordinates [14]. These equations apply under the following assumptions [14]:

a. The shell is thin, that is the thickness-to-radius ratio is much less than 1 ($h/R << 1$).

b. The strains are small compared to unity.

c. Transverse shear and normal stresses are negligible (plane stress condition).

d. The middle surface strains are of the order of magnitude of the total strain squared.

e. The rotations β_x and β_y are of the order of magnitude of the total strain.

f. The rotations relative to the normal to the middle surface are relatively small.

If one examines Equations (2.5) and (2.6), one sees that there are additional terms in the strain and curvature equations for a cylindrical shell brought about by the curvature of the shell. Thus, the curvature provides some additional strain energy to the structure. Given this, one would expect that a greater amount of force (or energy) would be required to deflect a curved shell the same amount as a flat plate. Or, looking at it from an impact damage point of view, it would require more force (or energy) to damage a cylindrical shell than it would to damage a flat plate of the same thickness and ply orientation. The extra energy is required to overcome the additional strain energy inherent in the structure.

With this brief introduction to impact and how the Dynatup calculates its results, we can proceed with a discussion of the impact testing.

Impact Testing Procedure

Since the Dynatup could not accommodate curved panels, curved aluminum blocks had to be manufactured to support the

panels during the impact tests. Figure 2.7 shows one of these blocks with a Graphite/Epoxy panel resting on it. A steel cover plate, also shown in Figure 2.7, was made to hold down the panels during the tests. A 5" x 5" cutout was made in both the cover plate and the aluminum support blocks to allow the impactor to strike the panel and to allow the panel to deflect. The clamped boundary conditions are simulated at all four edges. The panel is centered on the block such that the center of the panel is aligned with the centers of the cutouts. The cover plate is then bolted into place with its cutout aligned with the cutout of the support block. The final assembly of the panel on its support block is shown in Figure 2.8.

The panel-support block assembly is placed on an adjustable support plate underneath the impactor. As was mentioned earlier, the mass of the impactor used was approximately 5.5 lbs. Therefore, the impact velocity and subsequently the energy is varied by changing the drop height. For the Dynatup, the drop height was set using a tape measure. The height can be adjusted by using an Up-Down switch on the control panel shown in Figure 2.2.

A more accurate way to set the drop height is to calculate the impact velocity associated with the desired drop height using Equation (2.3). Then, placing a scrap panel on the support block, adjust the height of the impactor until the velocity determined by performing a

Figure 2.7 - Cover Plate, Panel, and Support Block

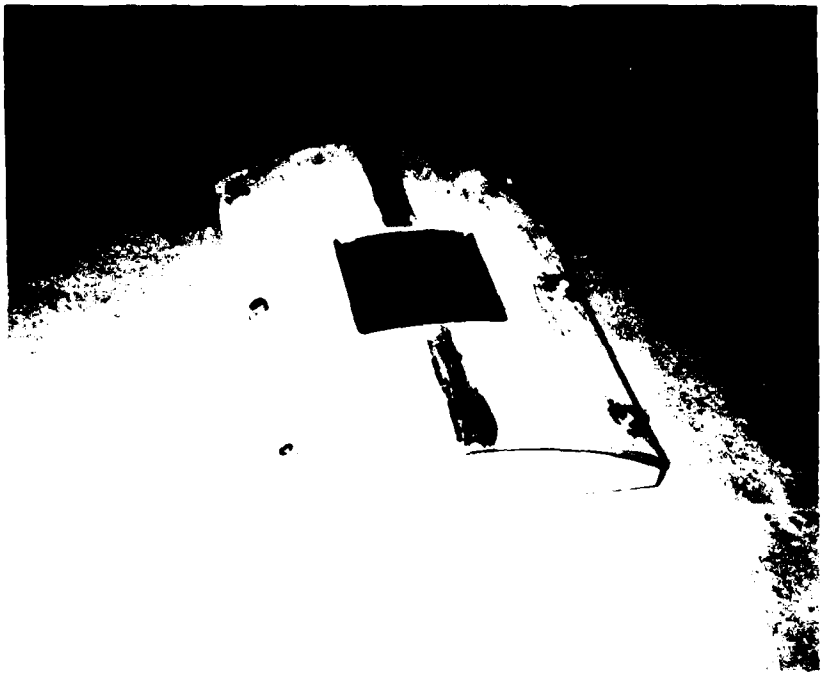

Figure 2.8 - Assembled Cover Plate, Panel, and Support Plate

velocity check [13] matches the calculated velocity. This method, however, is still not very easy to do on the Dynatup because there is no fine-tune or vernier adjustment capability on the drop height.

Once the drop height is set, a brake is set to catch the impactor as it rebounds off the panel, preventing multiple impacts. The impact test is ready to begin. The data acquisition system is started [13], a switch is thrown to arm the system, and a release button is pressed to electronically release the impactor. The test data is acquired and stored to disk so that at any time after the test, the data may be analyzed.

Minimum Damage Energy

O'Kane and Benham [5] showed in their work that there is an impact energy level below which no damage is sustained by a composite flat plate. Since the goal is to test panels for residual strength, the panels must be impacted with enough energy (or force) to cause damage. With this in mind, the minimum energy levels required to cause damage to Graphite/Epoxy panels with ply orientations of $[0/90]_{2s}$, $[\pm45/90/0]_{s}$, and $[0/90]_{3s}$ were determined.

A trial and error method was used to determine the minimum energy levels. The $[0/90]_{2s}$ and $[\pm45/90/0]_{s}$ orientations were initially impacted with a velocity of 9.67 ft/sec. The $[0/90]_{3s}$ was initially impacted with a velocity

of 11.85 ft/sec. These initial impacts were subjected to ultrasonic C-scan to determine the extent of the damage, if any. Based on the results of the C-scans, the impact velocity (energy) was increased or decreased accordingly. This process was repeated until the minimum energy level that caused damage was determined. Table 2.1 summarizes the minimum damage energies for the three types of Graphite/Epoxy panels.

Table 2.1
Minimum Damage Energy for Gr/Ep Panels

	$[0/90]_{2s}$	$[\pm 45/90/0]_{s}$	$[0/90]_{3s}$
Energy (ft-lbs)	1.27	0.99	2.46

By looking at Table 2.1, we see how the thickness and ply orientations affect the panels ability to absorb the impact. The $[\pm 45/90/0]_{s}$ panel was the most easily damaged, while the thicker $[0/90]_{3s}$ panel required more energy to damage it. A more in depth discussion of the impact damage will be presented in Chapter 3.

In order to insure that enough damage is present in the panel to see a difference in the residual strength tests, the impact energies used in the actual testing were increased 20% above those shown in Table 2.1. These increased energy levels are shown in Table 2.2.

Table 2.2
Energy Levels Used for Impact Tests

	$[0/90]_{2s}$	$[\pm 45/90/0]_{s}$	$[0/90]_{3s}$
Energy (ft-lbs)	1.52	1.19	2.92

Impact Tests

Using the impact energies shown in Table 2.2 and following the impact testing procedures described earlier, three Graphite/Epoxy and three Kevlar/Polyester panels were impacted with the same energy for the given ply orientation. For example, three $[0/90]_{2s}$ panels of each material were impacted with 1.52 ft-lbs of energy.

Figures 2.[illegible].14 show one Load and Energy vs. Time plot for each panel type. The small oscillations apparent in the Load vs. Time curve result from noise in the Dynatup as the impactor falls, strikes the panel, and rebounds. In the Graphite/Epoxy panels (Figures 2.9, 2.11, and 2.13), we notice larger oscillations in the force, corresponding to the panels being damaged. The Kevlar/Polyester panels hit with the same velocities show no such indications of damage. However, C-Scans indicate some damage resulted from the impact.

For each ply orientation, we also notice the impact generates a greater force in less time in the Graphite/Epoxy panels as compared to the Kevlar/Polyester panels. For instance, the maximum load for $[0/90]_{2s}$ Graphite/Epoxy is

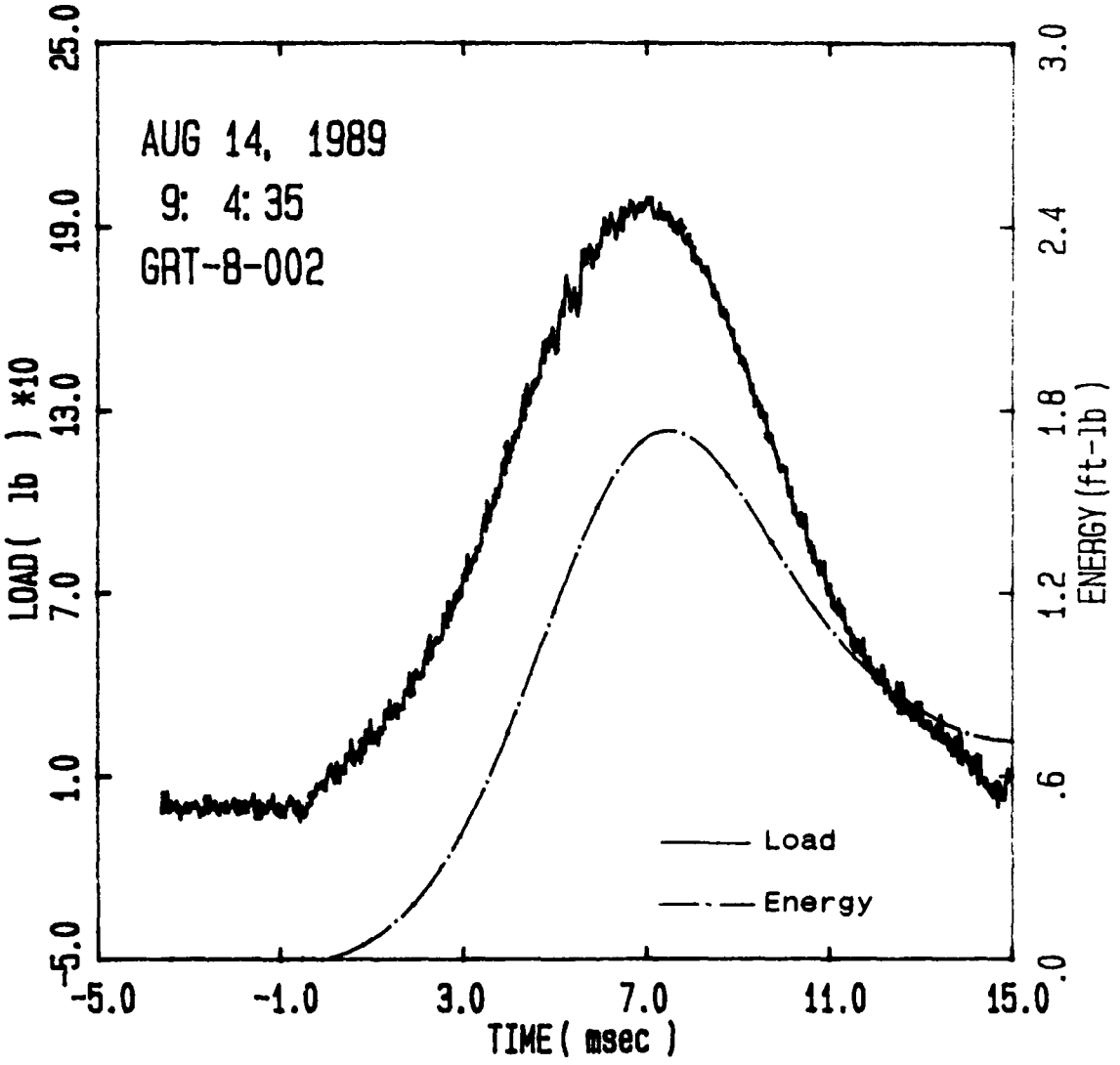

Specimen Id	Temp (f)	Impact Veloc. (ft/sec)	Impact Energy (ft-lb)	Time (msec) Max Ld	Time (msec) Total	Load (lb) Max	Energy (ft-lb) MaxLd	Energy (ft-lb) Total
GRT-8-002	72.	4.29	1.61	7.02	14.70	199.3	1.713	.718

Figure 2.9
Load and Energy vs. Time for $[0/90]_{2s}$ Gr/Ep Panels

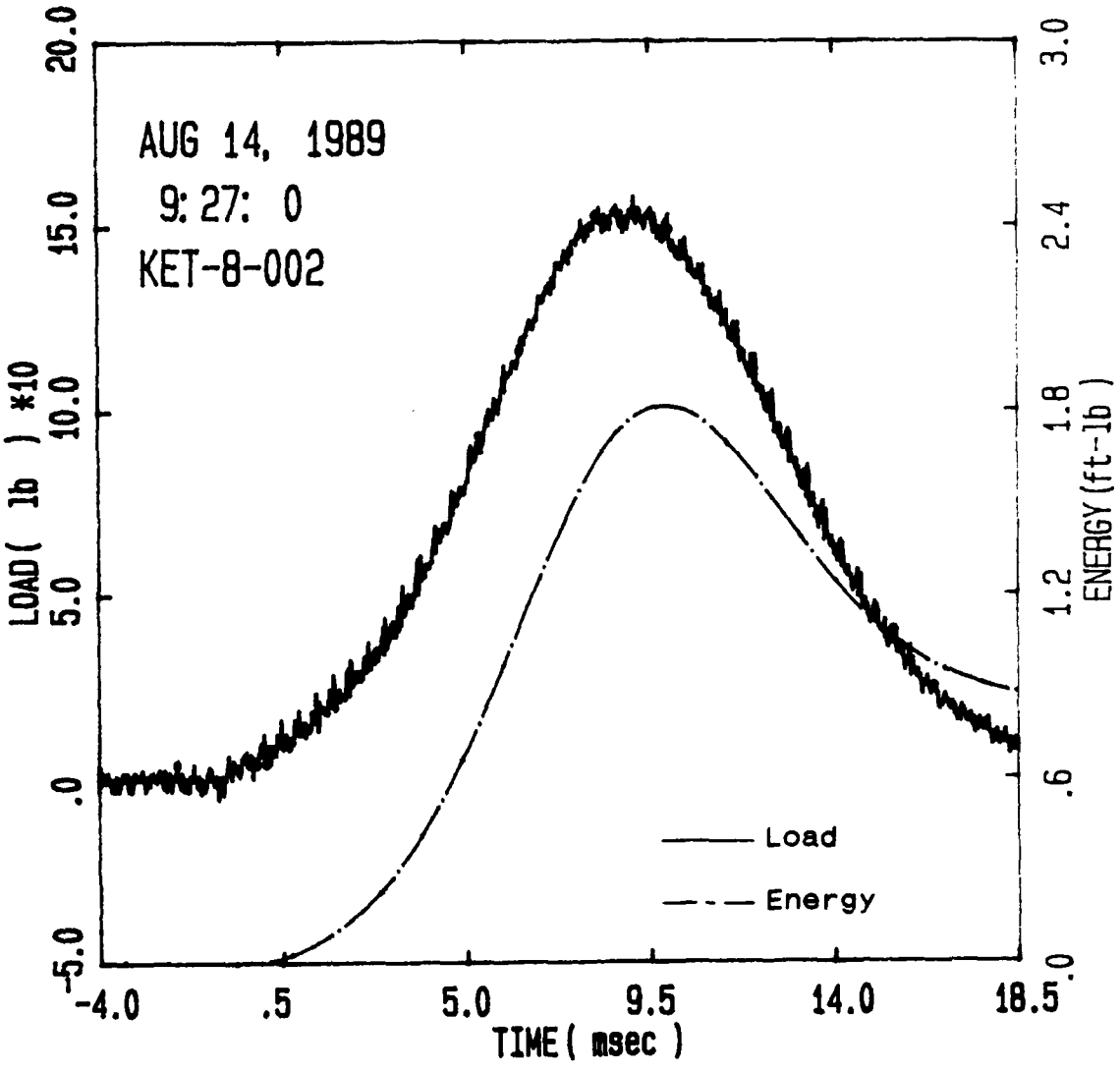

Specimen Id	Temp (f)	Impact Veloc. (ft/sec)	Impact Energy (ft-lb)	Time (msec) Max Ld	Time (msec) Total	Load (lb) Max	Energy (ft-lb) MaxId	Energy (ft-lb) Total
KET-8-002	72.	4.33	1.65	9.13	18.30	157.8	1.779	.882

Figure 2.10
Load and Energy vs. Time for $[0/90]_{2s}$ Kev/Poly Panels

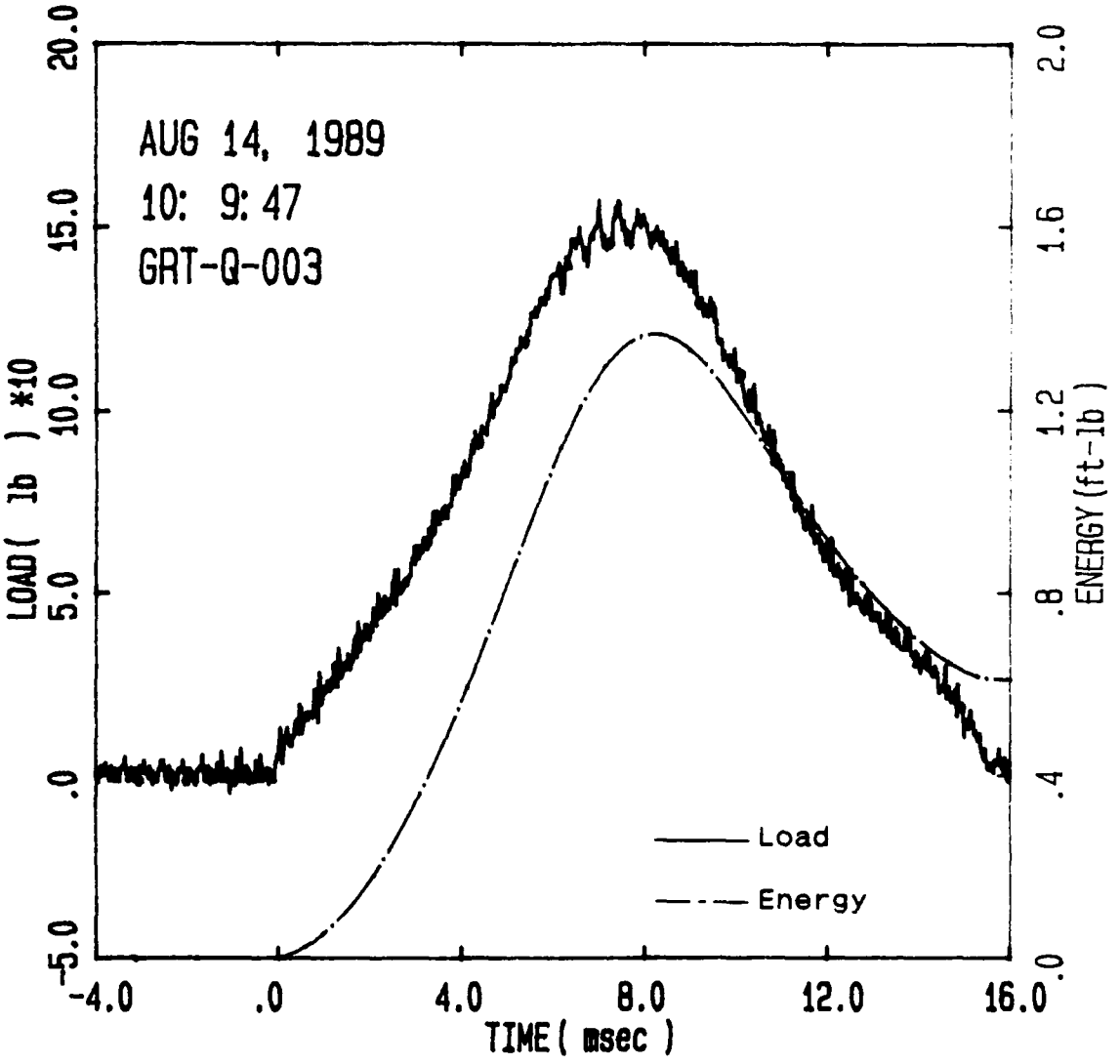

Specimen Id	Temp (f)	Impact Veloc. (ft/sec)	Impact Energy (ft-lb)	Time (msec) Max Ld	Time (msec) Total	Load (lb) Max	Energy (ft-lb) Max Ld	Energy (ft-lb) Total
GRT-Q-003	72.	3.78	1.25	7.00	15.95	157.3	1.278	.609

Figure 2.11
Load and Energy vs. Time for $[\pm 45/90/0]_s$ Gr/Ep Panels

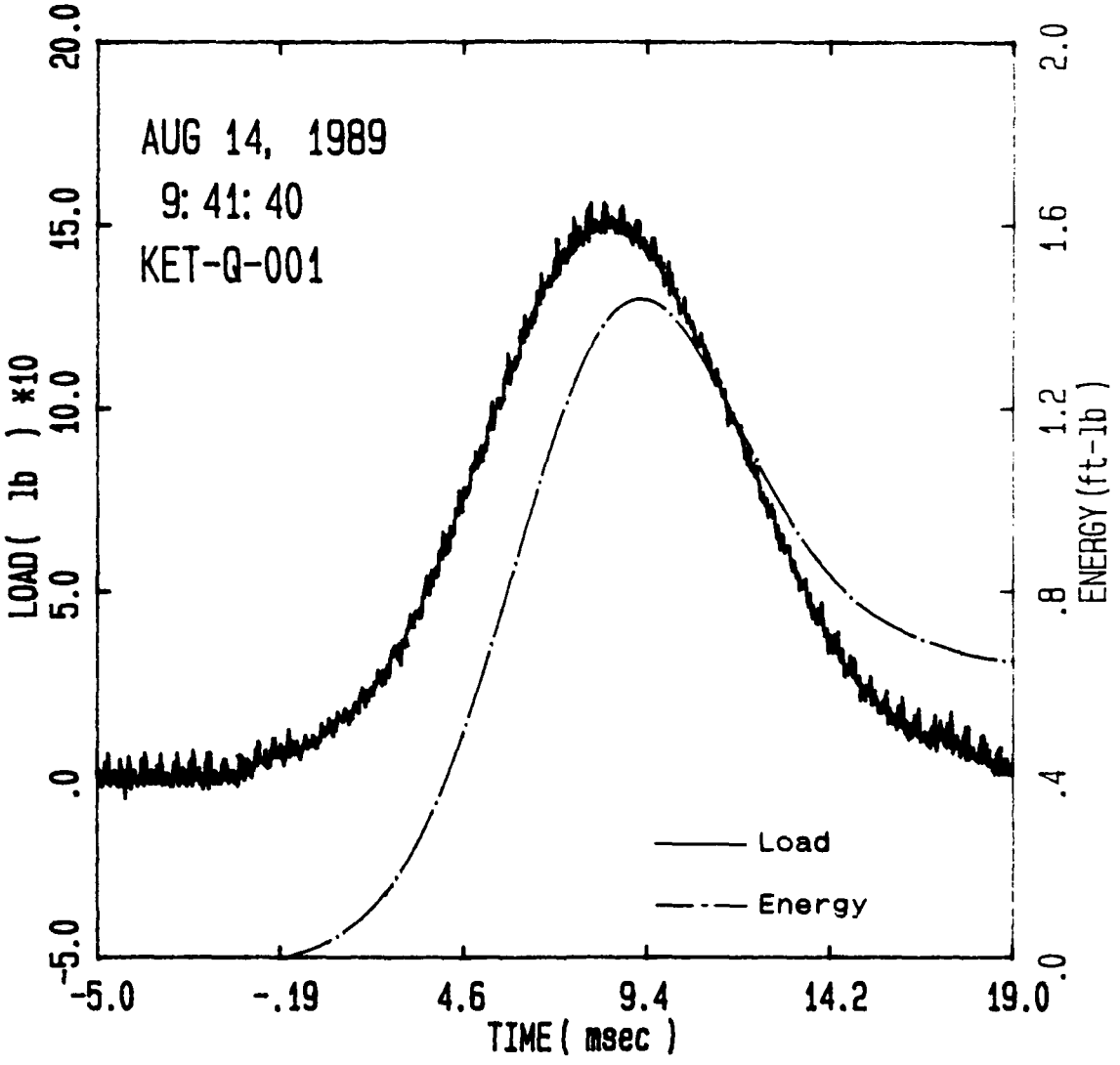

Specimen Id	Temp (f)	Impact Veloc. (ft/sec)	Energy (ft-lb)	Time (msec) Max Ld	Time (msec) Total	Load (lb) Max	Energy (ft-lb) Max Ld	Energy (ft-lb) Total
KET-Q-001	72.	3.85	1.30	7.93	18.55	156.1	1.337	.651

Figure 2.12
Load and Energy vs. Time for $[\pm 45/90/0]_s$ Kev/Poly Panels

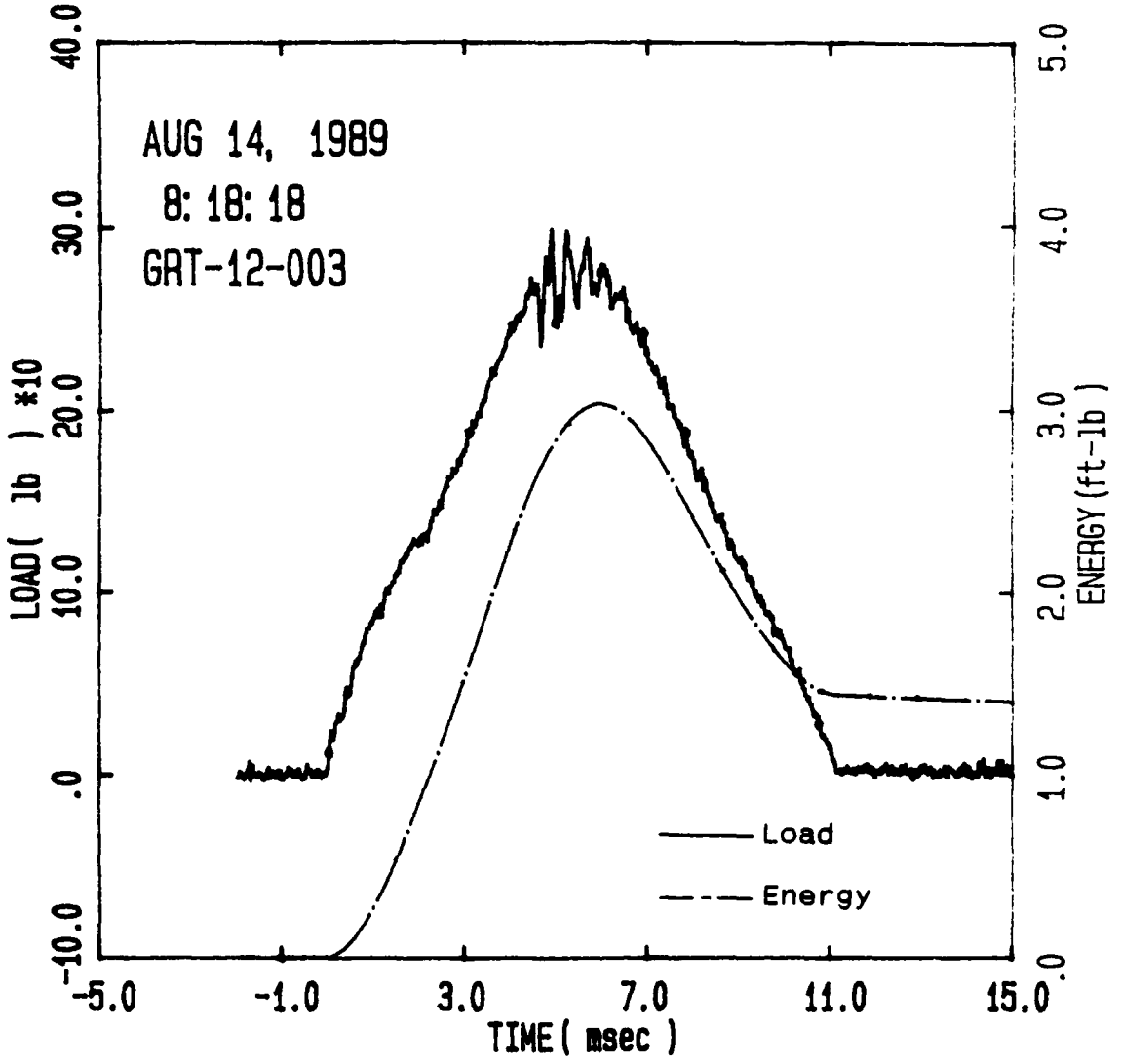

Specimen Id	Temp (f)	Impact Veloc. (ft/sec)	Impact Energy (ft-lb)	Time (msec) Max Ld	Time (msec) Total	Load (lb) Max	Energy (ft-lb) Max Id	Energy (ft-lb) Total
GRT-12-003	72.	5.77	2.92	4.90	12.00	208.8	2.809	1.429

Figure 2.13
Load and Energy vs. Time for $[0/90]_{3s}$ Gr/Ep Panels

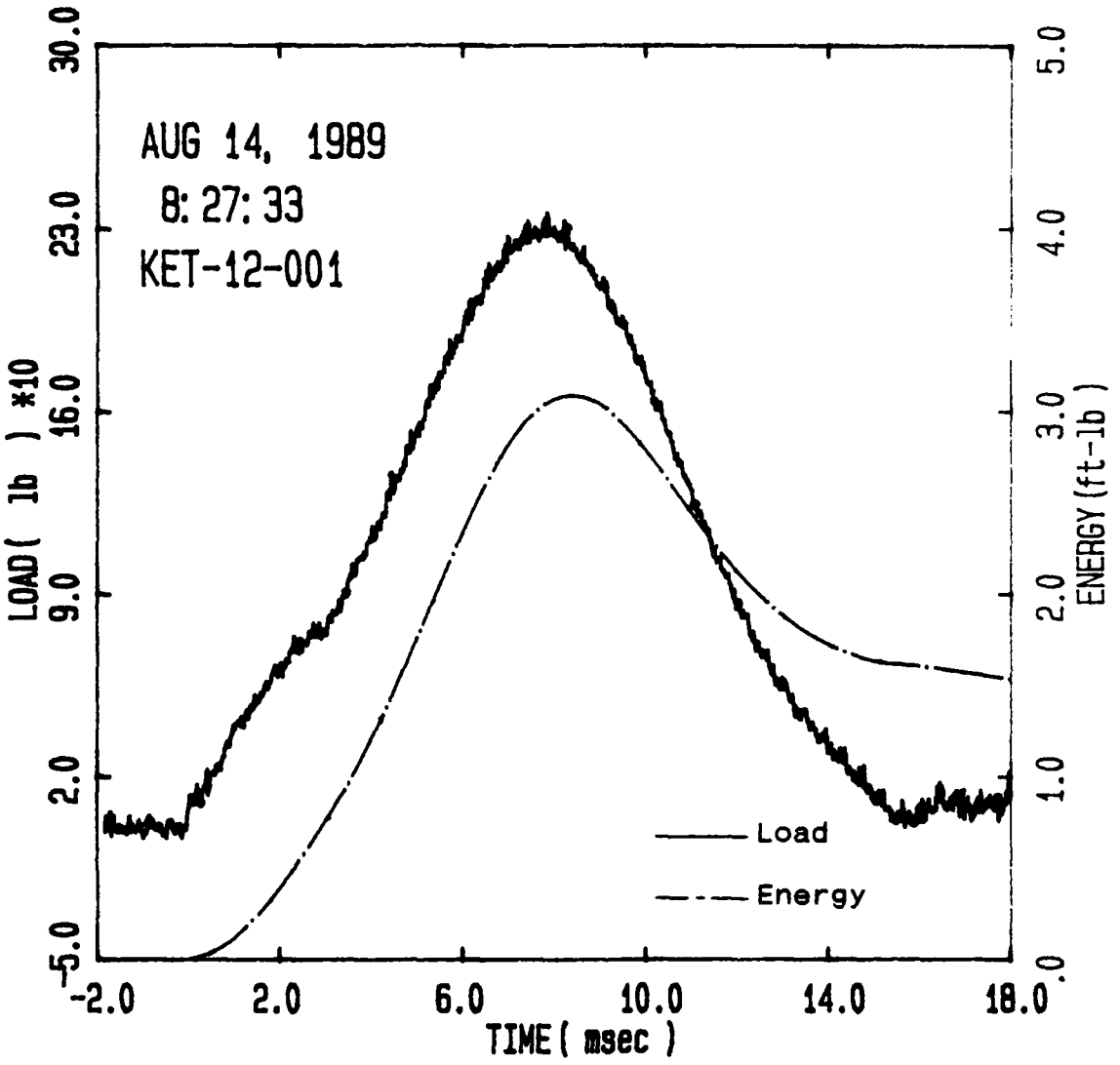

Specimen Id	Temp (f)	Impact Veloc. (ft/sec)	Energy (ft-lb)	Time (msec) Max Ld	Time (msec) Total	Load (lb) Max	Energy (ft-lb) MaxId	Energy (ft-lb) Total
KET-12-001	72.	5.76	2.91	7.85	18.18	236.3	3.059	1.528

Figure 2.14

Load and Energy vs. Time for $[0/90]_{3s}$ Kev/Poly Panels

199.3 lbs and occurs at 7.02 msec. For a $[0/90]_{2s}$ Kevlar/Polyester panel, the maximum load is 157.8 lbs occurring at 9.13 msec. The Kevlar/Polyester panel dissipates some of the energy by deflecting more because it is more flexible. This greater deflection shows up in the greater amount of time required for the panel to reach the peak load.

Compression Testing Procedure

The test fixture used to compress the panels, shown in Figure 2.15, was provided by the Air Force Flight Dynamics Laboratory. The panel is placed into the fixture between the top and bottom plates with the top and bottom curved edges of the panel clamped. The vertical edges are restrained by a simple support knife edge. The clamped edge condition is achieved by placing a series of six 1/2" steel chucks along the top and bottom edges. The edges of the chucks have a 12" radius of curvature so that they butt evenly against the panel. Each chuck is held in place by two set screws. See Reference [1] for a more complete description of the compression fixture. Mathematically, the boundary conditions are

Top edge:	$u=\text{free};\quad v=w=w_{,x}=w_{,y}=0$
Bottom edge:	$u=v=w=w_{,x}=w_{,y}=0$
Vertical edges:	$u=w_{,x}=\text{free};\quad v=w=w_{,y}=0$

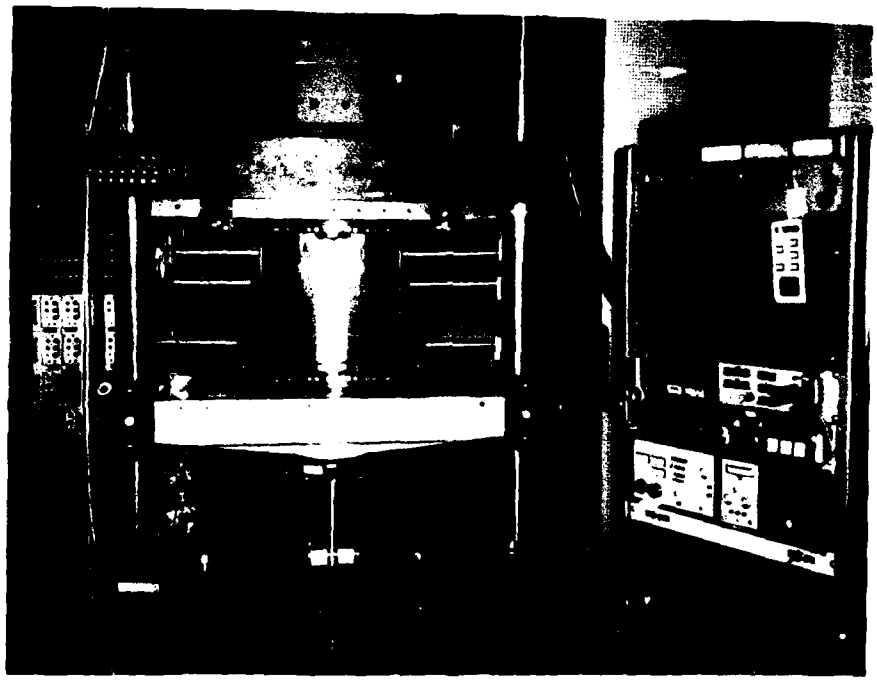

Figure 2.15 - Curved Panel Compression Fixture

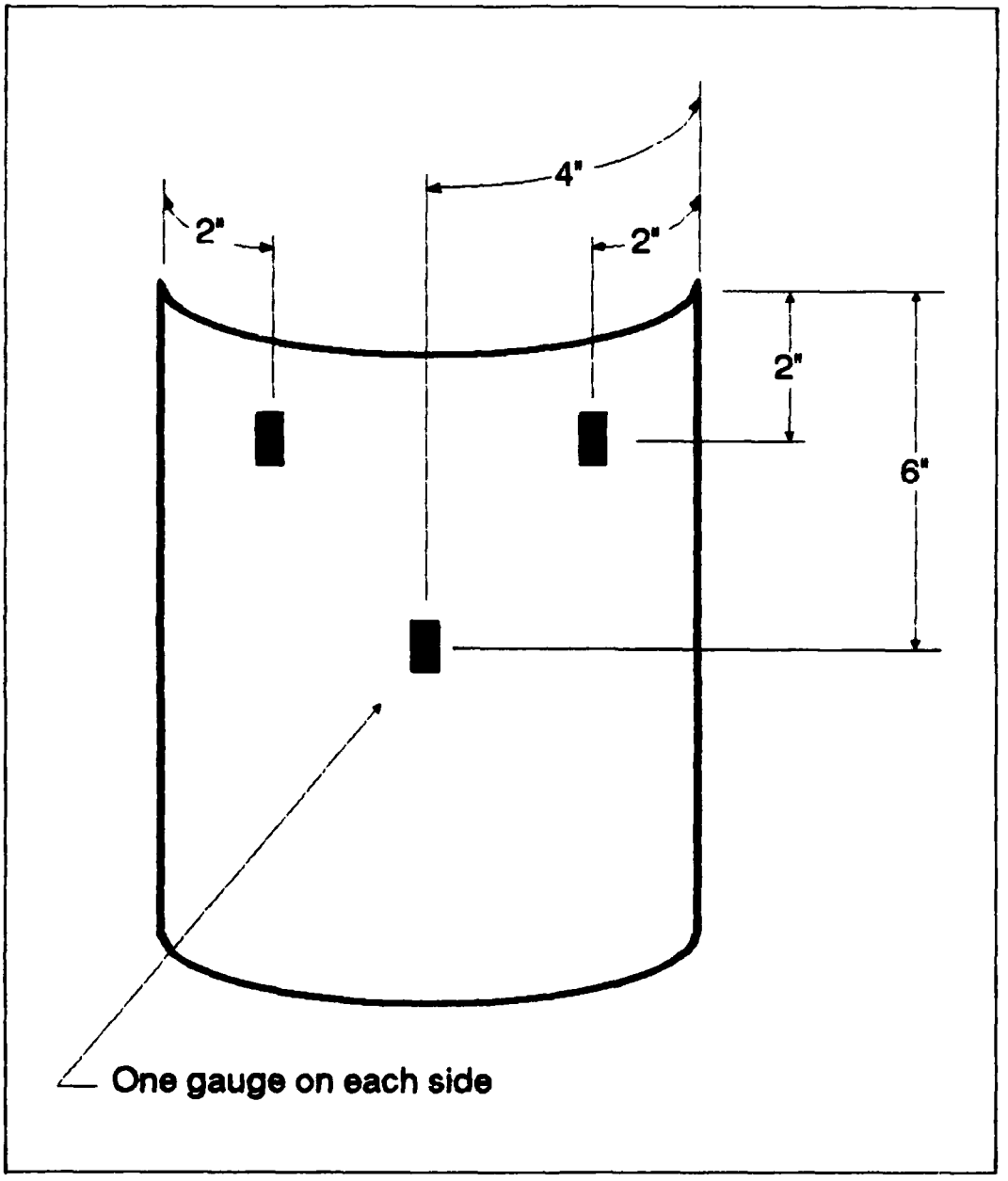

Figure 2.16 - Strain Gauge Placement

As the panel is compressed, a load cell measures the total load applied to the top edge while a LVDT (Linear Variable Differential Transformer) measures the vertical axial displacement, u. Additionally, unidirectional strain gauges were mounted on each panel as shown in Figure 2.16. The two strain gauges near the top edge of the panel provide information to insure the load is being applied as evenly as possible across the top edge. The two strain gauges in the center of the panel (placed back to back) measure the strain reversal that occurs when the panel buckles.

After a panel is placed in the fixture, the 1/2" chucks and vertical knife edges are loosely set in place. A preload of approximately 200 lbs for Graphite/Epoxy panels (100 lbs for Kevlar/Polyester panels) is applied. The preload makes sure the top and bottom edges of the panel are flush against the base plates. The support bolts and set screws are then tightened finger tight. The preload is then eased to approximately 100 lbs for Graphite/Epoxy panels (50 lbs for Kevlar/Polyester panels) and the support bolts and set screws tightened with a wrench and screwdriver. This preload procedure prevents movement of the panel before it begins to take on the load.

Once the preload procedure is complete, the panels are loaded in compression. A uniform displacement of 0.05 inches/minute is applied to the top edge with a load cell

measuring the resulting force and the vertical LVDT measuring the top edge displacement.

The load is applied until the panels buckle. For the Graphite/Epoxy panels, a loud "pop" can be heard when the panels snap into their buckled shape. For the Kevlar/Polyester panels, no "pop" was heard due to the greater flexibility of the material. The movement of the panel as it buckles is not as quick, thus it becomes more difficult to distinguish the buckling load. As a result, the output from the load cell was monitored and the test stopped when the load began to decrease. The maximum load observed was called the buckling load. Once the buckling load was determined, the test was stopped, the load removed, and the panel removed from the test fixture.

Compression of Panels

Three undamaged Graphite/Epoxy and three undamaged Kevlar/Polyester panels of each ply orientation were compressed to establish the baseline strength of the panels. The loads measured will be used for comparison purposes to determine how the impact damage weakens the panels. Table 2.3 summarizes the collapse loads of the undamaged panels.

Table 2.3
Collapse Loads of Undamaged Panels

		$[0/90]_{2s}$	$[\pm 45/90/0]_{s}$	$[0/90]_{3s}$
Load (lbs)	Gr/Ep	2802	3551	7667
	Kev/Pol	813	1103	2408

Three Graphite/Epoxy and three Kevlar/Polyester panels of each ply orientation were impacted with the energies shown in Table 2.2 using the procedures described earlier. These panels were then compressed to determine the residual strength of the panels. The residual strengths are summarized in Table 2.4.

Table 2.4
Collapse Load of Damaged Panels

		$[0/90]_{2s}$	$[\pm 45/90/0]_{s}$	$[0/90]_{3s}$
Load (lbs)	Gr/Ep	2750	3359	7492
	Kev/Pol	769	1118	2346

Comparing the values in Tables 2.3 and 2.4, the damaged panels were 2-6% weaker than the undamaged panels. The only exception is the $[\pm 45/90/0]_{s}$ Kevlar/Polyester panels. The average strength of the damaged panels was 15 lbs greater than that of the undamaged panels. One should not infer from this that this particular panel becomes stronger after

it is impacted. Recall, the values in Tables 2.3 and 2.4 were based on a sample of three panels. One must also keep in mind the relative insensitivity of the compression fixture alluded to earlier. And, there is always a certain amount of experimental scatter to live with. Thus, the results of this test for $[\pm 45/90/0]_s$ Kevlar/Polyester panels should be interpreted as the impact energy used having little or no effect on the panel's compressive strength. However, ultrasonic C-scans of the damaged panels taken after the one time compression load showed the damaged area in the panel had spread. The damaged area before the compression test was approximately 1/2" in diameter. After the compression testing of the damaged panels, the damaged area of the Graphite/Epoxy panels did not grow appreciably, while the damaged area of the Kevlar/Polyester panels grew to approximately 1-1/4" to 2" in diameter, depending on the ply orientation. It would be reasonable to assume that if the panels were loaded in compression again, they would buckle at lower loads than shown in Table 2.4.

The results of this experimentation tend to verify Wilder's technique [1] of implanting teflon inserts to simulate impact damage. His results showed a decrease in global strength of 13.2% for a quasi-isotropic ply orientation. One must bear in mind that Wilder's technique would only give one an idea of the global behavior of the panel. Near the impacted region, the behavior may be quite

different. In an impacted panel, the damaged area may still have some strength left in it depending on the amount of energy imparted to the panel. The teflon inserts Wilder used provides a totally debonded region. Thus, the teflon insert technique would tend to yield a conservative estimate of an impact damaged panel's global response to compression.

Figures 2.17-2.22 show plots comparing load vs. in-plane displacement, u, for damaged and undamaged panels of each material and ply orientation used to generate Tables 2.3 and 2.4. In each case, little difference in the stiffness of the damaged panels can be seen compared to the undamaged panels. Only the collapse load differs.

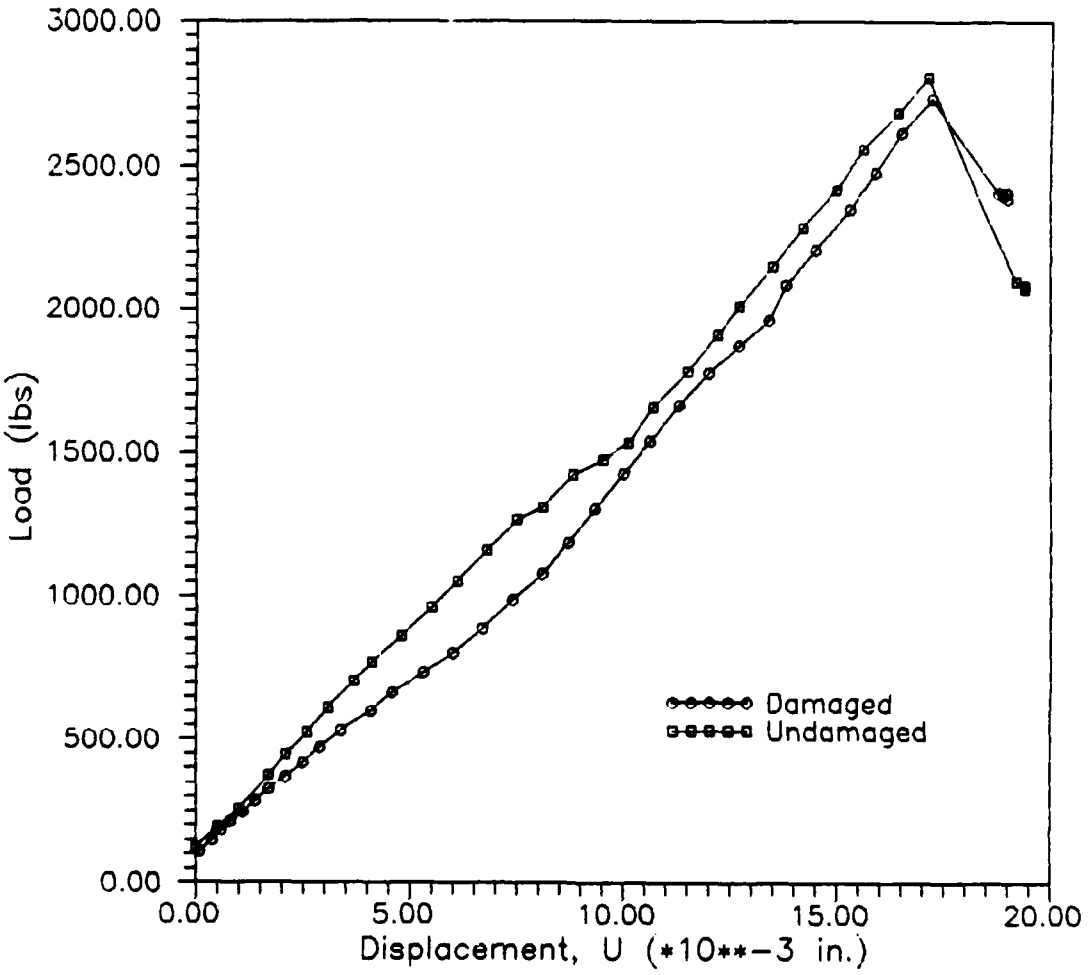

Figure 2.17
Load vs. Displacement for $[0/90]_{2s}$ Gr/Ep
Damaged and Undamaged Panels
(Impact Energy = 1.52 ft-lb)

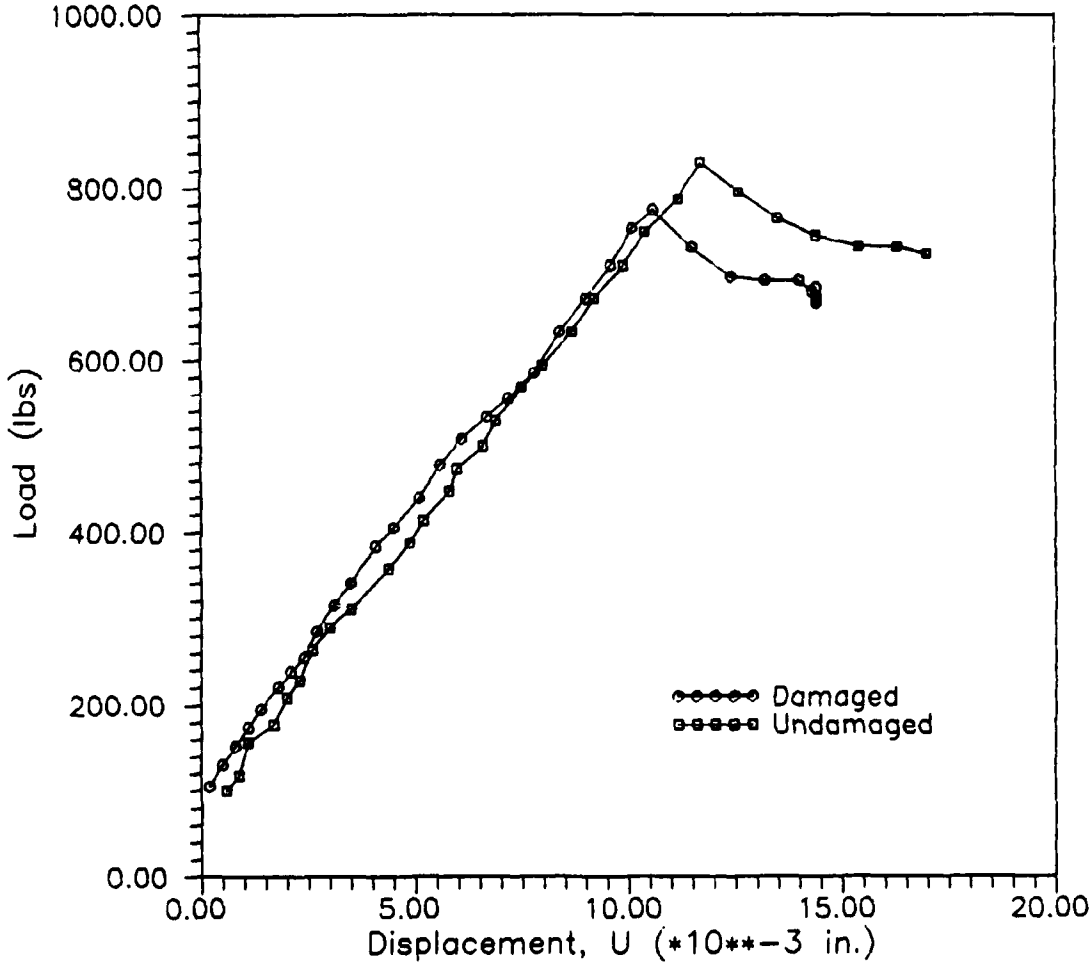

Figure 2.18
Load vs. Displacement for $[0/90]_{2s}$ Kev/Poly
Damaged and Undamaged Panels
(Impact Energy = 1.52 ft-lb)

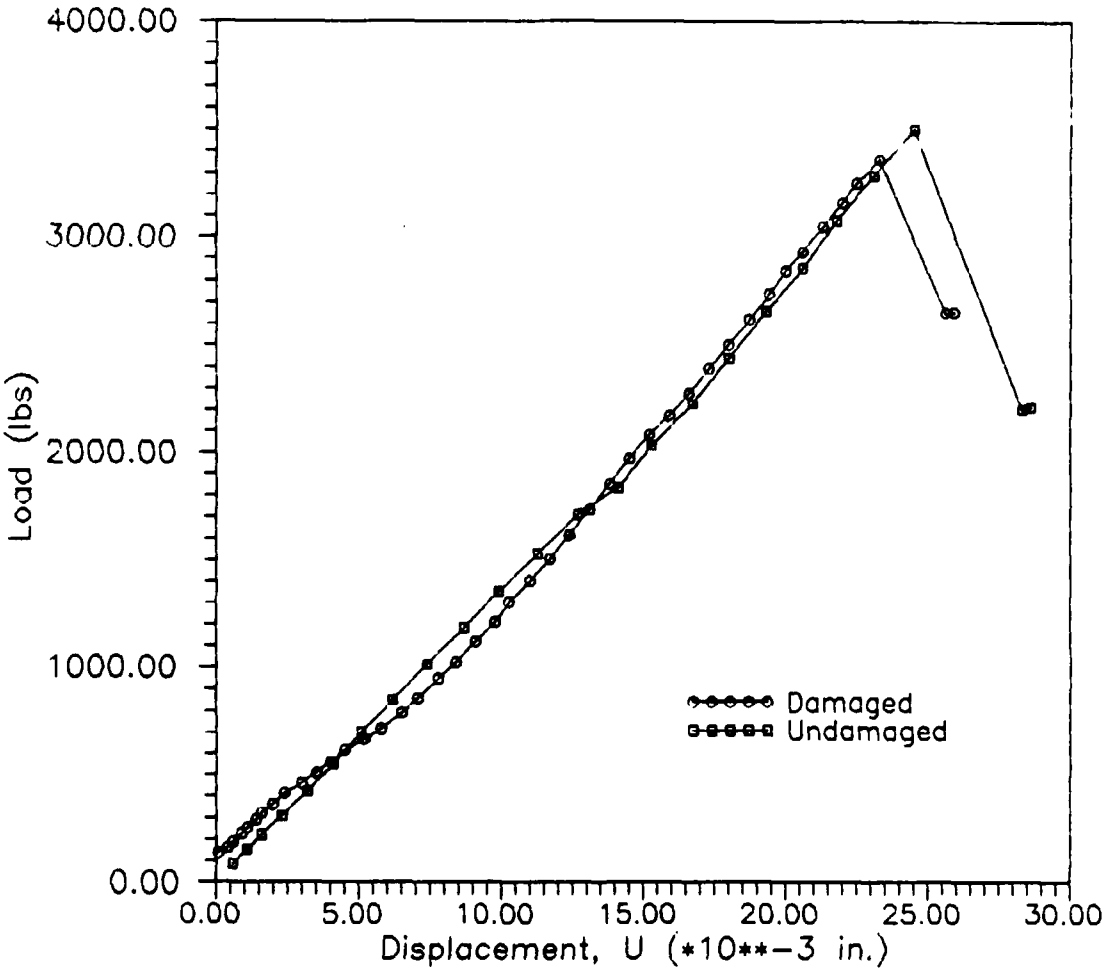

Figure 2.19
Load vs. Displacement for $[\pm 45/90/0]_s$ Gr/Ep
Damaged and Undamaged Panels
(Impact Energy = 1.19 ft-lb)

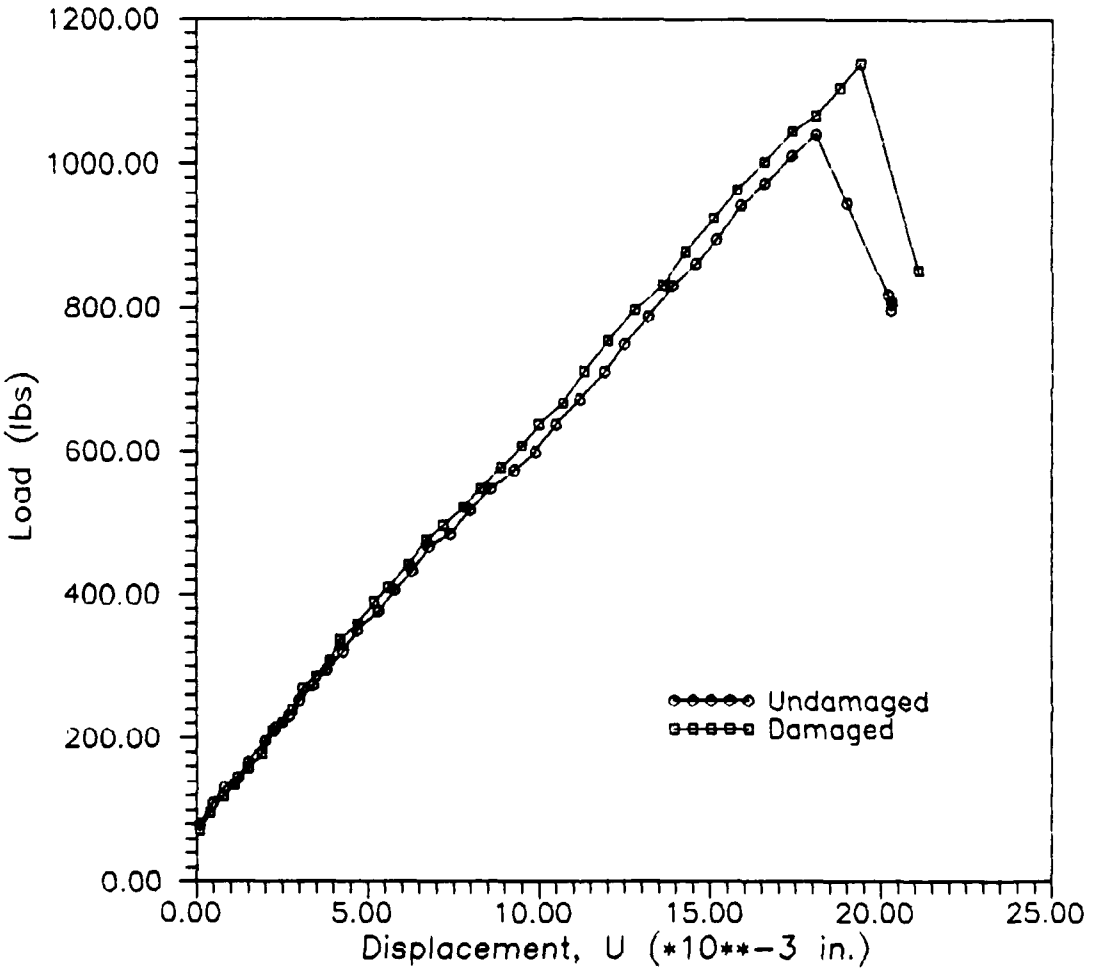

Figure 2.20
Load vs. Displacement for $[\pm 45/90/0]_s$ Kev/Poly
Damaged and Undamaged Panels
(Impact Energy = 1.19 ft-lb)

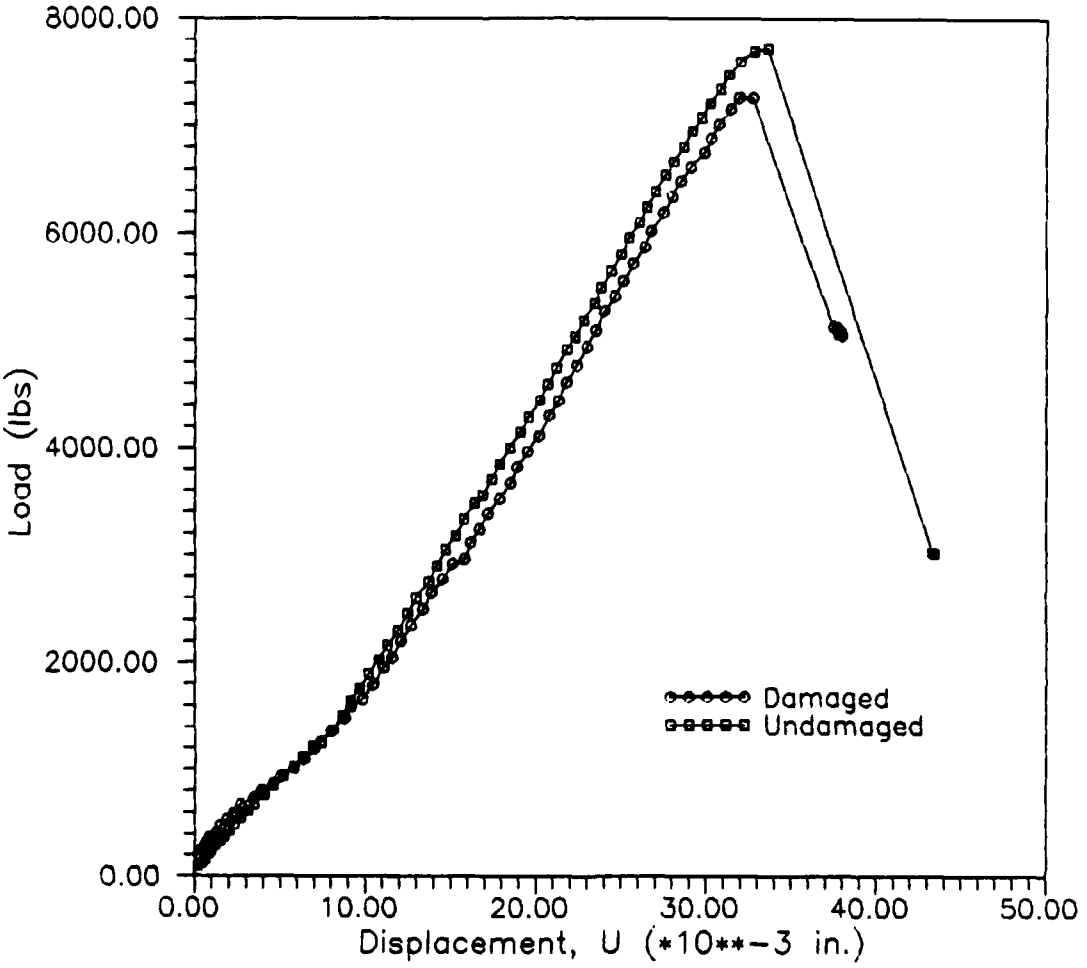

Figure 2.21
Load vs. Displacement for $[0/90]_{3s}$ Gr/Ep
Damaged and Undamaged Panels
(Impact Energy = 2.92 ft-lb)

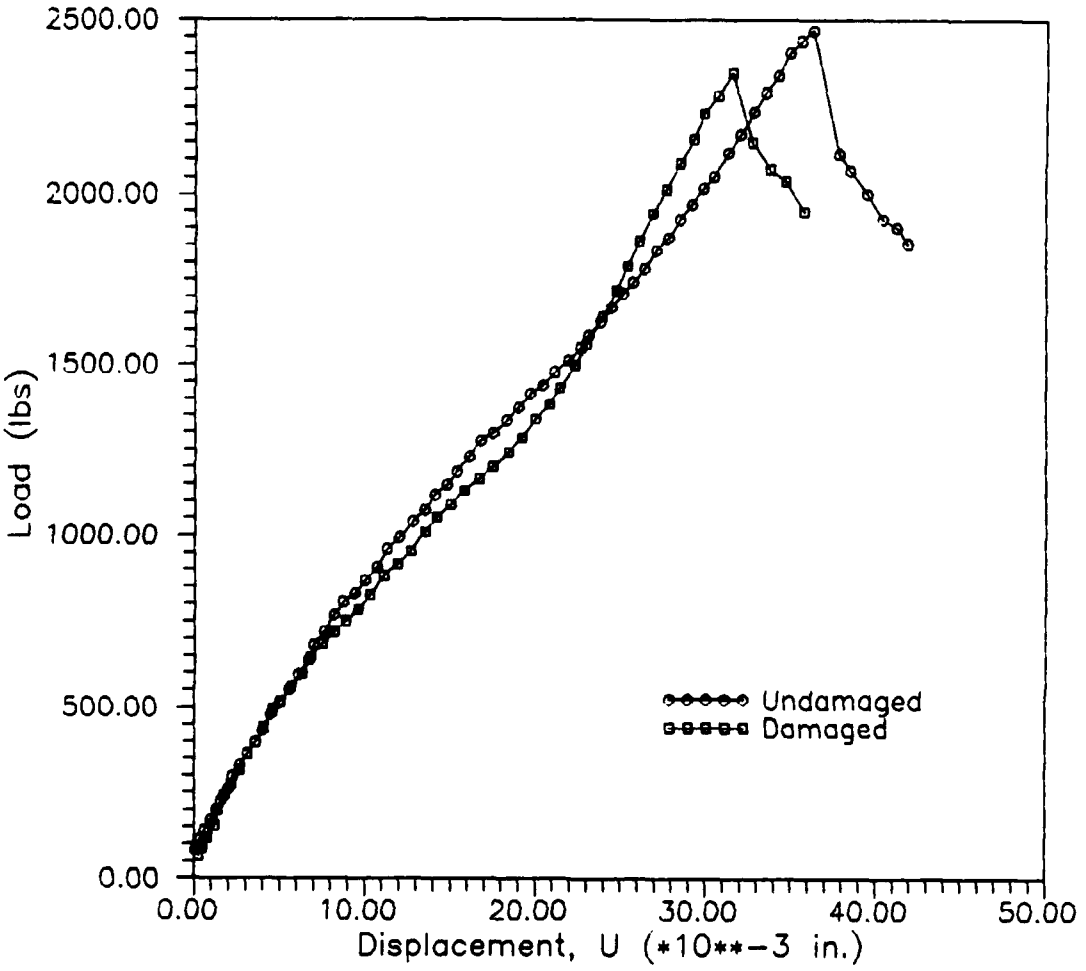

Figure 2.22
Load vs. Displacement for $[0/90]_{3s}$ Kev/Poly
Damaged and Undamaged Panels
(Impact Energy = 2.92 ft-lb)

3. DAMAGE CHARACTERIZATION

In this chapter, we take a closer look at the damage sustained by the panels from a low velocity impact. First, stereo X-rays were taken of the Graphite/Epoxy panels used to determine the minimum impact energy to cause damage. Second, a series of photographs and ultrasonic C-Scans were taken of Graphite/Epoxy and Kevlar/Polyester panels impacted with velocities ranging from 9.62-13.89 ft/sec (energies of 7.96-16.57 ft-lb). We therefore get an idea of what happens as the impact energy increases. Lastly, $[0/90]_{2s}$ Graphite/Epoxy, $[0/90]_{2s}$ Kevlar/Polyester, $[\pm 45/90/0]_{s}$ Graphite/Epoxy, and $[\pm 45/90/0]_{s}$ Kevlar/Polyester panels were cross-sectioned through the impact point and viewed under a microscope. This shows the damage through the thickness of the panel.

Stereo X-ray of Panels

Stereo X-rays provide a way of getting three-dimensional information on a damaged composite by combining two images taken at slightly different angles into one apparent three-dimensional image. The three-dimensional image is produced much the same way the human eye perceives it. Each eye sees an image at a slightly different angle due to the separation between the eyes. The brain then

merges the two images together to form a three-dimensional image.

For this thesis, the stereo X-rays were prepared as follows [15]. A 1/8" hole was drilled in the damaged area of the panel to allow a dye penetrant, tetrabromoethane (TBE), to soak into the damaged area via capillary action. The TBE provides a color contrast between the damaged and undamaged areas of the panel. Next, film is placed behind the panel and exposed by using an X-ray tube. Two exposures are taken at $\pm 15^{\circ}$ on either side of a plane perpendicular to the panel (see Figure 3.1). These two images may be recombined by using a "stereo viewer" to obtain a three-dimensional view of the damaged area.

Figures 3.2-3.4 are photographs of the X-rays for the minimum damage of each type of Graphite/Epoxy panel. In each figure, some damage to the fibers as well as some cracking of the fibers and matrix can be seen. The figures also show the extent and shape of the delamination that occurs. It is not very easy to pick out of the photographs by eye, but under the stereo viewer, one can see the delamination occurring at several different layers through the thickness of the panel. We only get a feel of relative positioning though. It is still difficult to pinpoint between which two plies the delaminations actually occur.

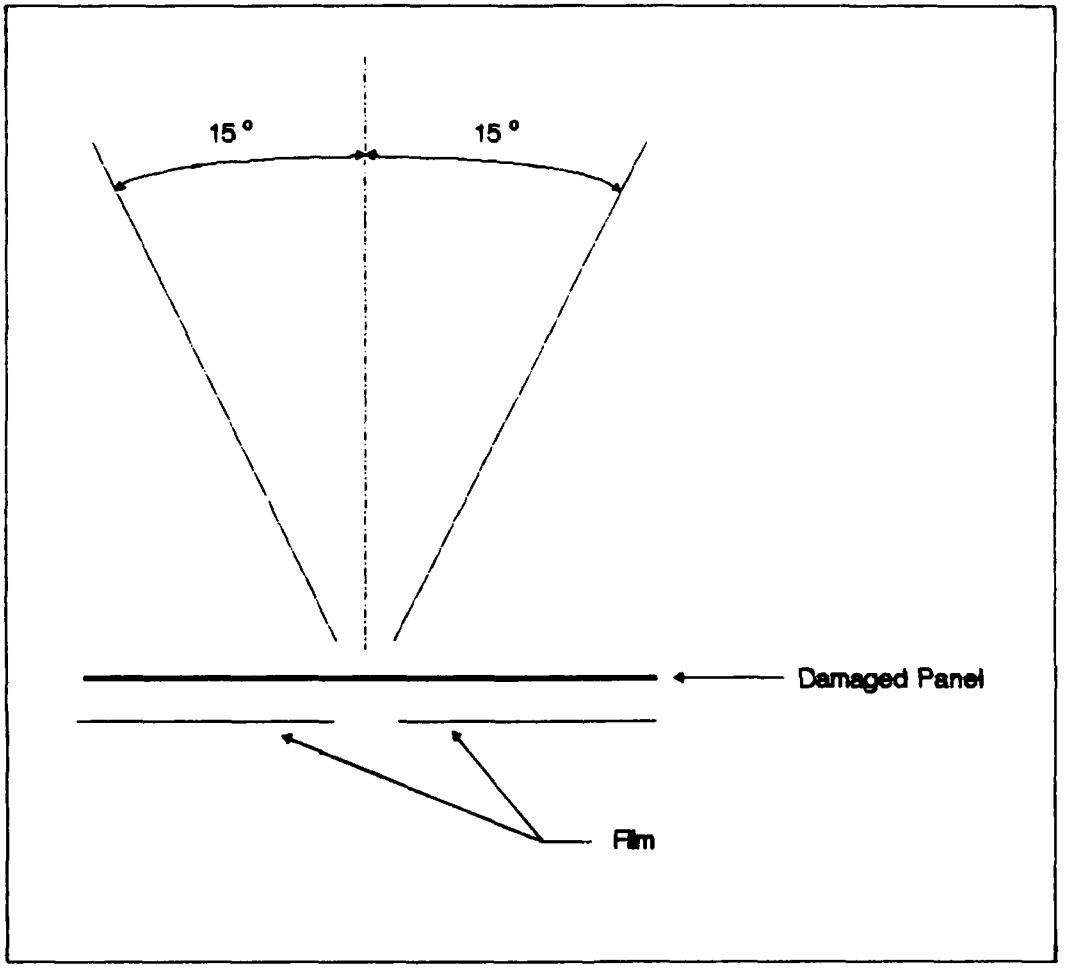

Figure 3.1 - Stereo X-Ray Geometry

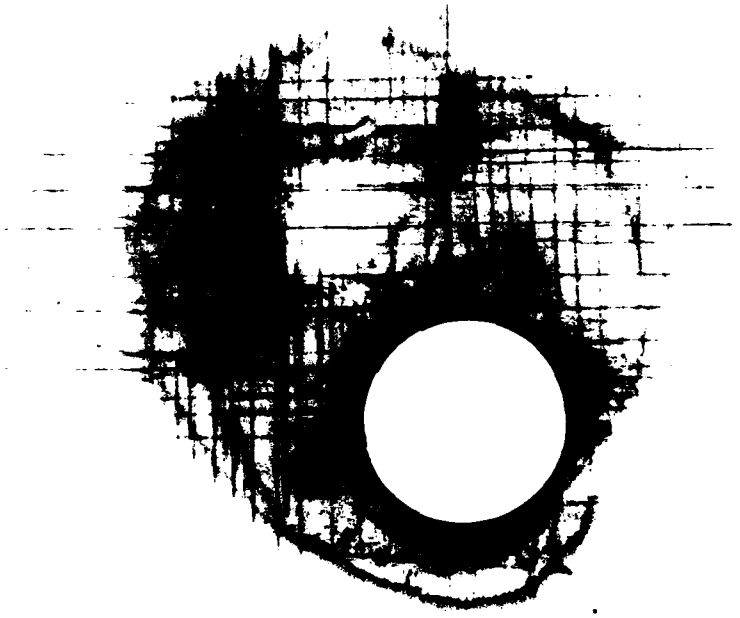

Figure 3.2
Stereo X-Ray of $[0/90]_{2s}$ Gr/Ep Impacted Panel
(Impact Energy = 1.27 ft-lb)

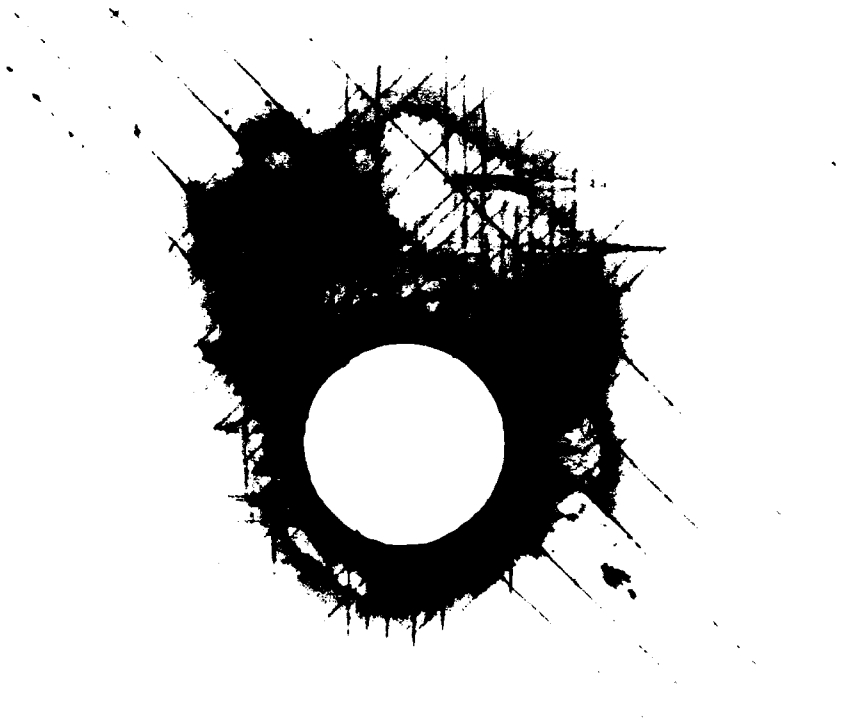

Figure 3.3
Stereo X-Ray of $[\pm 45/90/0]_s$ Gr/Ep Impacted Panel
(Impact Energy = 0.99 ft-lb)

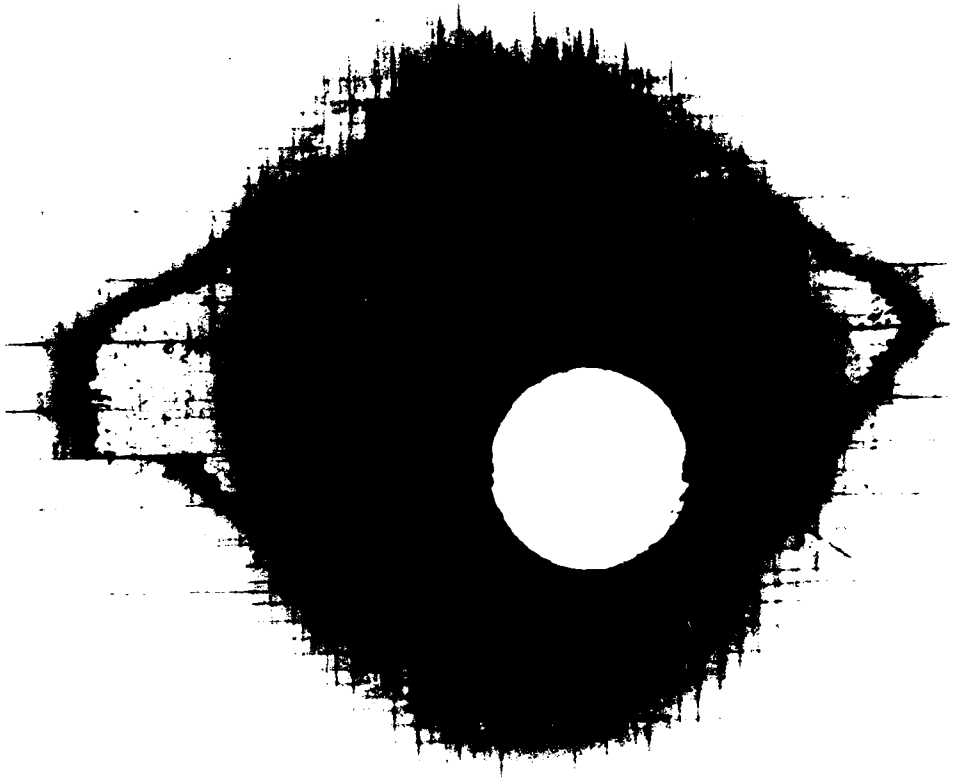

Figure 3.4
Stereo X-Ray of $[0/90]_{3s}$ Gr/Ep Impacted Panel
(Impact Energy = 2.46 ft-lb)

Photographs and C-Scans of Panels

In this phase of testing, Graphite/Epoxy and Kevlar/Polyester panels were impacted with increasing velocities and C-Scanned. By doing this, we can track how the damage spreads as the energy imparted to the panel increases.

We begin by considering $[0/90]_{2s}$ Graphite/Epoxy panels impacted with velocities ranging from 9.62-12.68 ft/sec. Figures 3.5-3.7 shows the impacted side, a C-Scan of the internal damage, and the back side of Graphite/Epoxy panels impacted at 9.62 ft/sec, 11.34 ft/sec, and 12.68 ft/sec respectively. As seen from the C-Scans, the internal damage increases as the impact velocity increases. The damage occurs in the form of a circular region at the point of impact and is approximately the same diameter as the impactor (1/2"). Additionally, two triangular regions are damaged on each side of the impact point in the circumferential direction. Since the impactor is hemispherical, one would not expect any directional preference of the damage. However, the curvature of the panel seems to dictate the direction of the damage. This also helps to explain the fiber splitting and fracture that occurs on the back side of the panel. Locally, the panel undergoes a high concentration of bending and tension. The panel is able to deflect circumferentially, but since it is

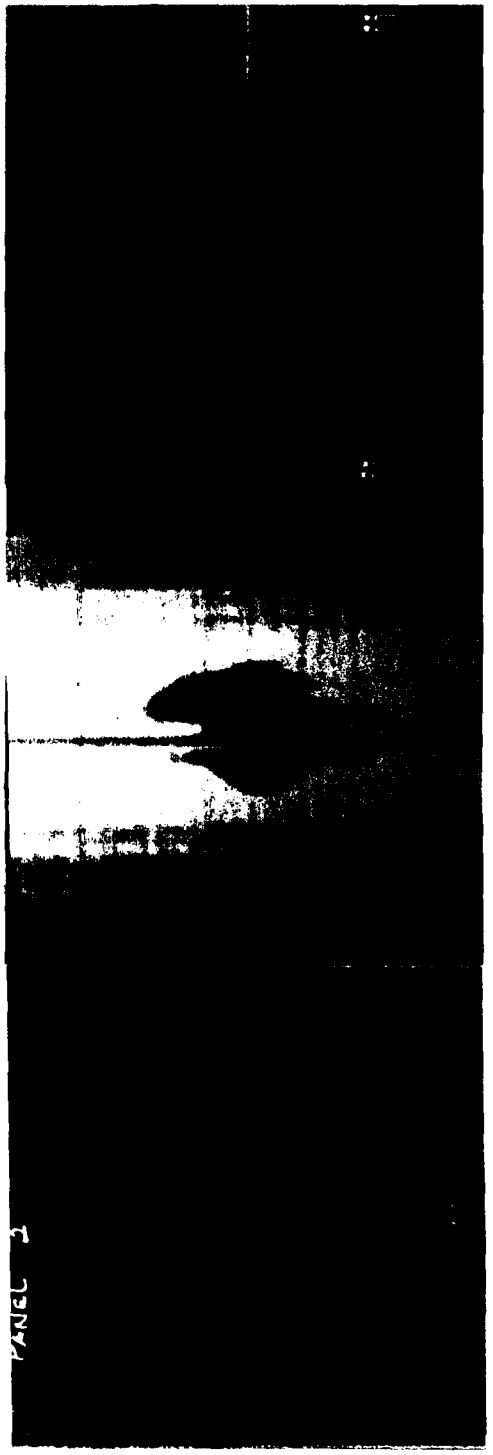

Figure 3.5 - Impacted $[0/90]_{2s}$ Gr/Ep Panel
(Velocity = 9.62 ft/sec; Impact Energy = 7.96 ft-lb)
(a) Impacted Side (b) C-Scan (c) Back Side

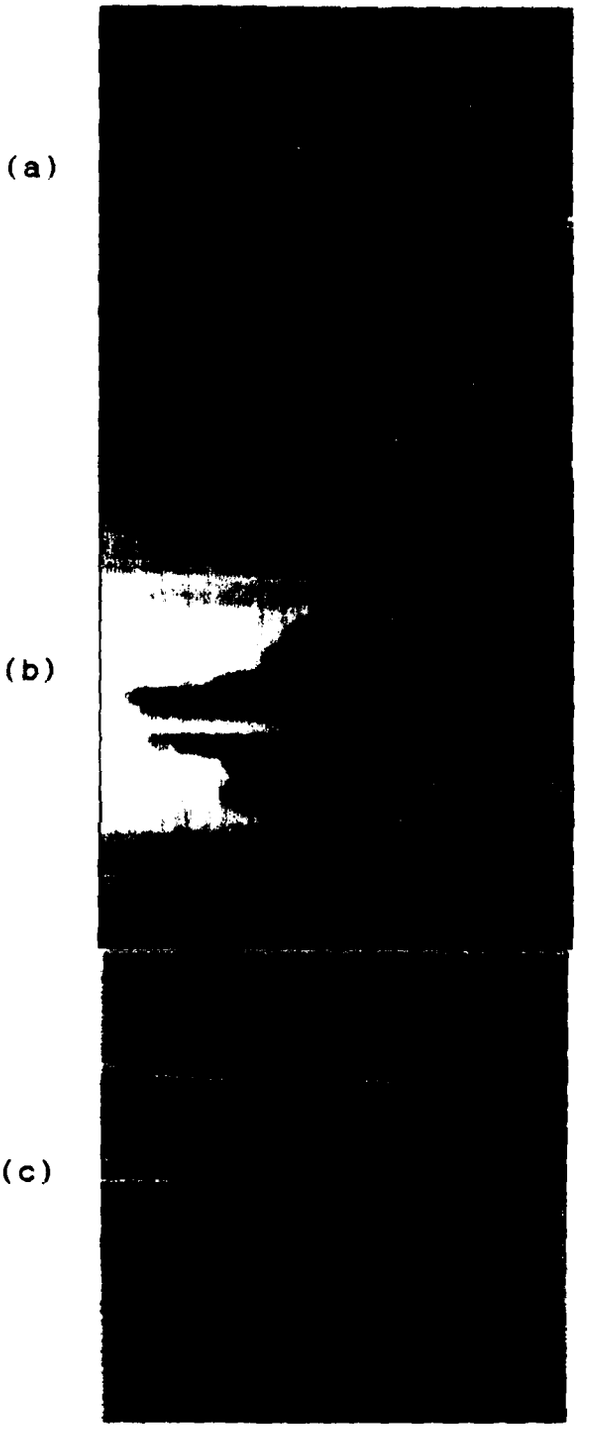

Figure 3.6 - Impacted $[0/90]_{2s}$ Gr/Ep Panel
(Velocity = 11.34 ft/sec; Impact Energy = 11.06 ft-lb)
(a) Impacted Side (b) C-Scan (c) Back Side

(a)

(b)

(c)

Figure 3.7 - Impacted $[0/90]_{2s}$ Gr/Ep Panel
(Velocity = 12.68 ft/sec; Impact Energy = 13.77 ft-lb)
(a) Impacted Side (b) C-Scan (c) Back Side

much stiffer longitudinally, the fibers break in response to the contact force created by the impact.

In Figures 3.8-3.10 we look at $[0/90]_{2s}$ Kevlar/Polyester panels impacted with the same velocities as the equivalent Graphite/Epoxy panels. The C-Scans show the damage growing in the circumferential direction as the impact velocity increases, just as for Graphite/Epoxy. The width of the damaged area remains approximately the diameter of the impactor. We do notice something different about the Kevlar/Polyester panels however. As the velocity increases from 11.34 ft/sec to 12.68 ft/sec, the shape of the internal damage becomes more circular. It appears as if the type or shape of damage that occurs depends on the impact velocity (or possibly energy). As the velocity increases, the damage to the back side changes from a slit where the fibers fracture to a cross where the fibers fracture in both directions. Also, we notice some damage occurring along diagonals extending from the impact point to the corners where the panel is supported by the support block and cover plate. A permanent indentation remains as a result of the impact. It appears that as a result of the transverse displacement, the material stretched, causing damage along the lines described.

Figure 3.11 shows a $[\pm 45/90/0]_s$ Graphite/Epoxy panel impacted with a velocity of 9.82 ft/sec. Only one panel of this type was available for testing, therefore no real

Figure 3.8 - Impacted $[0/90]_{2s}$ Kev/Poly Panel
(Velocity = 9.62 ft/sec; Impact Energy = 7.96 ft-lb)
(a) Impacted Side (b) C-Scan (c) Back Side

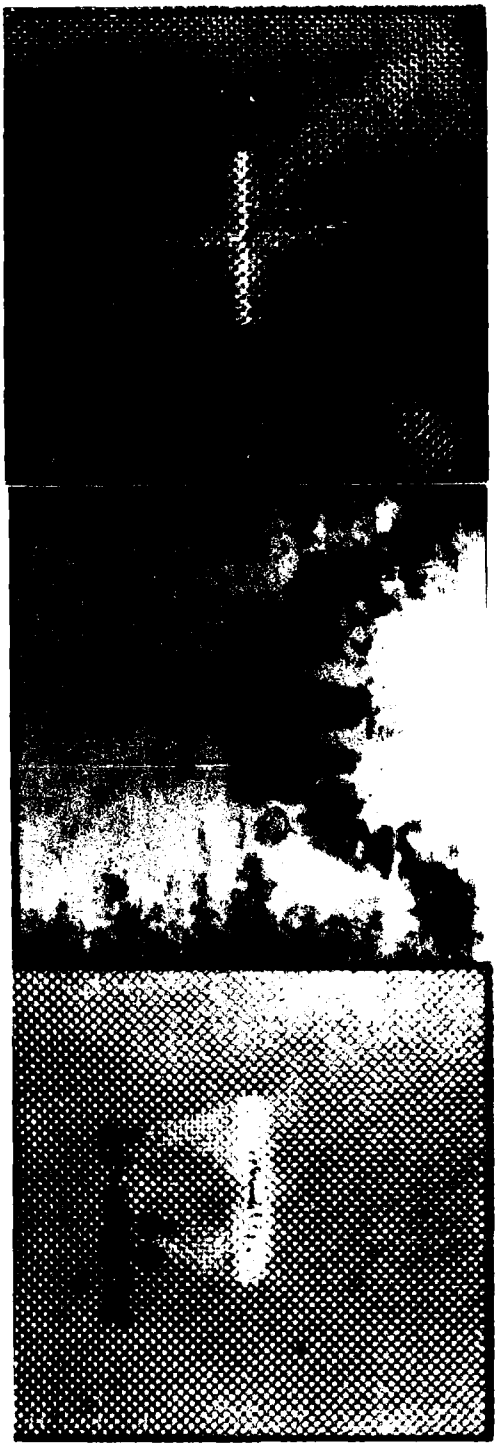

Figure 3.9 - Impacted $[0/90]_{2s}$ Kev/Poly Panel
(Velocity = 11.34 ft/sec; Impact Energy = 11.06 ft-lb)
(a) Impacted Side (b) C-Scan (c) Back Side

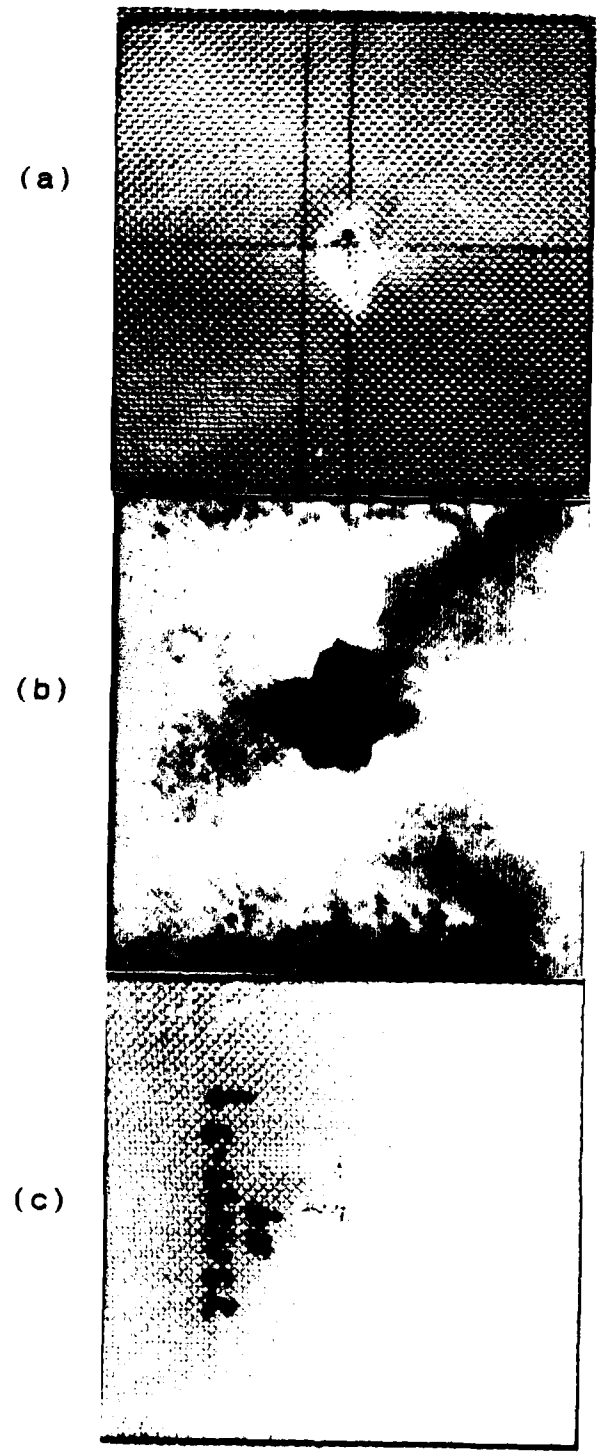

Figure 3.10 - Impacted $[0/90]_{2s}$ Kev/Poly Panel
(Velocity = 12.68 ft/sec; Impact Energy = 13.77 ft-lb)
(a) Impacted Side (b) C-Scan (c) Back Side

conclusions can be drawn by studying it alone. However, we can compare it to a Kevlar/Polyester panel to see how the two materials respond for the same ply orientation and impact velocity. The impacted side does not appear to be too badly damaged, however, on the back side, we see a great deal of fiber splitting and breakage. From the C-Scan, most of the internal damage appears to spread along the -45° direction. Comparing this panel to the equivalent Kevlar/Polyester panel shown in Figure 3.12, we see similar internal damage from the C-Scan. The damage is more circular and seems to show a tendency to spread in the ±45° directions. Again, the damage extending from the corners to the impact point is present.

Lastly, we consider $[0/90]_{3s}$ panels. Figures 3.13-3.16 illustrate the damage of Graphite/Epoxy panels where Figures 3.17-3.20 show damaged Kevlar/Polyester panels. Both sets of panels were impacted with velocities ranging from 11.75-13.89 ft/sec.

For the Graphite/Epoxy panels, we notice very little damage on the impacted side. This contrasts with the $[0/90]_{2s}$ panels which showed a little more damage on the impacted surface. The back sides however show the exact same features as the thinner panels (fiber splitting and breakage). The internal damage (delamination) evidenced from the C-Scans are somewhat different than for the $[0/90]_{2s}$ panels. While the shapes of the damaged areas

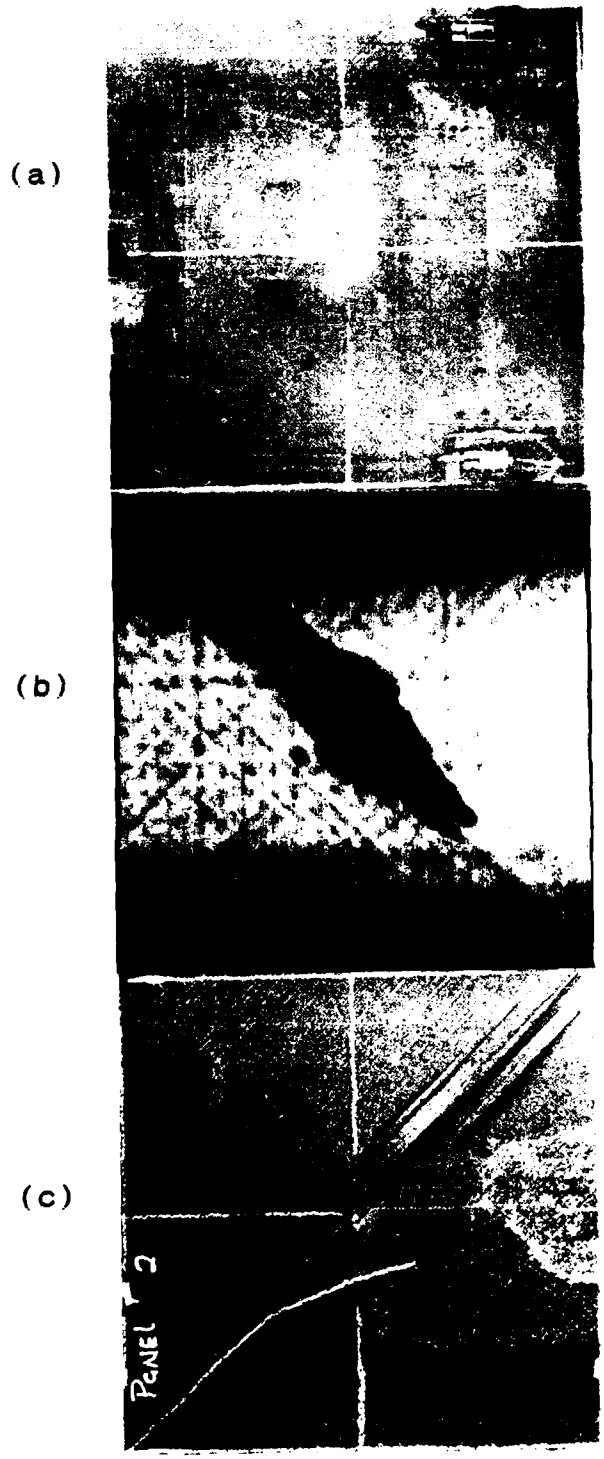

Figure 3.11 - Impacted $[\pm 45/90/0]_s$ Gr/Ep Panel
(Velocity = 9.82 ft/sec; Impact Energy = 8.25 ft-lb)
(a) Impacted Side (b) C-Scan (c) Back Side

Figure 3.12 - Impacted $[\pm 45/90/0]_s$ Kev/Poly Panel
(Velocity = 9.82 ft/sec; Impact Energy = 8.25 ft-lb)
(a) Impacted Side (b) C-Scan (c) Back Side

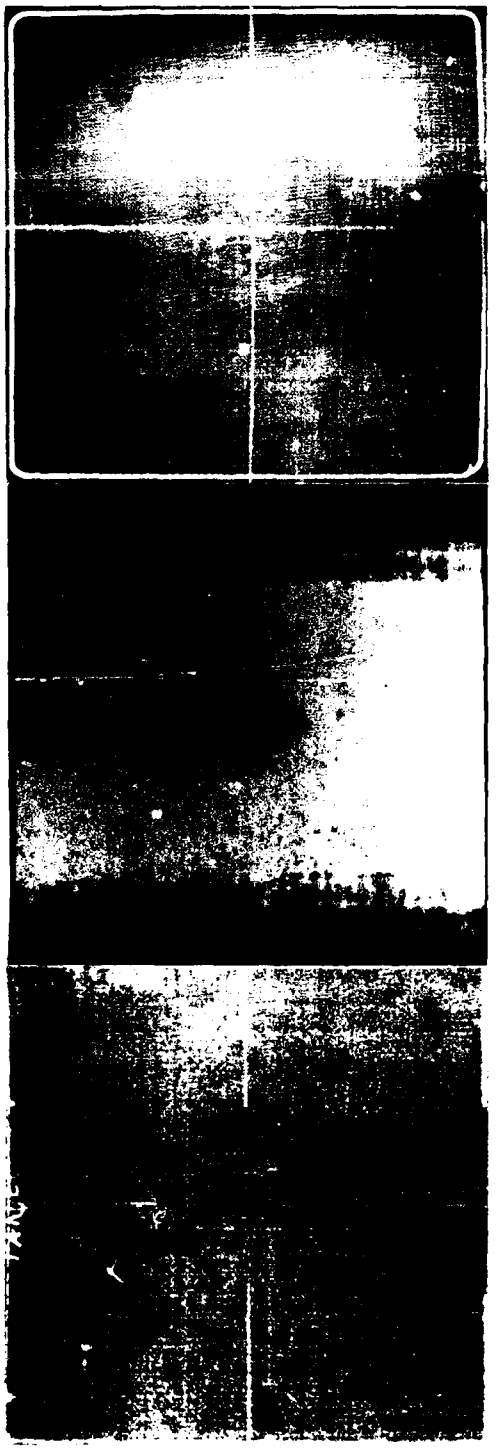

Figure 3.13 - Impacted $[0/90]_{3s}$ Gr/Ep Panel
(Velocity = 11.75 ft/sec; Impact Energy = 11.81 ft-lb)
(a) Impacted Side (b) C-Scan (c) Back Side

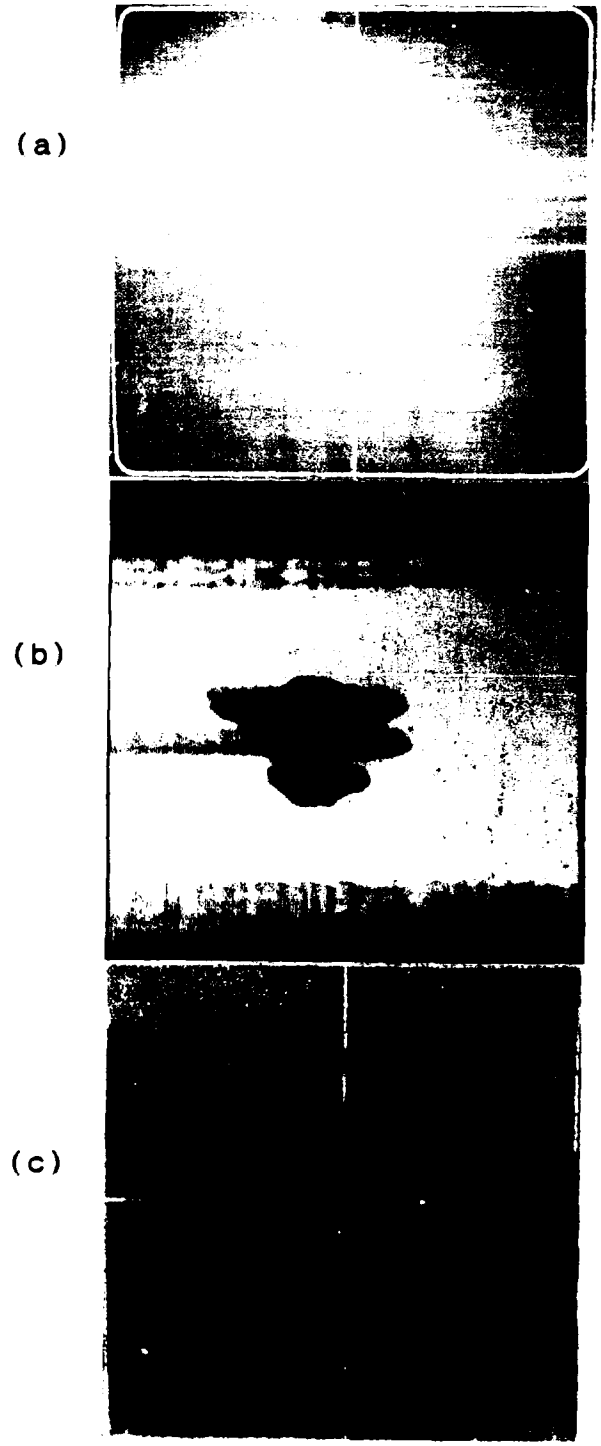

Figure 3.14 - Impacted $[0/90]_{3s}$ Gr/Ep Panel
(Velocity = 12.03 ft/sec; Impact Energy = 12.41 ft-lb)
(a) Impacted Side (b) C-Scan (c) Back Side

Figure 3.15 - Impacted $[0/90]_{3s}$ Gr/Ep Panel
(Velocity = 12.68 ft/sec; Impact Energy = 13.77 ft-lb)
(a) Impacted Side (b) C-Scan (c) Back Side

Figure 3.16 - Impacted $[0/90]_{3s}$ Gr/Ep Panel
(Velocity = 13.89 ft/sec; Impact Energy = 16.57 ft-lb)
(a) Impacted Side (b) C-Scan (c) Back Side

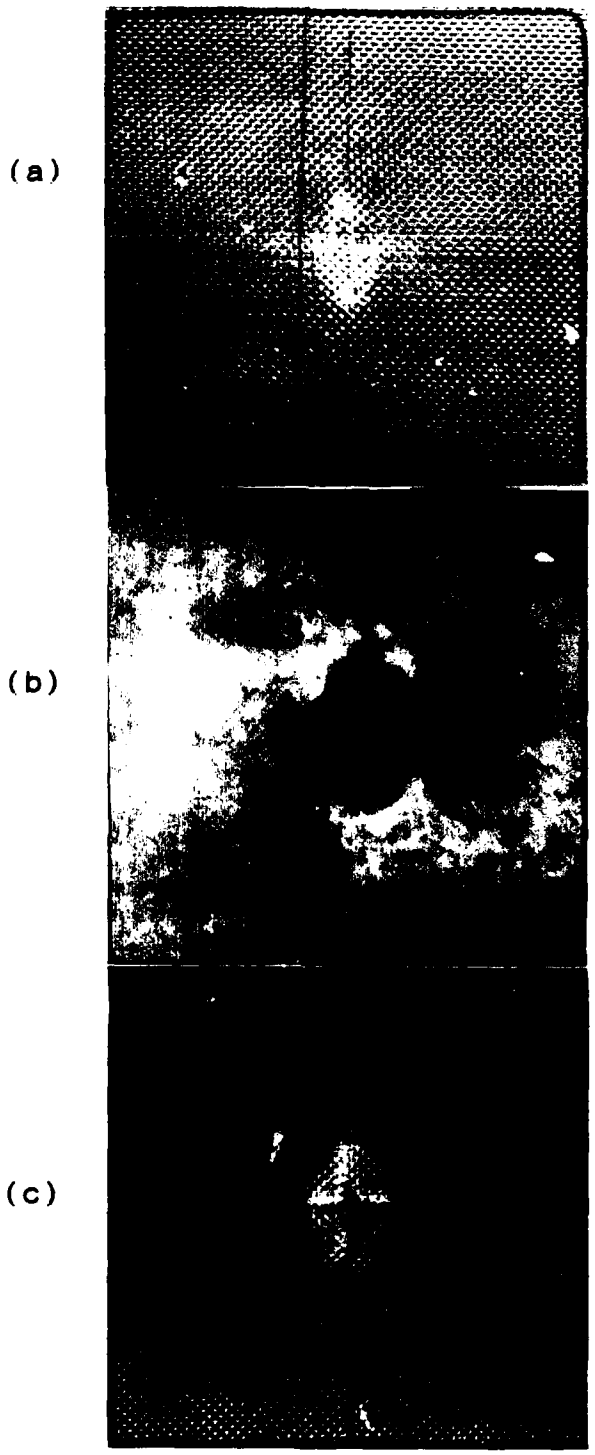

Figure 3.17 - Impacted $[0/90]_{3s}$ Kev/Poly Panel
(Velocity = 11.75 ft/sec; Impact Energy = 11.81 ft-lb)
(a) Impacted Side (b) C-Scan (c) Back Side

Figure 3.18 - Impacted $[0/90]_{3s}$ Kev/Poly Panel
(Velocity = 12.03 ft/sec; Impact Energy = 12.41 ft-lb)
(a) Impacted Side (b) C-Scan (c) Back Side

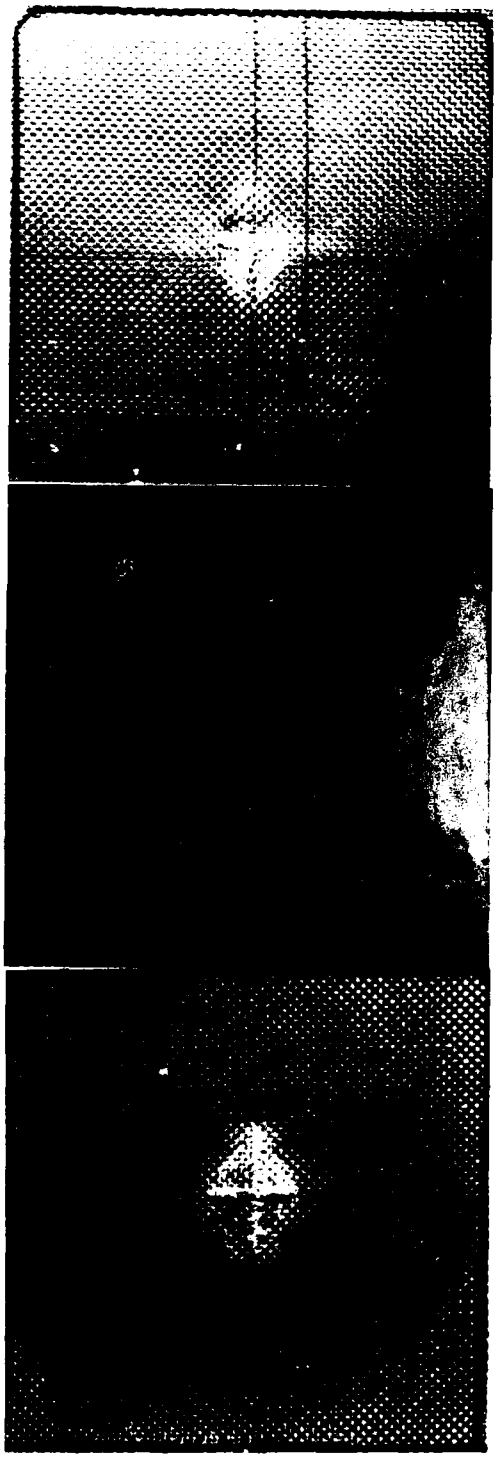

Figure 3.19 - Impacted $[0/90]_{3s}$ Kev/Poly Panel
(Velocity = 12.68 ft/sec; Impact Energy = 13.77 ft-lb)
(a) Impacted Side (b) C-Scan (c) Back Side

(a)

(b)

(c)

Figure 3.20 - Impacted $[0/90]_{3s}$ Kev/Poly Panel
(Velocity = 13.89 ft/sec; Impact Energy = 16.57 ft-lb)
(a) Impacted Side (b) C-Scan (c) Back Side

appear to be similar, it is surprising to note that the damage area did not increase very much (if at all) as the impact velocity increased. This leads one to suspect that there may be a range of impact energies (or velocities) where the amount of damage levels off. Indeed, O'Kane and Benham [5] plotted experimentally obtained damage areas as a function of impact energy. For several of the ply orientations they studied, the curves appear to flatten out indicating that the damage area becomes more or less constant over a range of impact energies. The same features are noticed for $[0/90]_{3s}$ panels made of Kevlar/Polyester shown in Figures 3.17-3.20. The damage does not appear to increase as the impact velocity increases.

To briefly summarize, damage to Graphite/Epoxy panels takes the form of fiber splitting, fiber breakage, and delamination. The delaminations seem to be oriented along the fiber directions. For the cases of $[0/90]_{2s}$ and $[0/90]_{3s}$ panels, the curvature of the panel seems to lend some preference as to which directions the delaminations spread.

The damage of Kevlar/Polyester panels remains much more contained and localized compared to Graphite/Epoxy panels. For Kevlar/Polyester, we see fibers breaking in a tensile mode, especially on the back side, and we see no fiber splitting as in Graphite/Epoxy, probably due to the weave construction of the material. Also, different modes of

damage may exist for Kevlar/Polyester, based on the observed changes in damage shape as the impact velocity increases.

Lastly, panels made of both materials exhibited the characteristic of a more or less constant damage area over a range of impact energies.

Microphotographs of Impacted Panels

The last part of investigating the impact damage consisted of cross-sectioning some of the panels and viewing them under a microscope. Microphotographs through the impact point were taken of these panels to be studied.

The following four panels were selected to be studied.

1. $[0/90]_{2s}$ Gr/Ep (Velocity = 12.68 ft/sec)
2. $[0/90]_{2s}$ Kev/Poly (Velocity = 12.68 ft/sec)
3. $[\pm 45/90/0]_{s}$ Gr/Ep (Velocity = 9.82 ft/sec)
4. $[\pm 45/90/0]_{s}$ Kev/Poly (Velocity = 9.82 ft/sec)

Metallographic specimens from each of these panels had to be prepared. The impacted panels were first cut along a line through the impact point as shown in Figure 3.21 using a water cooled diamond saw blade. The water prevented any localized heating during the cutting. A 3" section surrounding the impact point was removed from one of the half panels to use as the specimen.

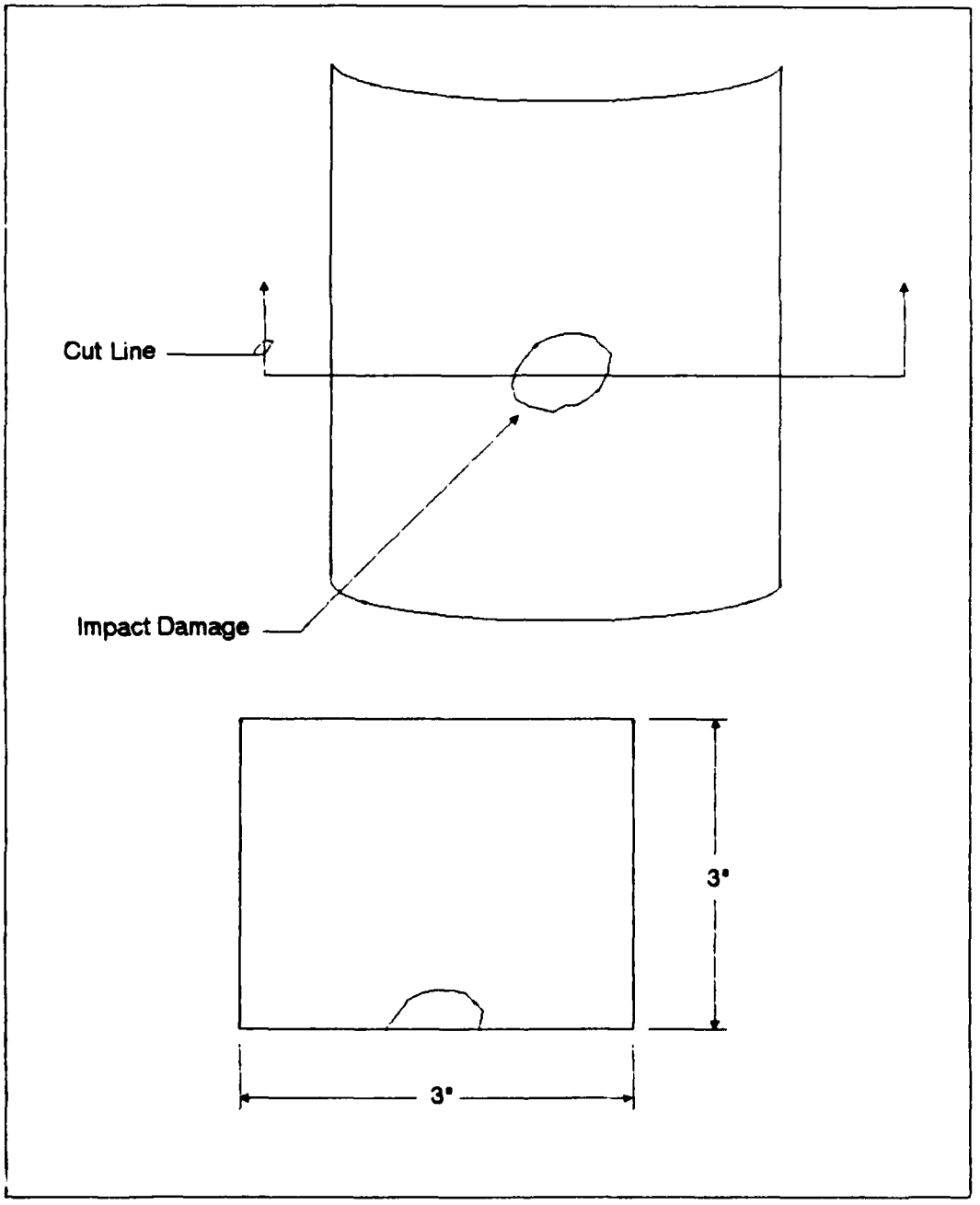

Figure 3.21 - Microphotograph Specimen Geometry

Each specimen was placed in an epoxy resin and allowed to set for approximately 48 hours. Setting the specimen in the epoxy made polishing easier and provided stability of the specimen for viewing under the microscope. After the epoxy had hardened, each specimen was ground on a grinding wheel until the cross-section through the thickness was exposed. Next, the surface was sanded using successively finer grits of sandpaper (240, 320, 400, 600 grit). Lastly, each specimen was polished with an alumina polishing cloth on a grinding wheel until the desired details could be seen under the microscope.

Figures 3.22-3.25 are microphotographs showing impact damage through the thickness. The actual width of the section photographed is approximately 1/2", the diameter of the impactor. The magnification used to view the specimens was 50X.

Figure 3.22 shows the cross-section of a $[0/90]_{2s}$ Graphite/Epoxy panel impacted with a velocity of 12.68 ft/sec. The top ply of 0° fibers debonded completely from the 90° ply beneath it. Delaminations, which appear as dark horizontal lines in the photograph, occur between every ply. We also see many cracks running through and along the 0° plies as well as numerous small cracks in the 90° plies. The horizontal cracks through the inner 0° plies suggest some shear failure, possibly resulting from a shear stress

σ_{yz}. The vertical cracks suggest tensile flexural stresses [6].

Figure 3.23 shows the cross-section of a $[0/90]_{2s}$ Kevlar/Polyester panel impacted by the same velocity (12.68 ft/sec). From this figure, one gets a good feel for the weave construction of Kevlar/Polyester. Through the thickness, there appears to be much less damage than in the equivalent Graphite/Epoxy panel. The fibers appear to remain intact, sustaining no visible damage. There are, however, a number of cracks in the matrix material between the fibers. Overall, we can also see the permanent deformation of the impacted region.

Moving on, the $[\pm 45/90/0]_s$ Graphite/Epoxy panel impacted at 9.82 ft/sec is shown in Figure 3.24. The cross-section appears to be literally destroyed. The fibers are broken into small pieces and a great deal of delamination has occurred between every ply.

Lastly, Figure 3.25 shows the $[\pm 45/90/0]_s$ Kevlar/Polyester impacted at 9.82 ft/sec. Again, we see much more damage (delamination and matrix cracks) than for the $[0/90]_{2s}$ ply orientation.

Figure 3.22 - Cross-Section of Impacted $[0/90]_{2s}$ Gr/Ep Panel
(Impact Velocity = 12.68 ft/sec; Impact Energy = 13.77 ft-lb)

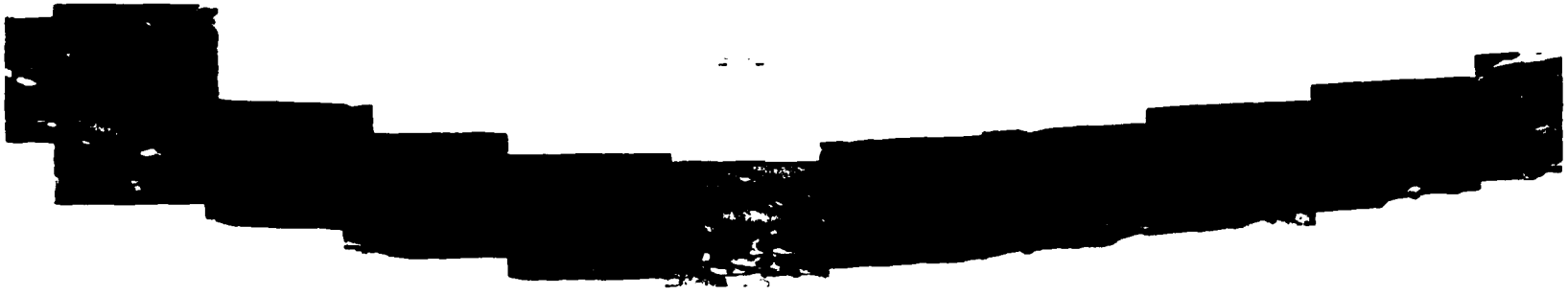

Figure 3.23 - Cross-Section of Impacted $[0/90]_{2s}$ Kev/Poly Panel
(Impact Velocity = 12.68 ft/sec; Impact Energy = 13.77 ft-lb)

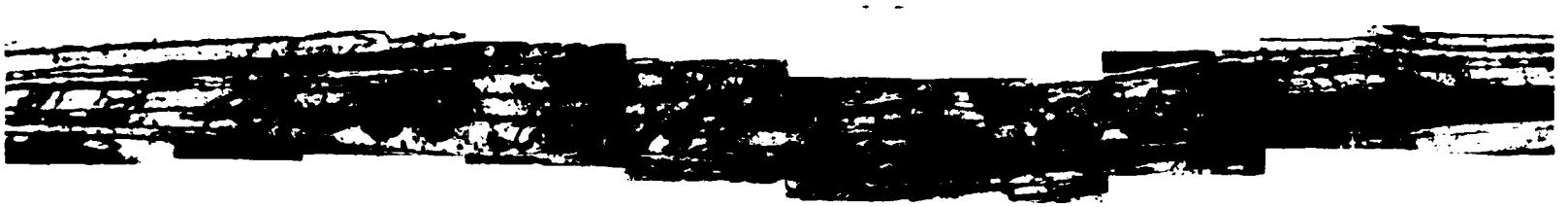

Figure 3.24 - Cross-Section of Impacted $[\pm 45/90/0]_s$ Gr/Ep Panel
(Impact Velocity = 9.82 ft/sec; Impact Energy = 8.25 ft-lb)

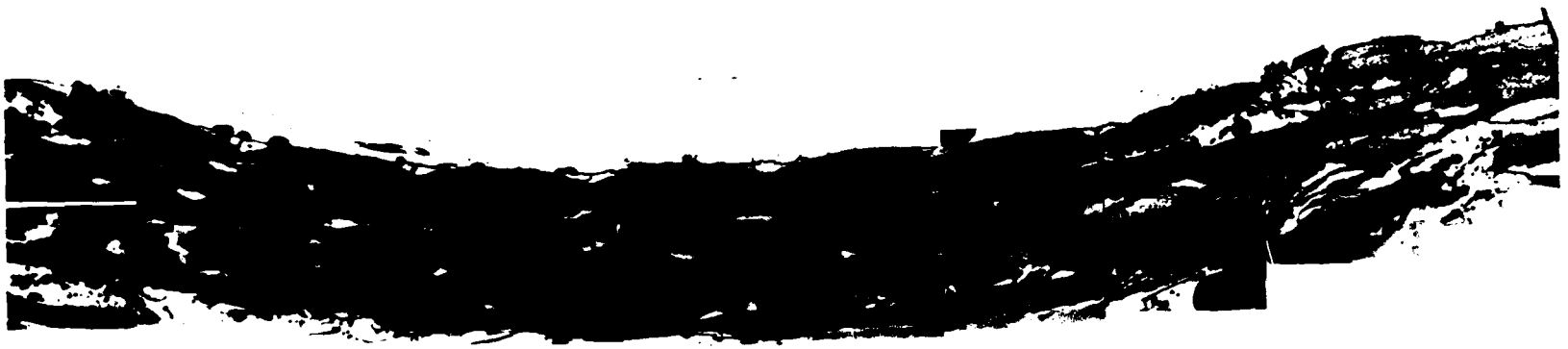

Figure 3.25 - Cross-Section of Impacted $[\pm 45/90/0]_s$ Kev/Poly Panel
(Impact Velocity = 9.82 ft/sec; Impact Energy = 8.25 ft-lb)

4. ANALYSIS

To the author's knowledge, no valid model exists for predicting the extent of damage and corresponding reduction in strength of composite cylindrical panels (or shells). That being the case, the analysis performed in this thesis concentrates on predicting the collapse load of undamaged panels.

An analysis first performed to determine the collapse load of the panels assumed a perfect geometry. The resulting collapse loads greatly disagreed with the experimentally measured loads of the undamaged panels. Depending on the ply orientation, the difference between the analytical and experimental load was as much as 62%. This prompted an investigation into geometrically imperfect panels.

Discrepancies were also noted between the displacements of the analytical vs. experimental panels. The actual panels were not as stiff as the analysis indicates, which by itself was not that surprising. However, the magnitude of the difference was puzzling. As a result, the boundary conditions were relaxed in order to allow more structural flexibility. While relaxing the boundary conditions does have an effect on the flexibility, it alone does not account for the large differences.

Nonlinear Collapse Analysis

The finite element program STAGSC-1 was used to perform the analysis of the composite cylindrical panels. STAGSC-1 is an energy based finite element code for performing structural analysis of shells. One of the advantages of STAGSC-1 is its ability to perform a nonlinear static analysis. Such an analysis enabled the determination of the collapse load of the panels studied in this thesis. In the finite element formulation of STAGSC-1, the kinematic relations of a cylindrical shell described by Equations (2.5) and (2.6) are replaced with the nonlinear kinematic relations of a flat plate. This is done because STAGSC-1 uses flat plate elements to approximate a shell. While the thin shell and small strains assumptions hold, the inclusion of the higher order terms allows for the large rotations that can occur when a shell deforms. A complete derivation of the relations is given in [16]. The middle surface strains used by STAGSC-1 are

$$\begin{aligned} \varepsilon_x^o &= u,_x + 1/2\ (u,_x^2 + v,_x^2 + w,_x^2\ ) \\ \varepsilon_y^o &= v,_y + 1/2\ (u,_y^2 + v,_y^2 + w,_y^2\ ) \\ \gamma_{xy}^o &= u,_y + v,_x + (u,_x u,_y + v,_x v,_y + w,_x w,_y) \end{aligned} \tag{4.1}$$

Applying the Kirchhoff-Love hypothesis (thin element with no distortion of the cross-section) and including the

curvatures, the strains at any point in the flat element may be expressed as [17]

$$\begin{aligned} \varepsilon_x &= \varepsilon_x^\circ - zw_{,xx} \\ \varepsilon_y &= \varepsilon_y^\circ - zw_{,yy} \\ \gamma_{xy} &= \gamma_{xy}^\circ - 2zw_{,xy} \end{aligned} \tag{4.2}$$

where ε_x° ε_y°, and γ_{xy}° are given by Equations (4.1). These strain relations are the ones used in the constitutive relations for composite materials. Appendix B provides a brief discussion of laminated plate theory. The result of an analysis using these nonlinear kinematic relations is the equilibrium path the structure follows as it deforms. The peak load on the curve is called the collapse load.

As was stated earlier, STAGSC-1 uses flat elements to model the curved surfaces of a shell. The two elements contained in STAGSC-1 primarily used for this type of analysis are the QUAF 410 and QUAF 411 elements. The QUAF 410 is a quadrilateral element with three translational and three rotational degrees of freedom per node, allowing 24 degrees of freedom per element. The QUAF 411 element, in addition to the same translations and rotations in the 410 element, allows an additional in-plane rotation at each corner and also includes a translational degree of freedom at the midpoint of each side of the element. This amounts to a total of 32 degrees of freedom for the QUAF 411

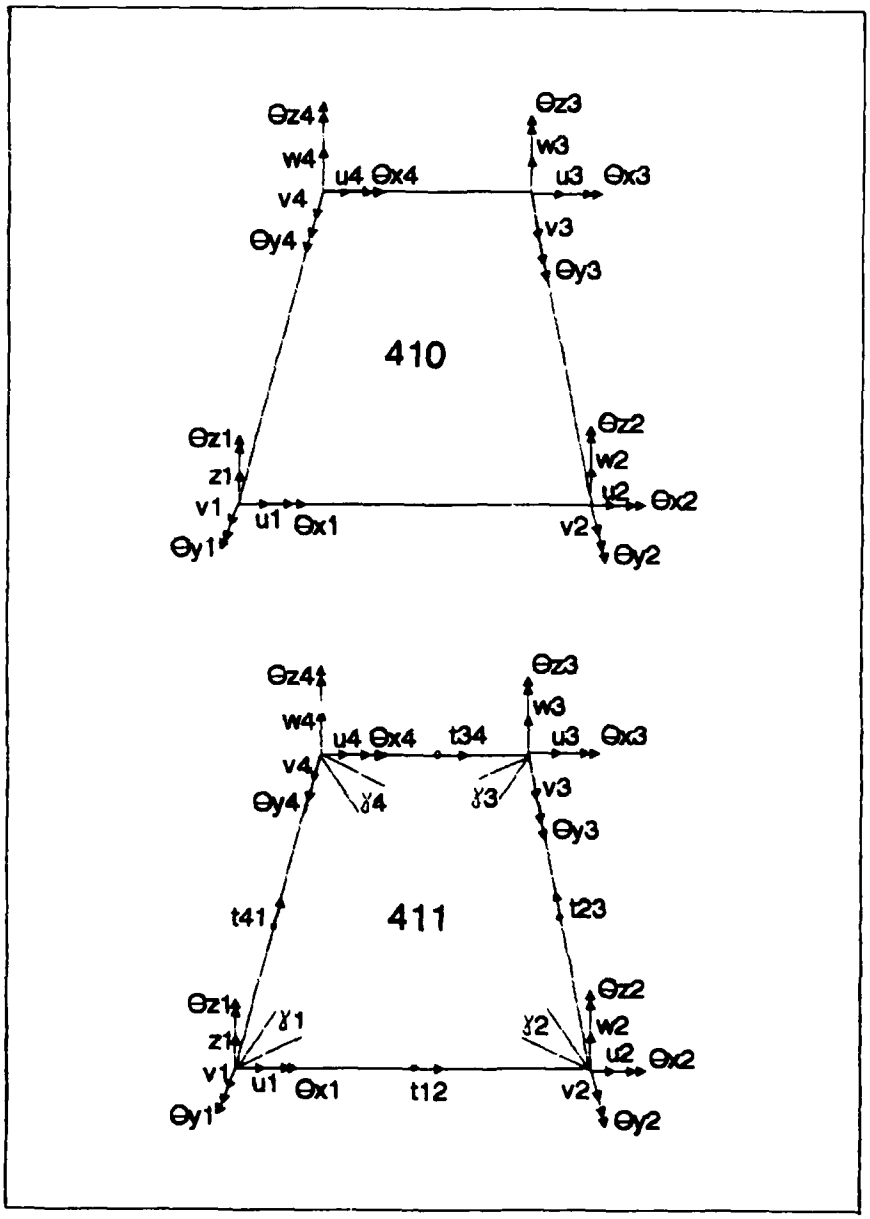

Figure 4.1 - QUAF 410 & QUAF 411 Elements

element. Figure 4.1 illustrates the two elements and their respective degrees of freedom [22].

Looking at Figure 4.1, we notice a degree of freedom not usually associated with plate elements. The normal rotation θ_z for the elements of Figure 4.1 is needed to account for the fact that two adjacent plate elements meet at an angle to represent a curved surface [17].

Solution Technique

The analysis of an elastic stability problem involving shell structures requires the solution of a large system of nonlinear equations using a finite element or finite difference method [18]. Bellini and Chulya [19] discuss the fact that when the nonlinear response curve (load vs. displacement) of a structure reaches a turning point, one of two things can happen. A limit point is reached where the solution stops, or a bifurcation point is reached with several possible branches.

The solution technique STAGSC-1 uses to solve the nonlinear equations is the Riks method [18,20] combined with the modified Newton-Raphson method as an iterative-incremental method [19]. The advantage of this technique is the response curve, which represents equilibrium states, can be solved for past a peak load. In essence, the solution continues and calculates a post-buckling equilibrium path. Interested readers are

referred to References [18,19,20] for in depth discussions on Riks method and nonlinear equation solution techniques using finite element methods.

Collapse of Undamaged Panels

Material properties of AS4/3501-6 Graphite/Epoxy were determined by standard tensile tests [21]. $[0]_8$ coupons were used to determine E_1 and ν_{12} while $[90]_{16}$ and $[\pm 45]_{2s}$ coupons were used to determine E_2 and G_{12} respectively. The material properties determined for the analysis of Graphite/Epoxy panels are

$$E_1 = 20.461 * 10^6 \text{ psi}$$
$$E_2 = 1.34036 * 10^6 \text{ psi}$$
$$\nu_{12} = 0.3131$$
$$G_{12} = 0.8638 * 10^6 \text{ psi}$$

Determining the material properties of Kevlar/Polyester is not as straight forward as for Graphite/Epoxy because Kevlar/Polyester can not be made into unidirectional coupons. Also, STAGSC-1 can not analyze a weave material, so an equivalent orthotropic laminate had to be developed to model Kevlar/Polyester. Therefore, laminates having the same ply orientations as the panels were tested. Appendix A details how the material properties were determined. The

properties used for the analysis of Kevlar/Polyester panels are

$$E_1 = 6.7932 * 10^6 \text{ psi}$$
$$E_2 = 0.44502 * 10^6 \text{ psi}$$
$$\nu_{12} = 0.50369$$
$$G_{12} = 0.1782 * 10^6 \text{ psi}$$

Graphite/Epoxy and Kevlar/Polyester cylindrical panels were analyzed using STAGSC-1 to predict their collapse load under compression. The dimensions of the panels used in the analysis are illustrated in Figure 2.1. The top curved edge was clamped and allowed only a displacement in the x direction. The bottom curved edge was fully clamped. The vertical edges were simply supported, allowing rotations and restraining any circumferential and radial displacements along the boundary. Mathematically, these boundary conditions may be expressed as

Top edge:	$u=\text{free};\ v=w=w_{,x}=w_{,y}=0$
Bottom edge:	$u=v=w=w_{,x}=w_{,y}=0$
Vertical edges:	$u=w_{,x}=\text{free};\ v=w=w_{,y}=0$

Once the boundary conditions are set, the next thing to consider is the finite element mesh size to be used to insure a correct answer is converged upon. Becker [2]

conducted a study to determine the optimum mesh size for the finite elements of composite cylindrical panels. He found that 1/2" x 1/2" elements were ideal for the panel geometries under consideration using the QUAF 410 or QUAF 411 elements. Also, Wilder [1] comments that accurate results are obtained with STAGSC-1, using QUAF elements, if the element size is between 1/2" to 2/3" square. As a result, 1/2" x 1/2" elements were used for all analysis performed in this thesis.

The last thing to consider before the analysis can begin is the type of element to be used. The QUAF 410 element was chosen for use in the analysis done in this thesis. It was felt that since the vertical edges were supported, the moderate rotations encountered could be adequately modeled by the 410 element. The 411 element would be the element of choice for large rotations. Another reason for selecting the 410 element is the difference in the resulting computational time between the use of the two elements. An analysis using the 411 element with its eight additional degrees of freedom can take up to four times longer than an analysis using the 410 element.

Table 4.1 shows the collapse load for each material and ply orientation studied assuming a geometrically perfect panel with the above stated boundary conditions. The experimental loads that were shown in Table 2.3 ranged from 24-62% below these analytical loads. These large

discrepancies can partially be explained by considering geometric imperfections of the curved panels.

Table 4.1
STAGSC-1 Collapse Load of Undamaged Panels

		$[0/90]_{2s}$	$[\pm 45/90/0]_{s}$	$[0/90]_{3s}$
Load (lbs)	Gr/Ep	5926	4652	10124
	Kev/Poly	2117	1504	5524

STAGSC-1 Imperfection Analysis

The manufacture of geometrically perfect cylindrical panels is nearly impossible to achieve. Janisse [3] in his work showed that imperfections do exist in panels and can have a profound effect on their load carrying capability for certain ply orientations. The imperfections he measured were on the order of the thickness of a single ply (0.005").

STAGS has a built in capability to impose a geometric imperfection into the panel. The imperfection is constant through the thickness of the panel and of the form [22]

$$W_0 = WAMP * \cos\left[(x-X1) * \pi/XL\right] * \cos\left[(y-Y1) * \pi/YL\right] \quad (4.3)$$

where

WAMP = Amplitude of Imperfection

X1,Y1 = Location of Center of Imperfection

XL,YL = Half-wavelength of Imperfection in x and y direction respectively

The question that must be answered at this point is, "What imperfection pattern will best model the actual imperfect panel?". To determine the appropriate pattern, two ply orientations were examined, $[0/90]_{2s}$ and $[\pm 45/90/0]_{s}$. The material analyzed was Graphite/Epoxy. It is assumed that the Kevlar/Polyester panels would respond similar to the Graphite/Epoxy panels since the imperfections are geometrical, not material related. First, consider $[0/90]_{2s}$ Graphite/Epoxy panels. Table 4.2 shows the collapse loads calculated by STAGSC-1 from a nonlinear collapse analysis of panels with imperfection of the type described by Equation (4.3). Four different imperfection patterns were analyzed.

(1) 0.005" with one half-wave in each direction.

(2) 0.04" with one half-wave in each direction.

(3) 0.04" with three half-waves in each direction.

(4) 0.005" with three half-waves in each direction.

Table 4.2
Imperfection Analysis of $[0/90]_{2s}$ Gr/Ep Panels
(Collapse Load of "Perfect" Panel = 5926 lbs)

		Imperfection Amplitude	
	# of half waves	0.005"	0.04"
Load (lbs)	1	6334	4995
	3	2880	6516

The surprising result of this analysis is that for two of the imperfection patterns studied, the panel actually strengthens as a result of the imperfection. To understand this, consider the shape of the "perfect" panel at the collapse load as calculated by STAGSC-1 shown in Figure 4.2. Figure 4.2 actually shows the deformed shape of the "perfect" panel's centerlines.

First consider imperfection pattern (1). The geometry of this imperfect panel is very close to that of the "perfect" panel. Janisse [3] showed in his work that the imperfect panels tended to displace in the same pattern as the imperfection. If one thinks of tne imperfection as being imposed on the panel, then for this first case, we have a panel that wants to deform into 3 half waves longitudinally and 5 half waves circumferentially being forced to deform into one half wave in each direction. One can see that it will require some extra energy to pop the

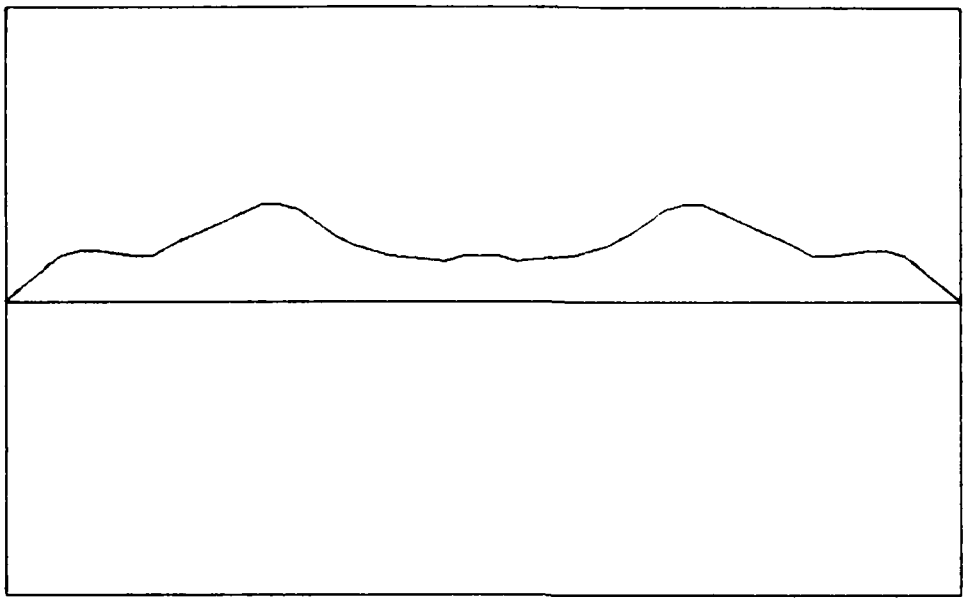

(a)

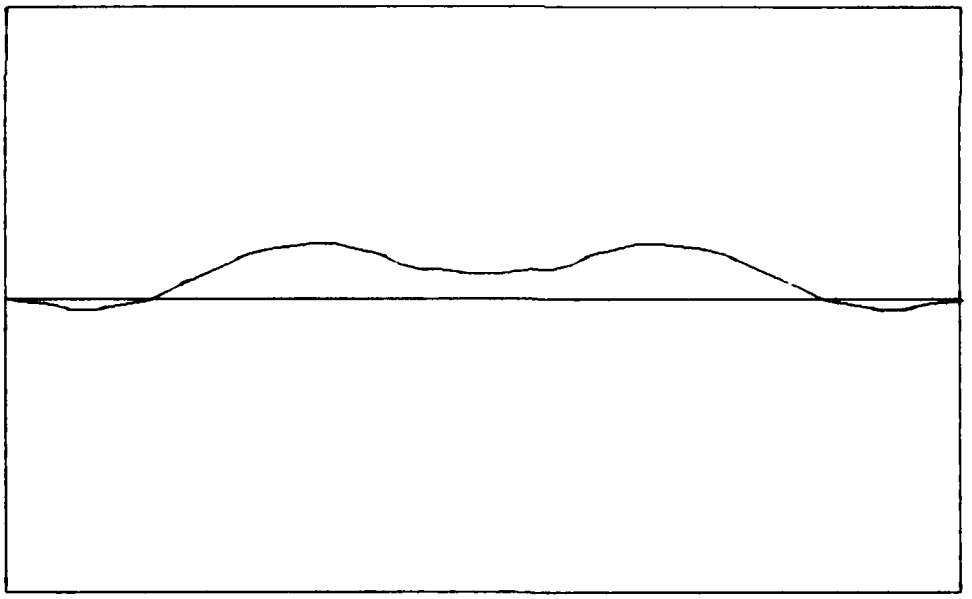

(b)

Figure 4.2
Shape of "Perfect" $[0/90]_{2s}$ Gr/Ep Panel at Collapse
(a) Longitudinal Shape (b) Circumferential Shape

extra waves through until the panel deforms into one half wave in each direction. Hence, the collapse load is higher than that of the perfect panel.

Next, consider imperfection pattern (2). Here we see that as the amplitude of the imperfection is increased, the panel weakens somewhat. With an imperfection as large as 0.04", the applied load not only causes membrane stresses but also begins to impart some bending to the panel. This additional bending weakens the panel.

Third, consider imperfection pattern (3). Again we see the collapse load increases beyond that of the "perfect" panel. In this instance, the imperfections are large enough and the curvatures in the panel change often enough that the panel responds similar to a folded plate. The effective longitudinal length of the panel is decreased, causing an increase in the collapse load.

Lastly, consider imperfection pattern (4). The collapse load of 2880 lbs is within 3% of the experimental collapse load. This imperfection pattern is closest to the deformed shape of the "perfect" panel determined by analysis. Therefore, less energy is required to cause the panel to collapse because the imperfections present in the panel are in the direction the panel wants to naturally move. The exact geometry of the imperfections is not known and in general is random and can vary from panel to panel. However, the pattern of three half waves longitudinally and

circumferentially seems to model the actual imperfections very well by smearing them out evenly over the entire panel geometry.

Consider now the same four imperfection patterns imposed on a $[\pm 45/90/0]_s$ Graphite/Epoxy panel. Table 4.3 shows the collapse loads computed by STAGSC-1 for these cases.

Table 4.3
Imperfection Analysis of $[\pm 45/90/0]_s$ Gr/Ep Panels
(Collapse Load of "Perfect" Panel = 4652 lbs)

		Imperfection Amplitude	
	# of half waves	0.005"	0.04"
Load (lbs)	1	4692	4930
	3	4065	6200

We see the same trends here for the $[\pm 45/90/0]_s$ orientation as for the $[0/90]_{2s}$ orientation with one exception. For imperfection pattern (2), STAGSC-1 computes a greater collapse load than that of a "perfect" panel. Recall the collapse load was lower for the $[0/90]_{2s}$ orientation. The two ply orientations see the load applied in the same way, but the $[\pm 45/90/0]_s$ orientation has a greater bending stiffness than does the $[0/90]_{2s}$ orientation. The $\pm 45^\circ$ plies are the reason for the

increased bending stiffness. This also accounts for the dramatic increase in the collapse load of a panel with imperfection pattern (3). The angled plies help resist the bending moments in addition to the geometry decreasing the effective length of the panel.

One last aspect of the imperfection analysis to comment on involves the sensitivity of the panels to initial geometric imperfections. We see by the analysis that the ply orientation determines the sensitivity of the panel to imperfections. $[\pm 45/90/0]_s$ was least sensitive to imperfections while $[0/90]_{2s}$ was most sensitive. The author feels that the ply orientation is critical in characterizing a cylindrical panel's imperfection sensitivity.

Now that the appropriate imperfection pattern has been determined, we perform the analysis for each ply orientation and material. An imperfection was located at the center of each panel with three half waves in each direction. The amplitude was set equal to 0.005". Thus, the following parameters are substituted into Equation (4.3).

$$X1 = 6.0"$$

$$Y1 = 19.0986^{\circ}$$

$$XL = 4.0"$$

$$YL = 12.7324^{\circ}$$

Figure 4.3 shows the shape of the imperfection along the center of the panel in the x-direction. Table 4.4 shows the collapse loads of the panels accounting for the imperfection.

Table 4.4
Collapse of Imperfect Panels

		$[0/90]_{2s}$	$[\pm 45/90/0]_{s}$	$[0/90]_{3s}$
Load (lbs)	Gr/Ep	2880	4065	7473
	Kev/Pol	833	1320	2338

While the imperfections that are actually in the panel are not exactly modeled by this sinusoidal imperfection, the experimental loads are within 3-16% of the loads in Table 4.4.

Figures 4.4 - 4.9 shows the Load-Displacement curves for each panel. The displacements are in the direction of the applied load. STAGSC-1 curves for a perfect and imperfect panel are shown as well as experimental data.

The curves show the same features for each case studied. Note that the STAGSC-1 curves for a perfect and imperfect panel show some post-buckling strength for the $[0/90]_{2s}$ and the $[0/90]_{3s}$ ply orientations. However, the experimentation was halted after the panel buckled as it was not the intention of the research to investigate

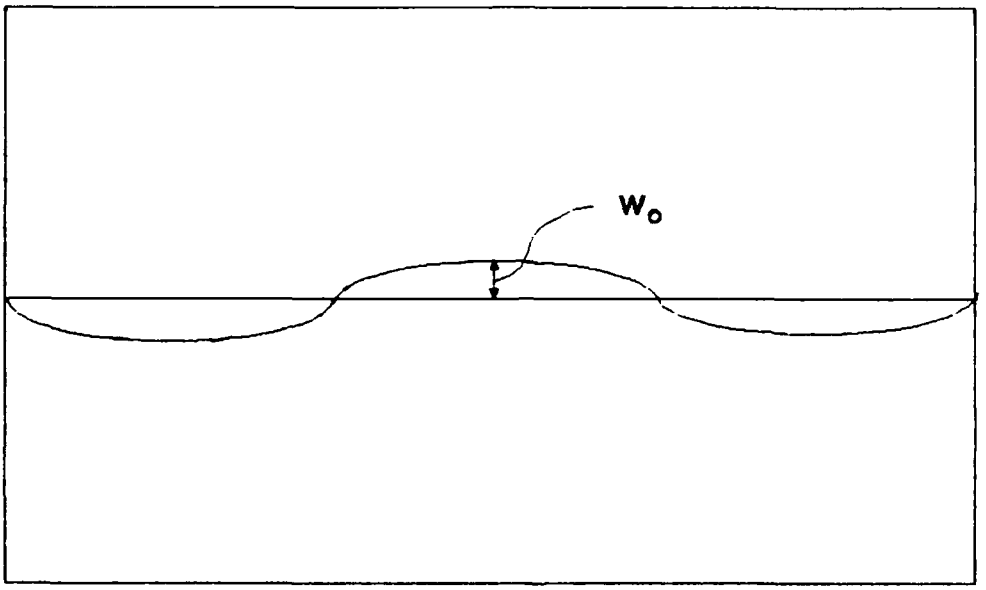

Figure 4.3 - Imperfection Shape (Three Half Waves)

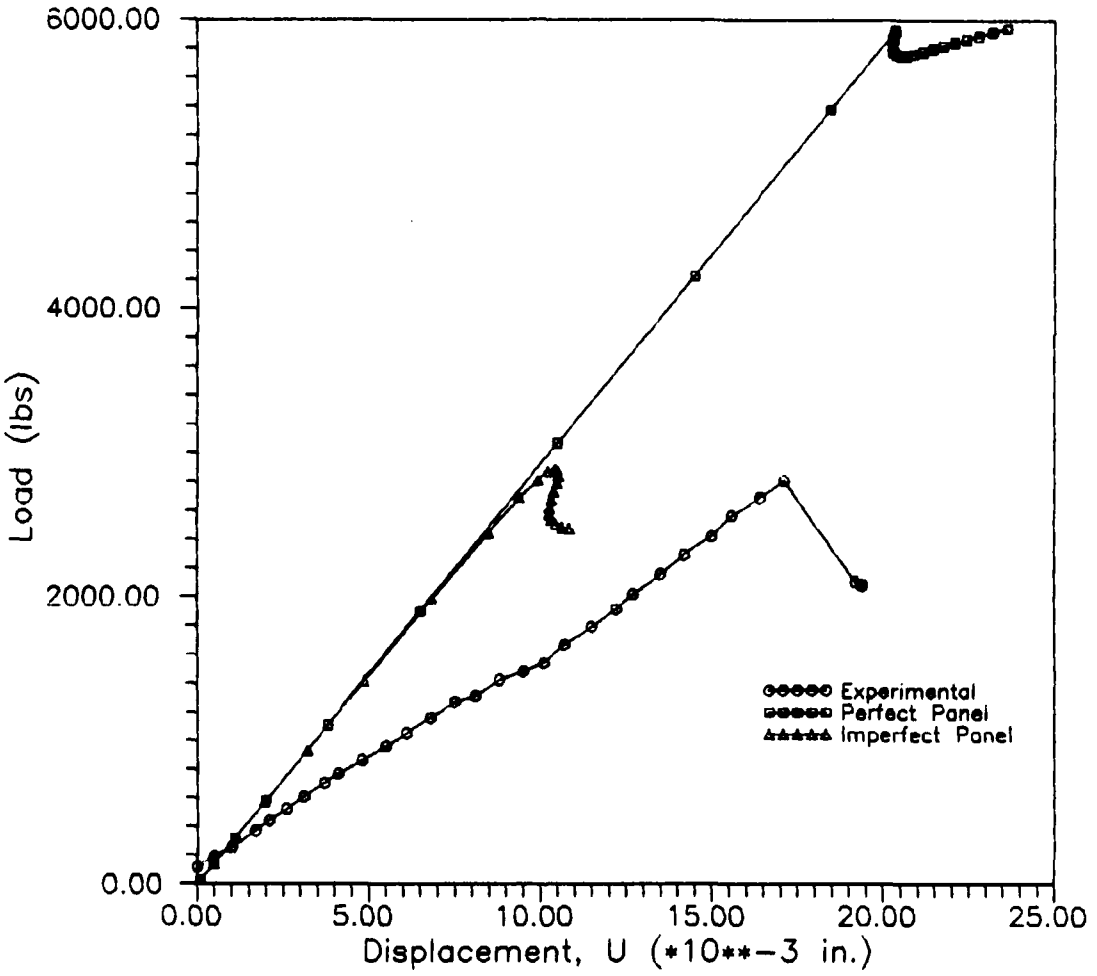

Figure 4.4
Load-Displacement Curves for $[0/90]_{2s}$ Gr/Ep Panels

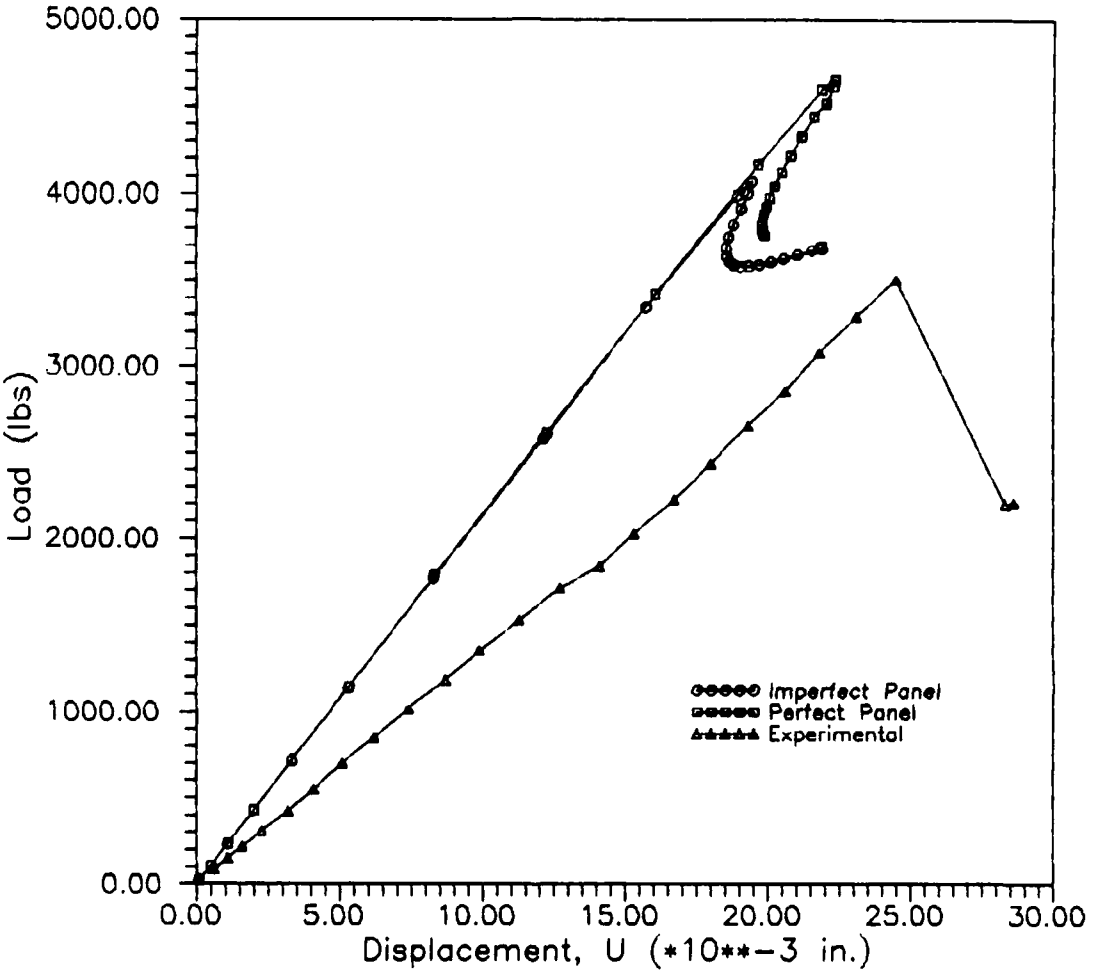

Figure 4.5
Load-Displacement Curves for $[\pm 45/90/0]_s$ Gr/Ep Panels

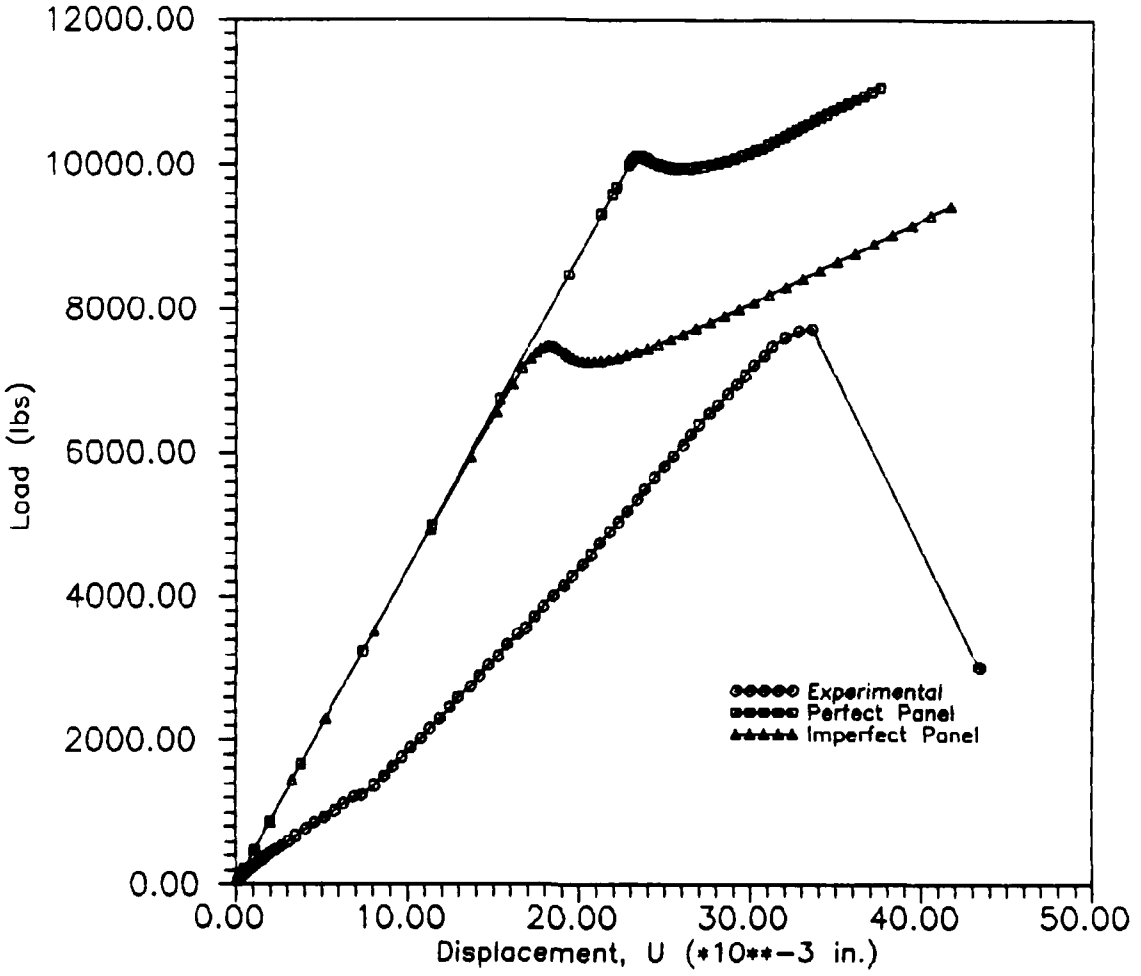

Figure 4.6
Load-Displacement Curves for $[0/90]_{3s}$ Gr/Ep Panels

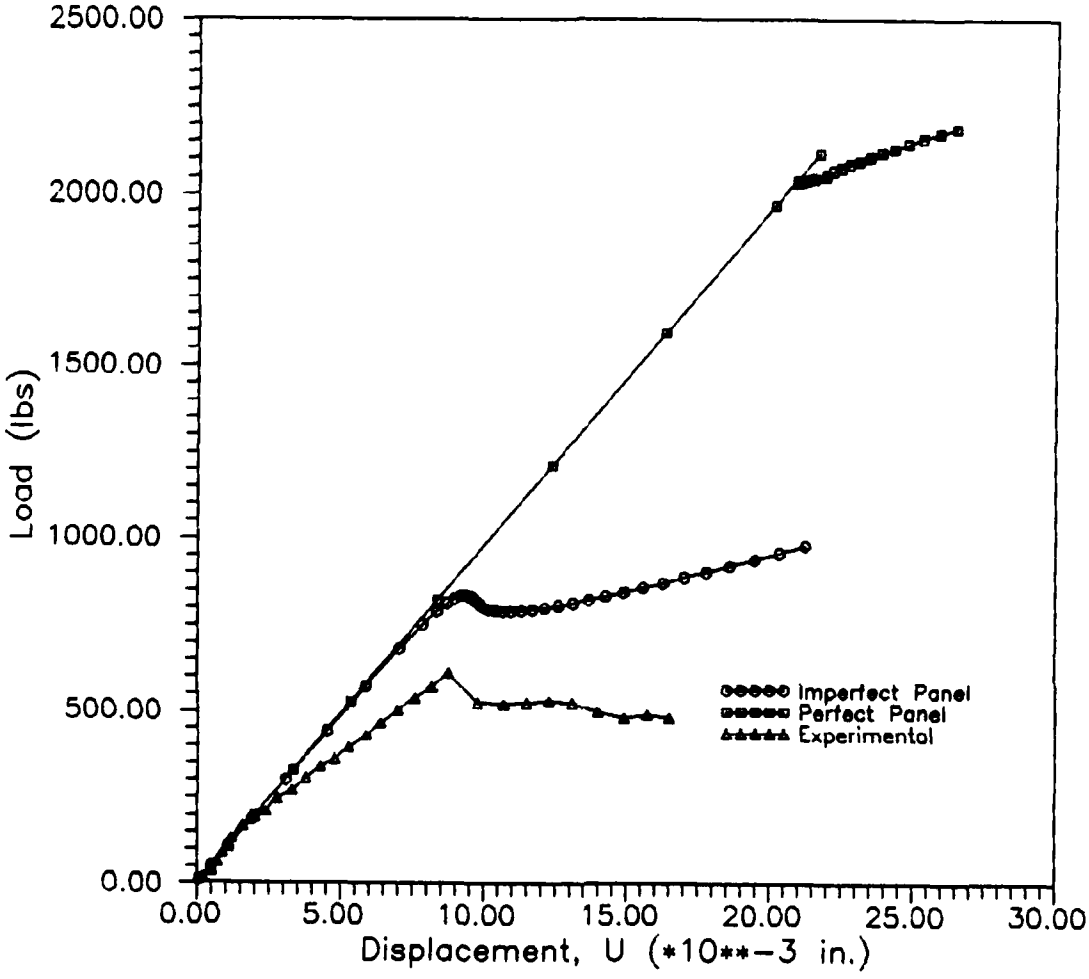

Figure 4.7
Load-Displacement Curves for $[0/90]_{2s}$ Kev/Poly Panels

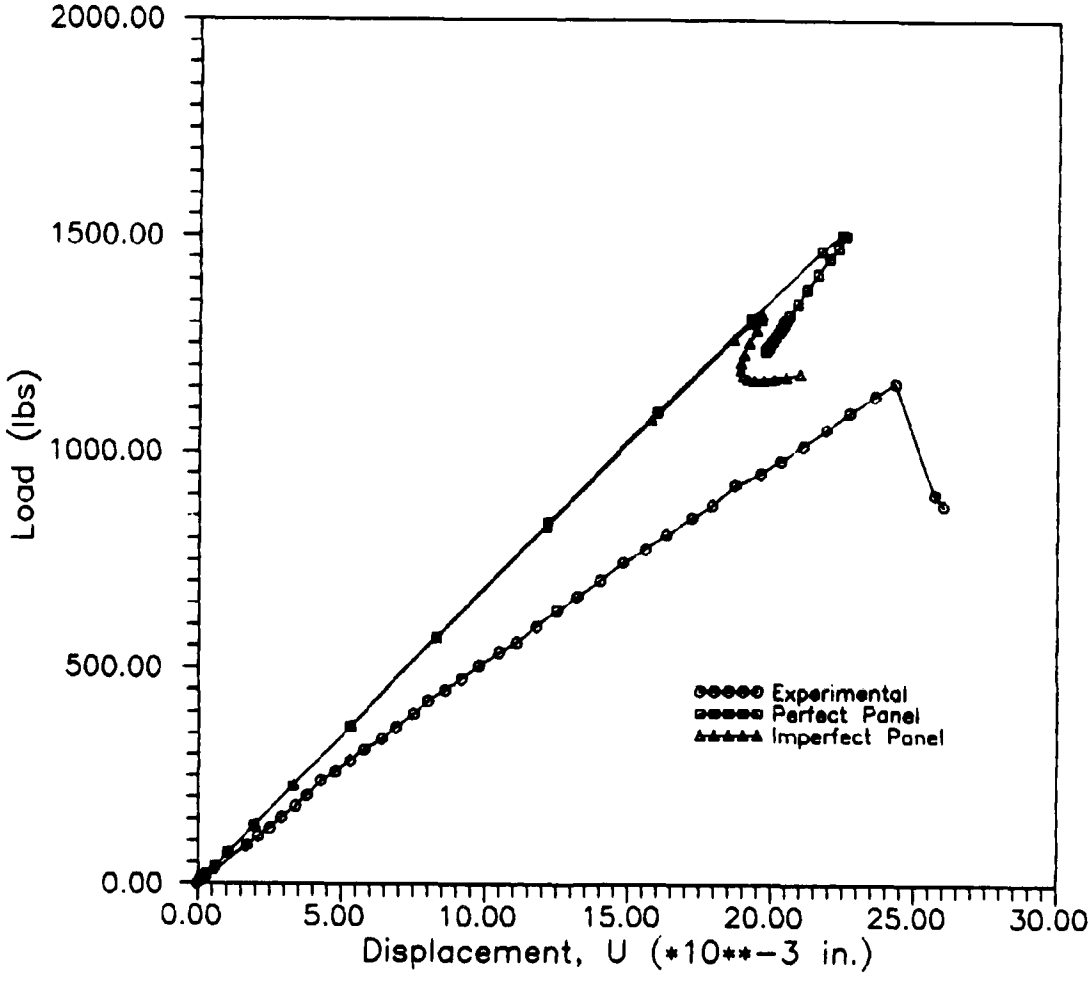

Figure 4.8
Load-Displacement Curves for $[\pm 45/90/0]_s$ Kev/Poly Panels

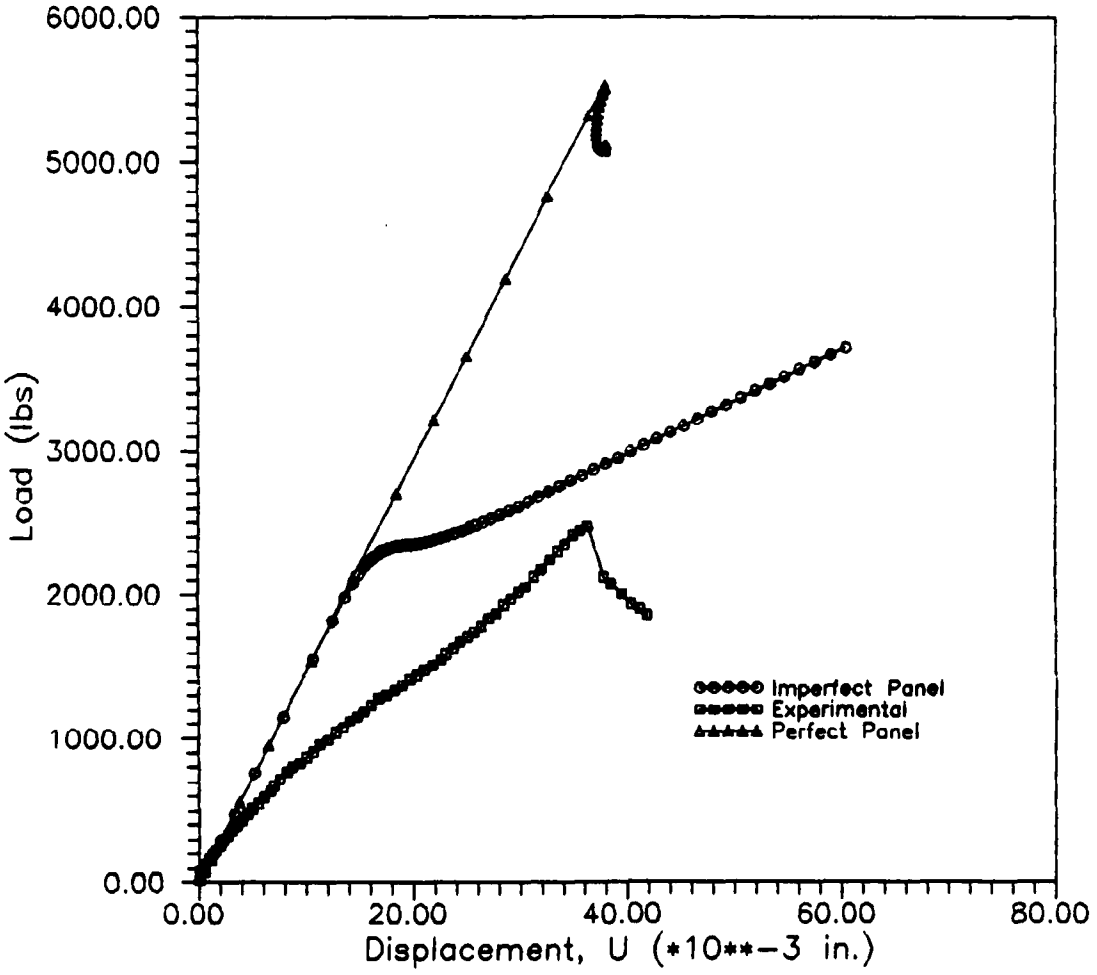

Figure 4.9
Load-Displacement Curves for $[0/90]_{3s}$ Kev/Poly Panels

post-buckling strength of cylindrical panels. We see that the imposed imperfection pattern has little or no effect on the initial stiffness of the structure. In fact, no difference in stiffness is noticed until the collapse load of the imperfect panel is reached. One other thing that we did not expect to see was the large difference in the stiffness between the two analytical panels and the actual panel.

Analytical vs. Experimental Stiffness

Looking at Figures 4.4-4.9, one notices the slopes of the analytical curve are much steeper than that of the experimental curve. The finite element model is thus stiffer than the actual panel, which is expected. However, the amount of the difference is somewhat surprising.

On first glance, one must suspect the model being used. Since boundary conditions play a role in the stiffness or flexibility of a structure, changing the boundary conditions was considered. A STAGSC-1 analysis was performed on $[0/90]_{2s}$ and $[\pm 45/90/0]_{s}$ Graphite/Epoxy panels allowing the circumferential displacement, v, to be free. Figures 4.10 and 4.11 compare the analytical imperfect panel, with both v fixed and v free, and the experimental panel for the ply orientations considered.

As expected, changing the boundary conditions changed the response of the panel. However, little or no change is

apparent in the initial stiffness of the structure when considering the in-plane displacement, u. For the $[0/90]_{2s}$ panel, no change can be seen, where as for the $[\pm 45/90/0]_{s}$ panel, a slight increase in flexibility is noticed. Figures 4.10 and 4.11 show that while boundary conditions do have an effect on the stiffness, it is still most likely the imperfections in the panel which cause the increased flexibility. Even though the two analytical curves have imperfections modeled in them, they do not, by any means, model the actual imperfections exactly. Therefore, the author feels it is the actual imperfections of the panels that cause the increased flexibility.

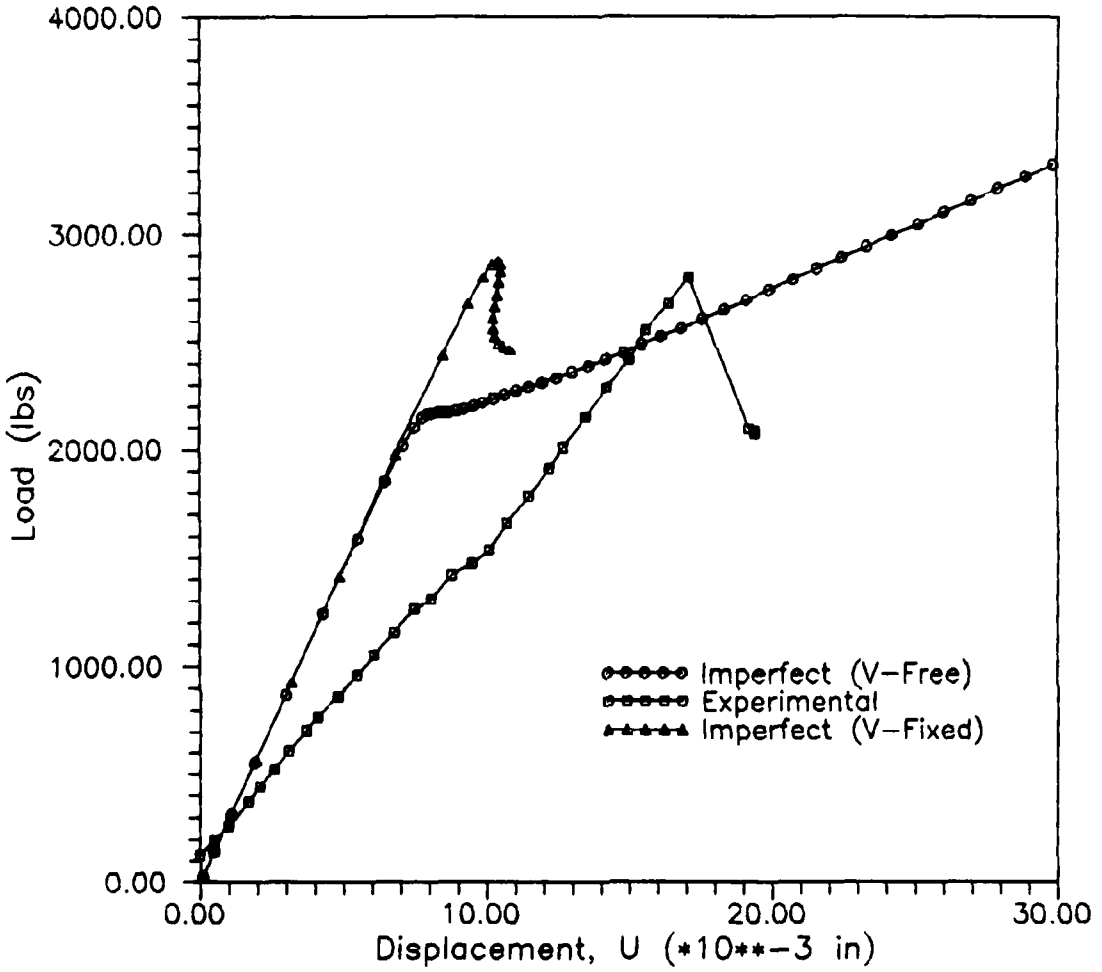

Figure 4.10
Boundary Condition Analysis for $[0/90]_{2s}$ Gr/Ep Panels

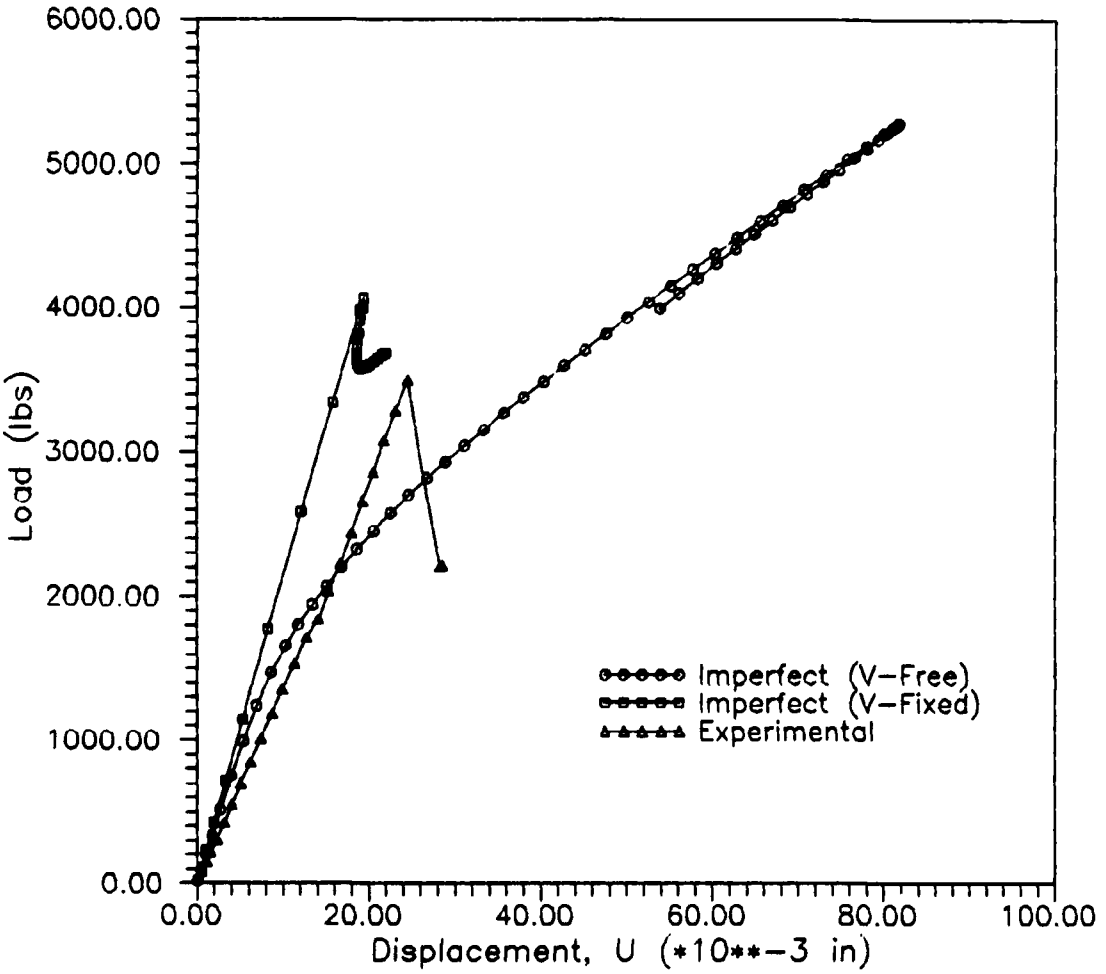

Figure 4.11
Boundary Condition Analysis for $[\pm 45/90/0]_s$ Gr/Ep Panels

5. CONCLUSIONS

Based on the analysis and experimentation performed in this thesis, the following conclusions may be drawn.

1. For composite cylindrical panels, there is a minimum impact energy below which no damage is sustained by the panel. This minimum energy depends on the ply orientation and the thickness. The quasi-isotropic orientations are the most easily damaged where the thicker cross-ply orientations require more energy to cause damage.

2. Photographs and C-Scans show that the damage area appears to remain relatively constant for a range of impact energies. However, we can not say the total damage remains constant because we don't know how the damage propagates through the thickness as the impact energy increases.

3. Panels impacted with energies between 1-3 ft-lbs show little decrease in compressive strength (2-6%) as a result of the impact. However, the delamination caused by the impact spread as a result of the compression test. Thus, impact damage can be quite catastrophic, even though the damage may not be visible, particularly if the structure is subjected to fatigue.

4. Simulating impact damage by implanting teflon inserts as Wilder [1] did may be used to get an idea of the effect impact has on the global collapse load of the panel. Wilder's technique would yield conservative results since

the teflon inserts provide a totally debonded region. The damaged area may still have some strength left in it depending on the amount of energy imparted to the panel. This technique has only been tested on quasi-isotropic laminates. This conclusion can not be extended to cross-ply or any other laminates without further testing.

5. Imperfections must be accounted for when determining the collapse load of undamaged cylindrical panels. This is especially true for cross-ply laminates. Not accounting for imperfections led to differences in analytical vs. experimental loads of 24-62%.

6. The imperfection pattern of 3 sinusoidal half waves in each direction (longitudinal and circumferential), with an amplitude equal to the thickness of one ply (0.005"), seems to most accurately model the random imperfection present in a 8" x 12" cylindrical panel.

7. Quasi-isotropic ply orientations are relatively insensitive in the longitudinal direction (x) to geometric imperfections where as cross-ply laminates are extremely sensitive to imperfections.

8. Changing the boundary conditions on the circumferential displacement (v-fixed vs. v-free) had little effect on the flexibility of the panels. Thus, it is primarily the actual imperfections of the panel that cause the larger than expected displacements in the u-direction.

9. Microphotographs of the cross-section of damaged composite panels show a great deal of cracking and delamination through the thickness of the laminate not visible from C-Scans or stereo X-rays. Information gained from microphotographs will be essential to develop a model to predict damage.

10. The assumption that E_1/E_x, E_2/E_y, and ν_{12}/ν_{xy} are the same for Kevlar/Polyester as they are for Graphite/Epoxy was valid. The resulting equivalent orthotropic material properties were within 5% of the measured properties of the woven laminates.

Appendix A: Material Properties of Kevlar/Polyester

Kevlar/Polyester is a weave material that cannot be made into unidirectional coupons like Graphite/Epoxy. Therefore, determining the material properties is not straight forward. Also, STAGSC-1 can not analyze a weave material, so an equivalent orthotropic laminate had to be developed to model the Kevlar/Polyester.

Kevlar/Polyester coupons with ply orientations of $[0/90]_{2s}$ and $[0/90]_{3s}$ were tested in tension. The results from testing these coupons yielded E_x, E_y, and ν_{xy} for Kevlar/Polyester. G_{12} was determined from the $[\pm 45]_{2s}$ coupons. From the tensile tests,

$$E_x = 3.6371 * 10^6 \text{ psi}$$
$$E_y = 3.6371 * 10^6 \text{ psi}$$
$$\nu_{xy} = 0.061936$$
$$G_{12} = 0.1782 * 10^6 \text{ psi}$$

Next, in order to calculate E_1, E_2, and ν_{12} for Kevlar/Polyester, a relation between these laminate properties had to be assumed. The assumption is that the ratio of laminate properties to unidirectional properties for Kevlar/Polyester is the same as for Graphite/Epoxy. Therefore the effective laminate engineering properties for

Graphite/Epoxy were calculated for ply orientations of $[0/90]_{2s}$ and $[0/90]_{3s}$ using the following equations [23].

$$\begin{aligned} E_x &= (A_{11}A_{22} - A_{12})/hA_{22} \\ E_y &= (A_{11}A_{22} - A_{12}^2)/hA_{11} \\ \nu_{xy} &= A_{12}/A_{22} \end{aligned} \qquad (A.1)$$

where the A_{ij}'s are elements of the extensional stiffness matrix and h is the laminate thickness. Equations (A.1) are only valid for balanced ply orientations (equal numbers of $+\theta$ and $-\theta$ layers) symmetric about the middle plane. For $[0/90]_{2s}$ and $[0/90]_{3s}$ Graphite/Epoxy,

$$\begin{aligned} E_x &= 10.9549 * 10^6 \text{ psi} \\ E_y &= 10.9549 * 10^6 \text{ psi} \\ \nu_{xy} &= 0.0385 \end{aligned}$$

In order to obtain an initial guess for the equivalent orthotropic engineering properties of Kevlar/Polyester, we now use the assumption that the ratios E_1/E_x, E_2/E_y, and ν_{12}/ν_{xy} were the same for both materials. Using these ratios, the following equation was used to calculate E_1 for Kevlar/Polyester.

$$(E_1)_{Kev/Poly} = \beta \left(E_x \right)_{Gr/Ep} \qquad (A.2)$$

where

$$\beta = \left(\frac{E_1}{E_x} \right)_{Gr/Ep} \qquad (A.3)$$

Similar expression were used to calculate E_2 and ν_{12}. The values obtained were

$$E_1 = 6.7932 * 10^6 \text{ psi}$$
$$E_2 = 0.44502 * 10^6 \text{ psi}$$
$$\nu_{12} = 0.50369$$
$$G_{12} = 0.1782 * 10^6 \text{ psi}$$

Using these values, E_x, E_y, and ν_{xy} for Kevlar/Polyester were calculated using Equations (A.1) and compared to the experimentally determined laminate properties as a double check. The calculated values are within 5% of the experimental values. Thus the above values for E_1, E_2, ν_{12}, and G_{12} were used in STAGSC-1 for Kevlar/Polyester.

Appendix B: Classical Laminated Plate Theory

Since the present study deals with composite panels, a brief review of classical laminated plate theory is presented. Interested readers are referred to Jones' [24] text for a detailed presentation of classical laminated plate theory.

For an orthotropic material in a state of plane stress, the stress-strain relations may be written as

$$\begin{Bmatrix} \sigma_1 \\ \sigma_2 \\ \tau_{12} \end{Bmatrix} = \begin{bmatrix} Q_{11} & Q_{12} & Q_{16} \\ Q_{12} & Q_{22} & Q_{26} \\ Q_{16} & Q_{26} & Q_{66} \end{bmatrix} \begin{Bmatrix} \varepsilon_1 \\ \varepsilon_2 \\ \gamma_{12} \end{Bmatrix} \tag{B.1}$$

The Q_{ij}'s are the reduced stiffnesses and are functions of the material constants.

$$\begin{aligned} Q_{11} &= E_1 \,/\, (1 - \nu_{12}\nu_{21}) \\ Q_{12} &= (\nu_{12}E_2) \,/\, (1 - \nu_{12}\nu_{21}) \\ Q_{22} &= E_2 \,/\, (1 - \nu_{12}\nu_{21}) \\ Q_{66} &= G_{12} \end{aligned} \tag{B.2}$$

Equations (B.1) are defined in the principal material directions. However, these directions often do not coincide with the body or laminate axis system natural to the given structure. Therefore, a coordinate transformation must be made. Transforming from the material axis system (1-2

directions) to the structural axis system (x-y directions) we obtain

$$\begin{Bmatrix} \sigma_x \\ \sigma_y \\ \tau_{xy} \end{Bmatrix} = \begin{bmatrix} \bar{Q}_{11} & \bar{Q}_{12} & \bar{Q}_{16} \\ \bar{Q}_{12} & \bar{Q}_{22} & \bar{Q}_{26} \\ \bar{Q}_{16} & \bar{Q}_{26} & \bar{Q}_{66} \end{bmatrix} \begin{Bmatrix} \varepsilon_x \\ \varepsilon_y \\ \gamma_{xy} \end{Bmatrix} \tag{B.3}$$

where

$$\begin{aligned}
\bar{Q}_{11} &= Q_{11}\cos^4\theta + 2(Q_{12} + 2Q_{66})\sin^2\theta\cos^2\theta + Q_{22}\sin^4\theta \\
\bar{Q}_{12} &= (Q_{11} + Q_{22} - 4Q_{66})\sin^2\theta\cos^2\theta + Q_{12}(\sin^4\theta + \cos^4\theta) \\
\bar{Q}_{22} &= Q_{11}\sin^4\theta + 2(Q_{12} + 2Q_{66})\sin^2\theta\cos^2\theta + Q_{22}\cos^4\theta \\
\bar{Q}_{16} &= (Q_{11} - Q_{12} - 2Q_{66})\sin\theta\cos^3\theta + (Q_{12} - Q_{22} + 2Q_{66})\sin^3\theta\cos\theta \\
\bar{Q}_{26} &= (Q_{11} - Q_{12} - 2Q_{66})\sin^3\theta\cos\theta + (Q_{12} - Q_{22} + 2Q_{66})\sin\theta\cos^3\theta \\
\bar{Q}_{66} &= (Q_{11} + Q_{22} - 2Q_{12} - 2Q_{66})\sin^2\theta\cos^2\theta + Q_{66}(\sin^4\theta + \cos^4\theta)
\end{aligned} \tag{B.4}$$

The angle θ is the angle between the 1-axis and the x-axis shown in Figure B.1.

Knowing how the stresses and strains vary through the thickness of a laminate is necessary in order to define the extensional and bending stiffnesses of the laminate. Here, we assume the individual laminae are perfectly bonded together, infinitesimally thin, and are non-shear deformable. The displacements through the thickness are continuous so that no laminae can slip relative to another. We also make the following assumptions, collectively known

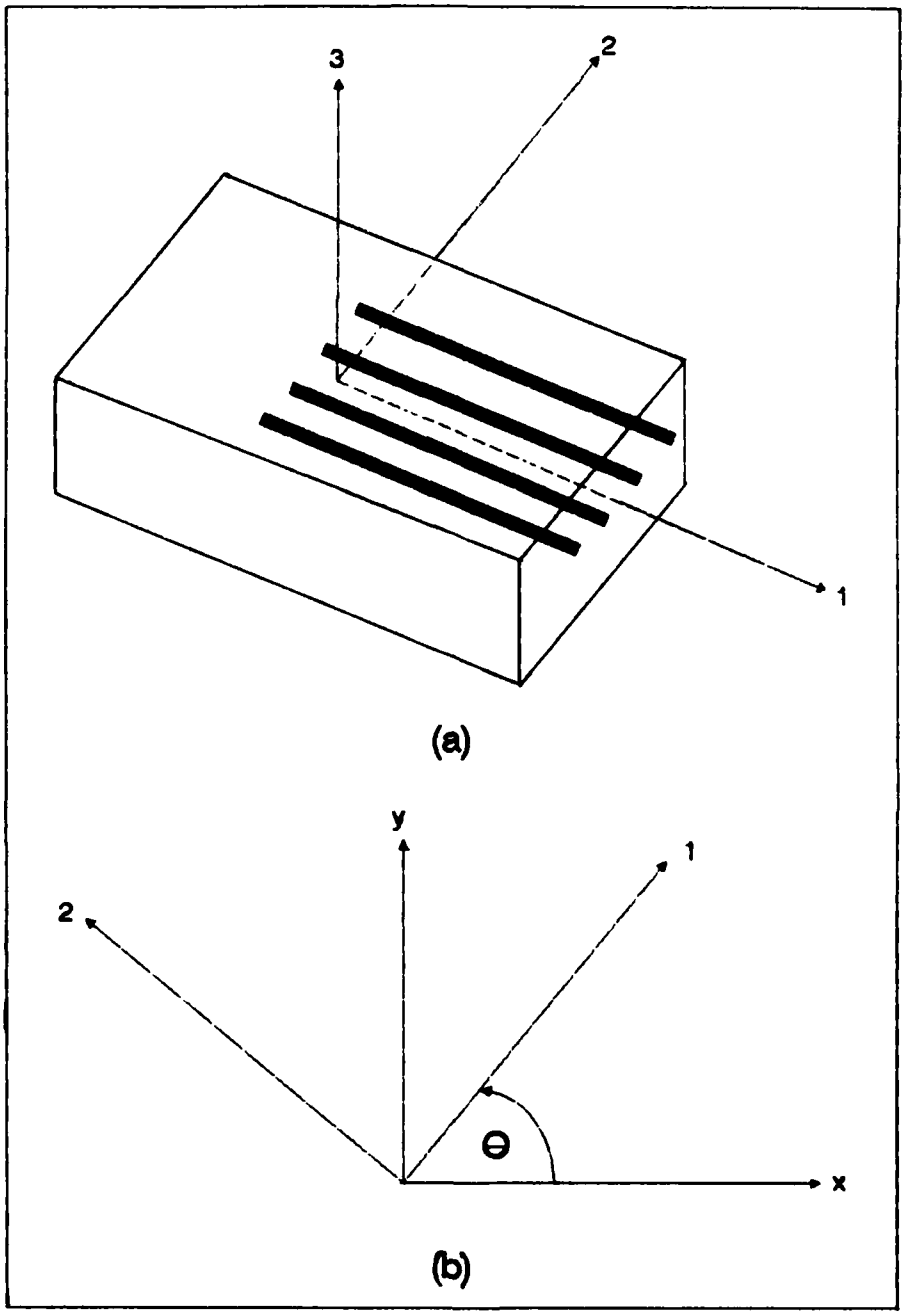

Figure B.1

(a) Fiber (1-2) Axis System (b) Transformation into Structural Axis System

as the Kirchhoff hypothesis for plates or Kirchhoff-Love hypothesis for shells.

(a) A line originally normal to the middle surface of the laminate remains normal after the laminate is deformed (i.e. shear strains γ_{xz} and γ_{yz} are negligible).

(b) Normals have constant length ($\varepsilon_z = 0$).

The strains for the laminate, as long as they are assumed to be small, may be written as

$$\begin{Bmatrix} \varepsilon_x \\ \varepsilon_y \\ \gamma_{xy} \end{Bmatrix} = \begin{Bmatrix} \varepsilon_x^o \\ \varepsilon_y^o \\ \gamma_{xy}^o \end{Bmatrix} + z \begin{Bmatrix} K_x \\ K_y \\ K_{xy} \end{Bmatrix} \qquad (B.5)$$

where the middle surface strains are

$$\begin{Bmatrix} \varepsilon_x^o \\ \varepsilon_y^o \\ \gamma_{xy}^o \end{Bmatrix} = \begin{Bmatrix} u_{o,x} \\ v_{o,y} \\ u_{o,y} + v_{o,x} \end{Bmatrix} \qquad (B.6)$$

and the middle surface curvatures are

$$\begin{Bmatrix} K_x \\ K_y \\ K_{xy} \end{Bmatrix} = - \begin{Bmatrix} w_{o,xx} \\ w_{o,yy} \\ 2w_{o,xy} \end{Bmatrix} \qquad (B.7)$$

In Equations (B.6) and (B.7), u_o, v_o, and w_o are the displacements of the middle surface in the x, y, and z directions respectively.

Substituting Equation (B.5) into Equation (B.3) we obtain the stresses in the k^{th} layer of the laminate in terms of middle surface strains and curvatures.

$$\begin{Bmatrix} \sigma_x \\ \sigma_y \\ \tau_{xy} \end{Bmatrix}_k = \left[\bar{Q} \right]_k \left\{ \begin{Bmatrix} \varepsilon_x^o \\ \varepsilon_y^o \\ \gamma_{xy}^o \end{Bmatrix} + z \begin{Bmatrix} K_x \\ K_y \\ K_{xy} \end{Bmatrix} \right\} \qquad (B.8)$$

The resultant forces and moments acting on the laminate are obtained by performing the following integrations through the thickness of the laminate.

$$\begin{Bmatrix} N_x \\ N_y \\ N_{xy} \end{Bmatrix} = \int_{-h/2}^{h/2} \begin{Bmatrix} \sigma_x \\ \sigma_y \\ \tau_{xy} \end{Bmatrix} dz = \sum_{k=1}^{N} \int_{z_{k-1}}^{z_k} \begin{Bmatrix} \sigma_x \\ \sigma_y \\ \tau_{xy} \end{Bmatrix}_k dz \qquad (B.9)$$

$$\begin{Bmatrix} M_x \\ M_y \\ M_{xy} \end{Bmatrix} = \int_{-h/2}^{h/2} \begin{Bmatrix} \sigma_x \\ \sigma_y \\ \tau_{xy} \end{Bmatrix} z dz = \sum_{k=1}^{N} \int_{z_{k-1}}^{z_k} \begin{Bmatrix} \sigma_x \\ \sigma_y \\ \tau_{xy} \end{Bmatrix}_k z dz \qquad (B.10)$$

N is the number of layers in the laminate and z_k and z_{k-1} are shown in Figure B.2. Figure B.3 illustrates the forces and moments acting on the laminate.

Upon substitution for the stress vector of the k^{th} layer and performing the integrations, we obtain for the forces and moments

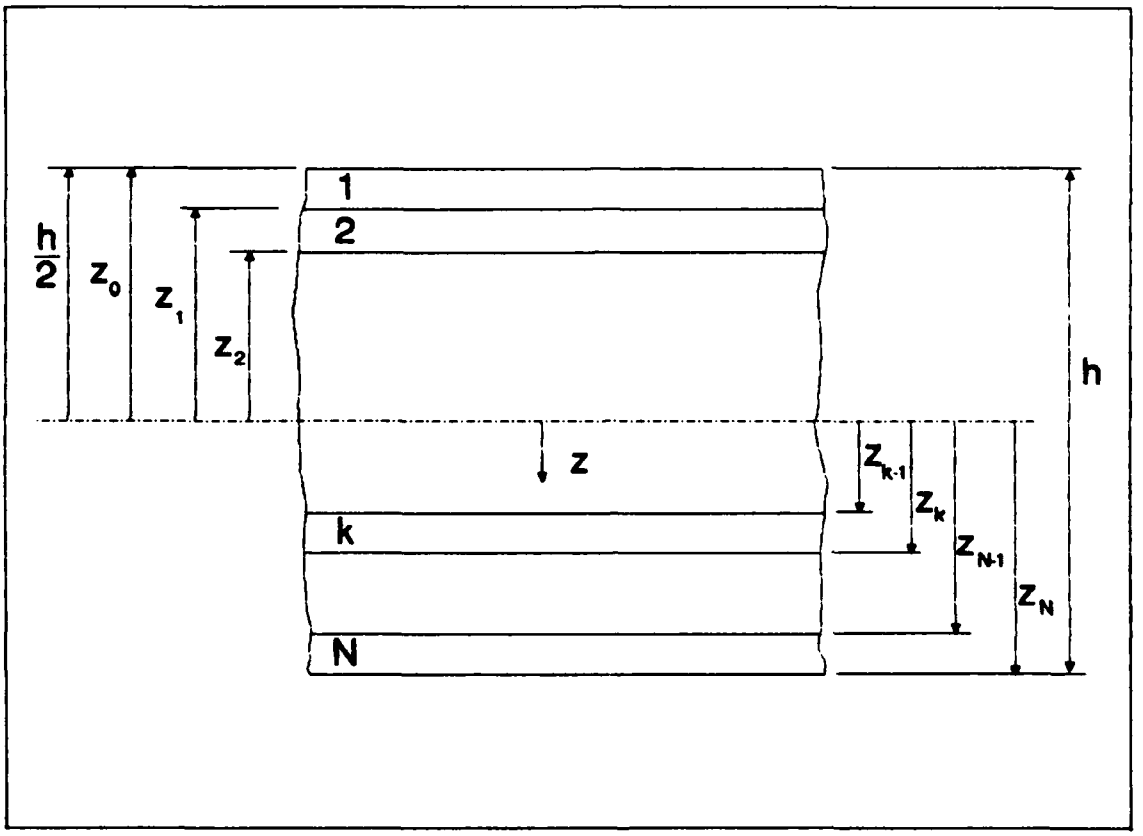

Figure B.2 - Laminate Geometry

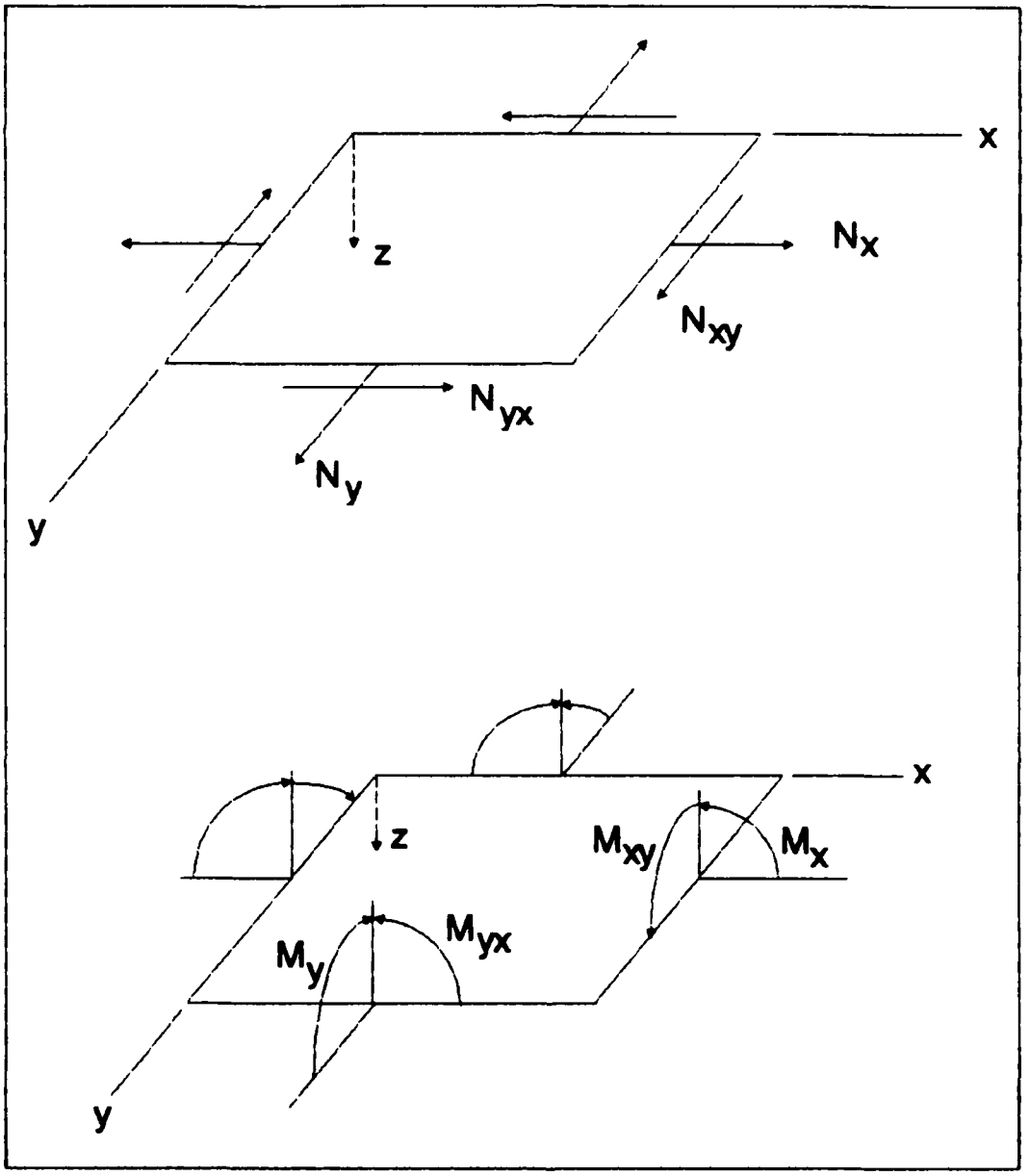

Figure B.3 - In-plane Forces and Moments on a Flat Laminate

$$\begin{Bmatrix} N_x \\ N_y \\ N_{xy} \end{Bmatrix} = \begin{bmatrix} A_{11} & A_{12} & A_{16} \\ A_{12} & A_{22} & A_{26} \\ A_{16} & A_{26} & A_{66} \end{bmatrix} \begin{Bmatrix} \varepsilon_x^\circ \\ \varepsilon_y^\circ \\ \gamma_{xy}^\circ \end{Bmatrix} + \begin{bmatrix} B_{11} & B_{12} & B_{16} \\ B_{12} & B_{22} & B_{26} \\ B_{16} & B_{26} & B_{66} \end{bmatrix} \begin{Bmatrix} K_x \\ K_y \\ K_{xy} \end{Bmatrix} \tag{B.11}$$

$$\begin{Bmatrix} N_x \\ N_y \\ N_{xy} \end{Bmatrix} = \begin{bmatrix} B_{11} & B_{12} & B_{16} \\ B_{12} & B_{22} & B_{26} \\ B_{16} & B_{26} & B_{66} \end{bmatrix} \begin{Bmatrix} \varepsilon_x^\circ \\ \varepsilon_y^\circ \\ \gamma_{xy}^\circ \end{Bmatrix} + \begin{bmatrix} D_{11} & D_{12} & D_{16} \\ D_{12} & D_{22} & D_{26} \\ D_{16} & D_{26} & D_{66} \end{bmatrix} \begin{Bmatrix} K_x \\ K_y \\ K_{xy} \end{Bmatrix} \tag{B.12}$$

The A, B, and D matrices are symmetric and are defined by

$$A_{ij} = \sum_{k=1}^{N} \left[\bar{Q} \right]_k \left(z_k - z_{k-1} \right) \tag{B.13}$$

$$B_{ij} = 1/2 \sum_{k=1}^{N} \left[\bar{Q} \right]_k \left(z_k^2 - z_{k-1}^2 \right) \tag{B.14}$$

$$D_{ij} = 1/3 \sum_{k=1}^{N} \left[\bar{Q} \right]_k \left(z_k^3 - z_{k-1}^3 \right) \tag{B.15}$$

BIBLIOGRAPHY

1. Wilder, Brenden L. A Study of Damage Tolerance in Curved Composite Panels, M.S. Thesis GA/AA/88M-3, School of Engineering, Air Force Institute of Technology (AU), Wright-Patterson AFB, OH, 1988.

2. Becker, Marvin L. Analytical/Experimental Investigation of the Instability of Composite Cylindrical Panels, M.S. Thesis GAE/AA/79D-3, School of Engineering, Air Force Institute of Technology (AU), Wright-Patterson AFB, OH, 1979.

3. Janisse, Thomas C. A Parametric Study of Surface Imperfections and Small Cutouts in a Composite Panel, M.S. Thesis GAE/AA/82D-15, School of Engineering, Air Force Institute of Technology (AU), Wright-Patterson AFB, OH, 1982.

4. Wu, Hsi-Yung T. and George S. Springer. "Impact Induced Stresses, Strains, and Delaminations in Composite Plates," Journal of Composite Materials, Vol. 22, pp. 533-560 (June 1988).

5. O'Kane, B.A.A. and P.P. Benham. "Damage Thresholds for Low Velocity Impact on Aircraft Structural Composites," Aeronautical Journal, pp. 368-372, (November 1986).

6. Joshi, S.P. "Impact-Induced Damage Initiation Analysis: An Experimental Study," Proceedings of the American Society for Composites, Third Technical Conference, pp. 325-333, (September, 1988).

7. Gosse, J.H. and P.B.Y. Mori. "Impact Damage Characterization of Graphite/Epoxy Laminates," Proceedings of the American Society for Composites, Third Technical Conference, pp. 344-353, (September, 1988).

8. Dost, Ernest F. et al. "Sublaminate Stability Based Modeling of Impact-Damaged Composite Laminates," Proceedings of the American Society for Composites, Third Technical Conference, pp. 354-363, (September, 1988).

9. Taske II, Leo E. and Azar P. Majidi. "Parametric Studies of Impact Testing in Laminated and Woven Architectures," Proceedings of the American Society for Composites, Third Technical Conference, pp. 374-383, (September 1988).

10. Joshi, S.P. and C.T. Sun. "Impact Induced Fracture in a Laminated Composite," Journal of Composite Materials, Vol. 19, pp. 51-66, (January 1985).

11. Meyer, P.I. "Low-Velocity Hard-Object Impact of Filament-Wound Kevlar/Epoxy Composite," Composites Science and Technology, Vol. 33, pp. 279-293, (1988).

12. Model 8250 Impact Test Machine Instruction Manual, Dynatup Products, General Research Corporation, Santa Barbara, CA, 1984.

13. GRC 730-I Instrumented Impact Test Data System Manual, Dynatup Products, General Research Corporation, Santa Barbara, CA, 1984.

14. Brush, D.O. and B.O. Almroth. Buckling of Bars, Plates, and Shells. New York: McGraw-Hill, Inc., 1975.

15. Rummel, Ward D. et al. Enhanced X-Ray Stereoscopic NDE of Composite Materials, AFWAL-TR-80-3053, Air Force Flight Dynamics Laboratory, Wright-Patterson AFB, OH, June 1980.

16. User's Manual for STAGS, Volume 1, Theory. Structural Mechanics Laboratory, Lockheed Palo Alto Research Laboratory, Palo Alto, CA, March 1978.

17. Egan, Gregory S. Nonlinear Finite Element Analysis of a General Composite Shell, M.S. Thesis GAE/AA/88D-12, School of Engineering, Air Force Institute of Technology (AU), Wright-Patterson AFB, OH, 1988.

18. Riks, E. "An Incremental Approach to the Solution of Snapping and Buckling Problems," International Journal of Solids and Structures, Vol. 15, pp. 529-551, (1979).

19. Bellini, P.X. and A. Chulya. "An Improved Automatic Incremental Algorithm for the Efficient Solution of Nonlinear Finite Element Equations," Computers and Structures, Vol. 26, No. 1/2, pp. 99-110, (1987).

20. Crisfield, M.A. "A Fast Incremental/Iterative Solution Procedure that Handles "Snap-Through"," Computers and Structures, Vol 13, pp.55-62, (1981).

21. Carlsson, Leif A. and R. Byron Pipes. Experimental Characterization of Advanced Composite Materials, Prentice-Hall, Inc., 1987.

22. Almroth, B.O. et al. Structural Analysis of General Shells, Volume II, User Instructions for STAGSC-1, Report No. LMSC-D633873, Lockheed Palo Alto Research Laboratory, Palo Alto, CA, 1983.

23. Whitney, James M. et al. Experimental Mechanics of Fiber Reinforced Composite Materials, Prentice-Hall, 1984.

24. Jones, Robert M. Mechanics of Composite Materials. Hemisphere Publishing Corporation, 1975.

VITA

Eugene A. Senn [redacted] He graduated from Thomas Kelly High School in Chicago, Illinois in 1981 and attended the Illinois Institute of Technology where he received a Bachelor of Science in Mechanical and Aerospace Engineering in 1985. Upon graduation he received a commission in the USAF through the ROTC program. His first assignment was as an F-111 Flight Test Ballistics Engineer at the Sacramento Air Logistics Center, McClellan AFB, CA. He was responsible for incorporating the capability for automatic weapon delivery of new weapons into the F-111. In May 1988, he began the graduate Aeronautical Engineering program at the Air Force Institute of Technology.

[redacted]